Investigating the mechanism of the Hsp90 molecular chaperone using photoinduced electron transfer fluorescence quenching

***

Untersuchungen zum Mechanismus des molekularen Chaperons Hsp90 mittels photoinduzierter Elektronentransfer-Fluoreszenzlöschung

Doctoral thesis for a doctoral degree
at the Graduate School of Life Sciences,
Julius-Maximilians-Universität Würzburg,
Sections Integrative Biology and Biomedicine

submitted by

Andrea Schulze

from

Bielefeld

Würzburg, 2017

Submitted on: ……

Members of the *Promotionskomitee*:

Chairperson: Prof. Dr. Christian Janzen

Primary Supervisor: PD Dr. Hannes Neuweiler

Supervisor (Second): Prof. Dr. Markus Sauer

Supervisor (Third): Prof. Dr. Thomas Müller

Date of Public Defence: ……..……

Date of Receipt of Certificates: ……

Affidavit

I hereby confirm that my thesis entitled *Investigating the mechanism of the Hsp90 molecular chaperone using photoinduced electron transfer fluorescence quenching* is the result of my own work. I did not receive any help or support from commercial consultants. All sources and / or materials applied are listed specified in the thesis.

Furthermore, I confirm that this thesis has not yet been submitted as part of another examination process neither in identical nor in similar form.

Würzburg, Signature

Eidesstaatliche Erklärung

Hiermit erkläre ich an Eides statt, die Dissertation *Untersuchungen zum Mechanismus des molekularen Chaperons Hsp90 mittels photoinduzierter Elektronentransfer-Fluoreszenzlöschung* eigenständig, d.h. insbesondere selbständig und ohne Hilfe eines kommerziellen Promotionsberaters, angefertigt und keine anderen als die von mir angegebenen Quellen und Hilfsmittel verwendet zu haben.

Ich erkläre außerdem, dass die Dissertation weder in gleicher noch in ähnlicher Form bereits in einem anderen Prüfungsverfahren vorgelegen hat.

Würzburg, Unterschrift

Zusammenfassung

Das molekulare Chaperon Hsp90 ermöglicht die korrekte Faltung und Aktivierung eines breiten Spektrums an strukturell und funktionell unterschiedlichen Klienten-Proteinen. Hsp90 bildet einen zentralen Knotenpunkt der Protein-Homöostase und ist an der Entstehung einer Vielzahl von humanen Erkrankungen beteiligt. Trotz des vielversprechenden Potentials, das Hsp90 als Zielprotein für die Behandlung von Erkrankungen besitzt, ist der Mechanismus, durch den Hsp90 seinen Klienten erkennt und dessen Reifung gewährt, noch unbekannt,

Die Gestalt des homodimeren Proteins ähnelt einer molekularen Klammer, die sich durch Bindung und Hydrolyse von ATP öffnet und schließt. Strukturelle Studien zeigen ein Netzwerk an weit voneinander entfernt liegenden lokalen Konformationsänderungen, die den langsamen Übergang (im Bereich von Minuten) in die Hydrolyse-aktive, geschlossene Konfiguration koordinieren. Allerdings sind die Kinetiken der lokalen Konformationsänderungen unbekannt, da es bisher noch keine spektroskopische Methode gibt, die diese detektieren könnte.

Die natürliche Aminosäure Tryptophan kann durch eine photoinduzierte-Elektronentransfer-(PET)-Reaktion die Fluoreszenz extrinsischer Fluorophore löschen. Fluorophor und Tryptophan müssen hierfür in einer Kontakt-Distanz im sub-nanometer Bereich stehen. Dieser Lösch-Mechanismus wurde zu einem 1-nm sensitiven, spektroskopischen Werkzeug entwickelt, das für die Detektion schneller Proteinfaltungsdynamiken angewendet werden kann. Im Rahmen der hier vorliegenden Dissertation wurden PET-Reporter-Systeme entworfen. Diese dienten der Untersuchung lokaler Konformationsänderungen, die Teil des mechanistischen Kerns des Hsp90-Chaperon-Zyklus sind. ATP-induzierte Kinetiken des ATP-Lid Schlusses sowie des Untereinheiten-Wechsels des N-terminalen ß-Faltblatts als auch der Assoziation der N-terminalen mit der mittleren Domäne wur-

den ermittelt. In Ensemble Experimenten konnte gezeigt werden, dass lokale Bewegungen auf ähnlichen Zeitskalen stattfinden und in guter Übereinstimmung mit der ATP-Hydrolyserate sind. Durch die Anwendung von Funktionsmutanten konnte demonstriert werden, dass die lokalen Bewegungen zusammenwirkend geschehen. Des Weiteren wurde gezeigt, dass der Lid anhand eines zweistufigen Prozesses schließt. Dieser besteht aus einer, durch die Bindung von ATP ausgelösten, raschen Lid-Rekonfiguration, gefolgt von der langsamen Schließung des Lids. Das Co-Chaperon Aha1 scheint den ATPase-Zyklus bereits in einem frühen Stadium, durch die Remodellierung der Lid-Konformation und die Stabilisierung des apo-Hsp90 in einer vor-assoziierten Konformation der NM-Domänen, zu beeinflussen

Des Weiteren wurde eine Zwei-Farben-Einzelmolekül-PET-Mikroskopie-Methode entwickelt, die es ermöglicht lokale Bewegungen an entfernten Positionen simultan und in Echtzeit zu beobachten. Dadurch kann festgestellt werden, ob eine Richtungscharakteristik innerhalb des Netzwerks lokaler Konformationsänderungen besteht. Hierfür wurde zunächst anhand von einfach markierten Hsp90 Konstrukten, die nur eine Bewegung darstellen, getestet ob die Detektion von PET-Komplexen auf der Einzelmolekülоberfläche möglich ist (Ein-Farben-Einzelmolekül-PET-Mikroskopie). Die Fluoreszenz PET-gelöschter Komplexe konnte mittels Oxidation durch molekularen Sauerstoff wiederhergestellt werden, wodurch eine Unterscheidung zu photogebleichten Fluorophoren möglich war. In Zwei-Farben-Experimenten konnte zudem ein gedimmter Zustand der PET-gelöschten Fluorophore festgestellt werden, allerdings nicht für jedes der verwendeten PET-Reportersysteme. Die Ergebnisse deuten auf ein innerhalb der Zeitauflösung des Experiments (0.3 sec) gleichzeitiges Auftreten der lokalen Bewegungen hin. Des Weiteren scheint der Mechanismus des Klammerschlusses komplexer zu sein, als der Mechanismus der Klammeröffnung. Während die Kinetiken der Klammeröffnung durch eine mono-exponentielle Fit-funktion angepasst werden konnten, benötigte der Klammerschluss eine bi-exponentielle Anpassungsfunktion.

Summary

The molecular chaperone Hsp90 facilitates the folding and activation of a wide array of structurally and functionally diverse client proteins. Hsp90 presents a central node of protein homeostasis and is frequently involved in the development of many human diseases. Although Hsp90 is a promising target for disease treatment, the mechanism by which Hsp90 facilitates client recognition and maturation is poorly understood.

The shape of the homodimeric protein resembles a molecular clamp that opens and closes in response to binding and hydrolysis of ATP. Structural studies reveal a network of distinct local conformational rearrangements that coordinate the slow transition into the hydrolysis-active, closed state configuration (time order of minutes). However, the kinetics of local conformational changes remain elusive because spectroscopic tools that can detect them have been missing so far.

Fluorescence quenching of extrinsic fluorophores by the natural amino acid Tryptophan is based on a photoinduced electron transfer (PET) reaction, which requires sub-nanometer contact between fluorophore and Tryptophan. This quenching mechanism has been developed into a 1-nm spectroscopic tool for the detection of rapid protein folding dynamics. Within the scope of this doctoral thesis, PET-reporter systems were designed to investigate the kinetics of local conformational motions that are part of the mechanistic core of the Hsp90 chaperone cycle. ATP-triggered kinetics of closure of the ATP-lid as well as swapping of the N-terminal ß-strand across subunits and association of the N-terminal and middle-domain were estimated in solution. Bulk experiments revealed that local motions occur on similar timescales and are in good agreement with the ATP-hydrolysis rate. Functional mutations demonstrated that local motions act cooperatively. Furthermore, the lid was shown to close via a two-step process consisting of a rapid lid-reconfiguration in direct response to ATP-binding, followed by slow closure of

the lid. The co-chaperone Aha1 seems to act early in the chaperone cycle by remodelling of the lid and by stabilization of apo Hsp90 in a NM-domain pre-associated conformation.

A two-colour single-molecule PET microscopy method was developed to observe local motions at remote positions simultaneously and in real-time. Thus, directionality within the network of local conformational changes could be revealed. In a first attempt, the feasibility of detecting PET-complexes on the single-molecule surface was tested on Hsp90 constructs that report on only one motion (one-colour single-molecule PET microscopy). PET-quenched complexes could be distinguished from photobleached fluorophores through oxidation by molecular oxygen, resulting in fluorescence recovery. In two-colour experiments, a dimmed state was identified for PET-quenched complexes, but not for all of the used PET-reporter systems. Results suggest that local motions occur simultaneously within the time-resolution of the experiment (0.3 sec). Furthermore, bi-exponential kinetics of transition into the closed clamp configuration indicate a more complex mechanism of clamp-closure than of clamp-opening, which could be well described by a mono-exponential function.

Abbreviations

ADP	adenosine diphosphate
Aha1	accelerator of Hsp90 ATPase activity
Aha1-C	carboxy-terminal domain of Aha1
Aha1-N	amino-terminal domain of Aha1
AMP-PNP	adenylyl-imidodiphosphate
ATP	adenosine triphosphate
bp	base pairs
$CaCl_2$	calcium chloride
CC	coiled-coil
CF	correction factor
CL	charged linker
CTD	carboxy-terminal domain of Hsp90
DDS	dichlorodimethylsilane
DMSO	dimethyl sulfoxide
DNA	deoxyribonucleic acid
DOL	degree of labelling
*d*STORM	direct stochastic optical reconstruction microscopy
DTT	dithiothreitol
E.coli	Escherichia coli
EDTA	ethylenediaminetetraacetic acid
EMCCD	electron-multiplying charge-coupled device
FCS	fluorescence correlation spectroscopy
FRET	fluorescence resonance energy transfer
FWHM	full-width half maximum
GHKL	gyrase, Hsp90, histidine kinase, MutL superfamily
HCl	hydrogen chloride

HEPES	4-(2-hydroxyethyl)-1-piperazineethanesulfonic acid
HILO	highly inclined and laminated optical sheet
Hop	Hsp70-Hsp90 organizing protein
Hsf	heat shock transcription factor
Hsp	heat-shock proteins
IPTG	isopropyl-β-D-thiogalactopyranosid
IS	ionic strength
kb	kilobase
KCl	potassium chloride
K_D	dissociation constant
kDa	kilodalton
KOH	potassium hydroxide
MD	middle domain of Hsp90
MgOAc	magnesium acetate
mRNA	messenger ribo nucleic acid
MWCO	molecular weight cut-off
NA	numerical aperture
NaCl	sodium chloride
NADH	nicotinamide adenine dinucleotide
NBD	nucleotide binding domain of Hsp70
Ni-NTA	nickel-nitrilotriacetic acid
NTD	amino-terminal domain of Hsp90
OD	optical density
Ops	optically pumped semiconductor
PCR	polymerase chain reaction
PDB	protein data bank
PEG	polyethylene glycole
PET	photoinduced electron transfer
PPIase	peptidyl-prolyl-cis-trans isomerase
QY	quantum yield
rpm	rounds per minute
SBD	substrate binding domain of Hsp70
SDS-PAGE	sodium dodecyl sulfate polyacrylamide gel electrophoresis

TB	transformation buffer
TBE	Tris-borate-EDTA buffer
TCEP	tris(2-carboxyethyl)phosphine
TIRF	total internal reflection fluorescence
TPR	tetratricopeptide repeat
tRNA	transporter ribo nucleic acid
TrpZip	tryptophan zipper
TY	tryptone yeast
wt	wildtype
WZA2	WinZipA2
WZB1	WinZipB1

Contents

1 Introduction

1.1 Quality control of protein folding - the role of chaperones

Almost all processes within living matter are carried out by a very complex network of macromolecules: the proteome. It describes the entire set of expressed proteins that can be found within a specific kind of cell at a given time. The proteome is a very dynamic system, highly influenced by external factors like temperature, pH and stress. These factors can lead to misfolding and aggregation of proteins. To preserve integrity of the proteome, organisms have evolved a protein homeostasis network consisting of chaperones and protein degradation machineries. Molecular chaperones are machineries that assist proteins to fold correctly within the crowded cellular environment. Especially large proteins that consist of multiple domains with different structures and functions would never reach their native form without the help of catalyzers and assistors of protein folding.

Protein folding refers to the process, by which a nascent polypeptide chain adopts its three-dimensional structure. How this is accomplished is one of the fundamental questions in protein science that is under investigation since more than four decades (Chen et al., 2008). Proteins are biological macromolecules that fulfill a vast ensemble of functions: they give cells their structure, transport molecules, serve as catalyzers of metabolic reactions and enable the response to an external stimuli, just to name a few. Their function and their destination within the cell are defined by the protein's sequence, consisting of 20 different amino acids that are connected via peptide bonds. This information is genetically encoded and translated into a polypeptide chain via complementary binding of amino-acid transporters, the tRNA, to a three-base codon in the messenger RNA (mRNA). After protein synthesis in the ribosome, the nascent polypeptide chain is released into the cytoplasm and adopts its three-dimensional structure. Early protein-folding

experiments have shown that some small proteins (< 100 amino acids) are capable to refold spontaneously into their native structure after denaturation at specific conditions. Based on this observation, the assumption was supported that all information needed for adoption of the three-dimensional structure is encoded in the amino acid sequence (Anfinsen, 1973). But as protein-folding is accomplished on time scales of milliseconds to seconds, it can't proceed by a random search of all possible conformations. Levinthal has proposed that folding happens via specific pathways in which the linear polypeptide chain has to pass partially structured intermediate states (Levinthal, 1968). The current model proposes that proteins exhibit rugged, funnel-like energy landscapes which allow the protein to progress along several downhill routes to their kinetically favorable native structure (Onuchic et al., 1997). But on its way to the native state, a protein often has to pass substantial kinetic energy barriers (Figure 1-1). Especially larger proteins are prone to populate kinetically trapped intermediate states. Hydrophobic chains or unstructured polypeptide backbones, which are buried in the native state, are often solvent-exposed in these conformations. Protein aggregation and misfolding due to non-native interactions are very likely. Thus, especially large proteins with complex domain folds need the assistance of chaperone molecules that promote their proper folding while counteracting nonnative, off-pathway interactions (Balchin et al., 2016).

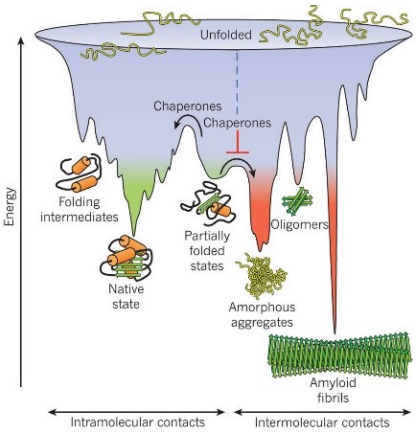

Figure 1-1: Nascent polypeptide chains on their journey to the native state along a rugged funnel-like energy landscape (green). Kinetic energy barriers lead to the population of partially folded intermediate states. Hydrophobic residues and unstructured polypeptide backbones, buried in the native state, are solvent exposed. Intermolecular contacts are favoured, leading to the formation of aggregates of varying sizes and morphologies. Chaperones circumvent these off-folding pathways (red) by lowering free energy barriers and preventing intermolecular interactions. Figure taken from (Hartl et al., 2011). Reuse permission has been granted.

Protein's secondary and tertiary structures are stabilised by a number of short-ranged (e.g. van-der Waals, hydrophobic, H-bonds, hard-sphere) and long-ranged (electrostatic) interactions (Chan and Dill, 1991). But a number of physical factors like temperature, salt concentration and pH can lead to disruption of these non-covalent interactions, shifting the balance towards a more destabilized or unfolded protein structure (Wang, 1999). Under such stress conditions, the real purpose of chaperones becomes clear. While under physiological conditions only about 20 % of proteins require assistance by chaperones to fold correctly, a massive upregulation of chaperone expression can be registered under stress (Hartl et al., 2011). Due to this effect, many chaperones have been termed heat-shock protein (Hsp) and are classified by their molecular weight in kDa.

Molecular chaperones are a diverse family of proteins in which each member possesses a dedicated role in de novo protein folding and refolding. Chaperones that assist broadly are so-called ATP-dependent "foldases", e.g. chaperonins (Hsp60), Hsp70 and Hsp90. They mainly recognize their specific unfolded or partially folded substrate by hydrophobic interactions (Balchin et al., 2016). Folding is then promoted via repeated ATP-driven cycles of binding and release. Upon release of the protein, folding can proceed and by rebinding, aggregation is blocked and misfolded structures may be reversed. An additional buffer of aggregation is provided by the ATP-independent small Hsps, the so-called "holdases". They bind to exposed hydrophobic residues and thus prevent non-native interactions (Kim et al., 2013).

1.2 Classes of molecular chaperones

Because of the complex interaction and regulation networks of chaperones and cochaperones and a large number of structural and functional diverse client proteins, the underlying mechanisms of chaperone mediated folding remain unclear. Different roles and chaperoning mechanisms can be ascribed to the respective Hsp families.

The Chaperonins are one of the most extensively studied chaperone classes. They form multisubunit complexes, arranged in a cylindrical order. Its central cavity provides a space where folding can occur protected from aggregation. Chaperonins are divided into two groups. Group I chaperonins can be found in the bacterial cytosol (GroEL), in mitochondria (Hsp60) and in chloroplasts. They are characterized by back-to-back stacked rings, each consisting of seven subunits. This barrel-like structure is closed by a lid-shaped ring consisting of seven subunits of GroES or Hsp10. Group II chaperonins are present in archaea and the cytosol of eukaryotes. They also form barrel-like structures of eight to nine subunits and contain a lid-domain to cover the cavity. The best investigated chaperonin is the bacterial group I GroEL/GroES system. Hydrophobic residues are exposed in the inner rim of GroEL, enabling interaction with a non-native substrate protein. ATP-binding leads to GroES mediated encapsulation of the bound protein and is accompanied by conformational changes of GroEL, forming a large hydrophilic cavity. The substrate is released into the hydrophilic cavity in which reduction of solvent-exposed hydrophobic residues is favoured and thus folding is promoted. Besides this passive assistance in protein folding, evidence is provided that GroEL/GroES can also accelerate protein folding by active folding mechanisms (reviewed in Motojima, 2015 and Hayer-Hartl et al., 2016).

Hsp70 is a central component of the cellular protein homeostasis network and is involved in a large number of cellular processes, including protein folding, refolding, disaggregation and transfer to the proteolytic machinery. It recognizes its non-native substrate proteins by a short degenerative, solvent exposed motif, consisting of a core of five to seven amino acids enriched in hydrophobic residues. These motifs are buried in the native state of a protein, explaining how Hsp70 explicitly binds to the unfolded or misfolded states (Mayer, 2013). Hsp70 consists of two domains: a nucleotide binding domain (NBD) and a substrate binding domain (SBD), connected by a flexible linker. In the ATP-bound state, substrate binding affinity is rather low due to a high substrate association and dissocation rate. Upon ATP-hydrolysis, Hsp70 undergoes a conformational change, by which an α-helical lid-segment, located in the SBD, folds over the bound substrate. This results in a low substrate association and dissociation rate and thus high affinity. ATP-hydrolysis is essential for chaperone function, reversing the chaperone from a low

to a high substrate affinity state. However, Hsp70s possess a very low inherent ATPase activity. For effective substrate binding and release cycles, cofactors are needed that regulate substrate binding by affecting the nucleotide state (Kampinga and Craig, 2010). Binding of a co-chaperone of the J-domain protein family (Hsp40) to the NBD and a substrate protein to the SBD synergistically trigger the ATPase activity by > 1000 fold (Kityk et al., 2015). Furthermore, a nucleotide exchange factor is needed to facilitate ADP-ATP exchange and thus opening of the lid and substrate release, enabling folding or transfer to downstream chaperone machineries or the ubiquitin-proteasome system (Balchin et al., 2016). One of these downstream chaperone machineries is Hsp90. Interaction is mediated by the co-chaperone Hop (Hsp70-Hsp90 organizing protein). Hop belongs to the tetratricopeptide repeat (TPR) domain containing co-chaperones that recognize their interaction partners by binding to a MEEVD-motif, located in the C-terminus of Hsp70 and Hsp90 (Li et al., 2012).

Unlike Hsp70, which binds to nascent polypeptide chains, Hsp90 acts at the late stages of folding. It does not only promote protein folding, but also the formation of the correct conformation and activation of a remarkable number of structurally and functionally diverse proteins, known as “clients”. This chaperone machinery is described in more detail in Section 1.4.

1.3 Molecular chaperones in disease

An increasing number of human diseases is connected with imbalances in protein homeostasis. Heat shock proteins are expressed at elevated levels at conditions at which proteins are likely to denature and aggregate. Chaperones help proteins to maintain their structure and function. This proteostasis network capacity declines with increasing age. Many age-related neurodegenerative diseases like Alzheimer’s disease, Parkinson’s disease or Huntington’s disease are associated with protein aggregation (Gorenberg and Chandra, 2017). Transcription and concomitant the expression of heat shock protein genes is controlled by heat shock transcription factors (Hsf). The activity of Hsf1 has been shown to be downregulated in neurodegenerative diseases. Hsf1 is the master regulator of the heat shock

response and its activity is controlled by a complex network of posttranslational modifications and interactions with regulatory proteins that include the expressed target proteins (Whitesell and Lindquist, 2009). For instance, the expression of Hsp70 and Hsp90 is controlled by Hsf1. Hsf1 is a client of Hsp90 and is kept in an inactive form by interaction with Hsp90 and Hsp70 at physiological conditions. This interaction is broken under stress conditions, inducing transcription of proteins involved in the heat shock response. Thus, some chaperone molecules are controlling their own transcription (Taipale et al., 2010). Studies in model organisms have shown that elevation of Hsf1 expression has therapeutic potential in neurodegenerative diseases (Neef et al., 2011). While neurodegenerative diseases are related to an impaired proteostasis network, this system is exploited by cancer cells to support their growth, survival and metastasis. Cancer cells have evaded the normal tissue control mechanisms that regulate production and release of growth-promoting signals to ensure homeostasis of cell numbers. This causes an uncontrolled cell proliferation and resistance to apoptosis are the results (Hanahan and Weinberg, 2011). The overexpression of oncogenes and an increasing number of mutations within the cancerous proteome (leading to oncogene activation and loss-of-function in tumor suppressor genes) are resulting in a higher demand for chaperone molecules, needed for folding, stabilization, activation and prevention of aggregation under this abnormal conditions. Different types of cancer are associated with elevated levels of different chaperone classes. Thus, the individual heat shock proteins as well as Hsf1 are interesting targets for cancer therapy (Chatterjee and Burns, 2017).

1.4 Hsp90 – a key player in cellular signal transduction

Hsp90 is an ubiquitous, highly conserved molecular chaperone that can be found in prokaryotes and all classes of eukaryotes. While it is dispensable in prokaryotes under non-stressed conditions, it is essential for viability of eukaryotes under all conditions. Being one of the most abundant proteins in the cytosol (~ 1-2 % of soluble protein under physiological and 4-6 % under stressed conditions (Lai et al., 1984; Finka and Goloubinoff, 2013; Prodromou, 2016)), it might not

surprise that the function of Hsp90 reaches much farer than assistance in protein folding. In contrast to other classes of molecular chaperones, Hsp90 binds to proteins at the late stages of folding and stabilizes and activates them. More than 200 "client" proteins have been identified, belonging to structurally and functionally highly diverse classes like transcription factors, protein kinases, telomerases and steroid hormone receptors (see https://www.picard.ch/downloads/Hsp90interactors.pdf). Many of its client proteins are part of signal transduction pathways, underscoring its importance to cellular processes.

1.4.1 Structure and conformational cycle

Hsp90 is a homodimeric protein. Each monomer consists of three domains: The N-terminal nucleotide binding domain (NTD), which is responsible for ATP-binding, the middle domain (MD), which is important for ATP-hydrolysis and client-interaction and the C-terminal domain (CTD), that is responsible for Hsp90 dimerization and interaction with TPR-domain containing cochaperones. The NTD and MD are connected by a long unstructured charged linker (CL) that contributes to the proteins high flexibility (Krukenberg et al., 2011). The overall architecture of Hsp90 resembles a molecular clamp that opens and closes during an ATP-driven cycle. Binding of ATP induces global conformational changes that lead to transient dimerization of the NTDs (closed state) lasting until ATP is hydrolysed, ADP is released accompanied by dissociation of the NTDs (open state). Hsp90 possesses a low affinity for ATP and a higher affinity for ADP (ATP K_D = 132 μM; ADP K_D = 29 μM in yeast Prodromou et al., 1997) and its ATPase activity is very low (~ 0.2 ATP/min in yeast (Meyer et al., 2003) and even about 10-times slower in human (McLaughlin et al., 2004; Richter et al., 2008)). Clamp-closure seems to be rate-limiting for ATP-hydrolysis, as suggested by experiments that determined the kinetics of NTD-dimerization applying FRET-reporter systems. Kinetics were in perfect agreement with the ATP hydrolysis rate (Hessling et al., 2009). However, structural analysis provides evidence that global conformational changes are coordinated by a network of local conformational rearrangements, stimulated by ATP binding. Mutational studies revealed the crucial role of these structural elements for ATP hydrolysis. But only little is known about the kinetics

of local conformational changes and their role in regulation of Hsp90 function, because methods that can detect them in solution have been missing so far.

The flexible nature of Hsp90 made it a challenging task to derive the crystal structure of full-length Hsp90. Truncation of the CL enabled crystallisation of yeast Hsp90 from *Saccharomyces cerevisiae* in the nucleotide bound, p23 interacting closed state conformation (Ali et al., 2006). Comparison to crystal structures of the isolated yeast Hsp90 domains, which are a model for domain structures in the open state, revealed that structural rearrangements are happening within the individual domains, relevant for clamp closure. To permit a deeper understanding of the role of specific structural elements within the Hsp90 ATPase cycle, each individual domain will be described in detail. The specific location of elements will belong to yeast Hsp90.

The nucleotide binding pocket is located within the NTD. Hsp90 belongs to the GHKL (gyrase, Hsp90, histidine kinase, MutL) superfamily. All members of this family share a similar nucleotide binding pocket topology. The core element of this binding pocket is an α/ß-sandwich consisting of four ß-sheets and three α-helixes. The most unique feature is a highly mobile ATP-lid, formed by a helix-loop-helix motif that possesses flexibility by a hinge region, created by glycine-residues (Dutta and Inouye, 2000). In Hsp90, the nucleotide binding pocket is exposed in the ATP-unbound open state and completely enclosed by the ATP-lid (residues 94-121) in the closed state. The open-state lid-conformation is stabilized by hydrophobic interactions with residues 10-27 (Prodromou et al., 1997). Rearrangement to the closed-lid conformation exposes hydrophobic surfaces that form the NTD dimerization interface. The lid is an important rate-determinant of ATPase activity. Closure of the clamp in the open-lid conformation would not be possible, because this element would sterically collide with its equivalent of the opposing subunit. Furthermore, the lid is essential for ATPase activity, as shown by lidless Hsp90 mutants that were not altered in nucleotide-affinity but absent of ATP-hydrolysis. Interestingly, removal of the lid of only one subunit within the Hsp90 dimer accelerates closure and ATPase-activity (Richter et al., 2006; Hessling et al., 2009). Burial of hydrophobic residues seems to stabilize the open-state, while exposure triggers rearrangement to the N-terminal dimerized closed state. This hypothesis is supported by mutation of polar Thr-101 to hydrophobic Ile (T101I),

causing stabilization of the open state and substantial reduction of ATPase-activity, while mutation of Ala-107 to polar Asn (A107N) accelerates ATPase-activity and stabilizes the closed lid conformation via polar interaction with Tyr-47 (Nathan and Lindquist, 1995; Prodromou et al., 2000; Siligardi et al., 2004; Vaughan et al., 2009).

Furthermore, deletion of the first 24 amino acids of Hsp90, consisting of an N-terminal ß-strand followed by an α-helix that forms the N-terminal dimerization interface, results in loss of ATPase activity and a higher flexibility of the ATP-lid. The N-terminal ß-strand swaps subunits upon closure of the clamp, accompanied by the movement of the adjacent α-helix. Deletion mutants lacking the first 16 amino acids are also incapable of ATP-hydrolysis, but can stimulate ATPase activity within the opposing subunit in heterodimers with WT-Hsp90. In contrast, deletion of the first 8 amino acids, forming the N-terminal ß-strand, accelerates ATPase activity, showing that they are dispensable for the ATP-hydrolysis reaction but provide a regulatory site (Richter et al., 2002; Richter et al., 2006). This is encouraged by the fact that human Hsp90 isoforms show an elongated, 10-50 amino acids N-terminal ß-strand accompanied by a lower ATPase activity. Truncation of the N-terminal strand of TRAP1 (mitochondrial isoform) to yeast Hsp90 length results in a 4-fold enhanced ATPase activity (Lavery et al., 2014).

The NTD contains all residues essential for binding and hydrolysis of ATP. Asp-79 is essential for adenine-nucleotide binding, a Mg^{2+}-ion connects the phosphate group to the protein via hydrogen bonds and a catalytic Glu-33 coordinates and activates the hydrolytic water molecule (Panaretou et al., 1998; Cunningham et al., 2008). Nonetheless, isolated NTDs show negligible ATPase activity. Presence of the MD is essential for minimal activity. Activity is completely rescued by introduction of a C-terminal Cys-residue facilitating covalent dimerization of NTD-MD constructs. This confirms the importance of the C-terminal dimerization site for ATPase activity (Richter et al., 2001; Wegele, 2003).

The middle-domain contains a highly conserved catalytic loop region (residues 370 – 390). Arg-380 acts as an ATP-sensor. It interacts with the γ-phosphate of the bound ATP-molecule, orientating it for ATP-hydrolysis and stabilizing the closed

state conformation. Mutation to an Alanine causes extremely weak ATPase activity and is lethal in yeast (Meyer et al., 2003). Evidence is provided that the catalytic loop Arg-380 is also a stabilizer of the apo-state via interactions with a conserved MD-loop (Meyer et al., 2003). Upon ATP-binding the catalytic loop is released, accompanied by a rotation of the NTD relative to the MD, facilitating NTD-dimerization (Cunningham et al., 2012). Cross-monomer hydrophobic interactions of the catalytic loop leucine-residues with Thr-22, Val-23, Tyr-24 further stabilize the closed-state conformation (Cunningham et al., 2008). Furthermore, a solvent exposed hydrophobic patch (residues 342-352) seems to be involved in correct positioning of Arg-380 in the hydrolysis-competent state and thus is essential for NTD and MD catalytic loop interaction (Meyer et al., 2003). Phe-349 forms the centre of this patch. Mutation to Ala results in very low ATPase activity.

Sequence and length of the CL, connecting NTD and MD, also influences ATPase activity. Eukaryotic forms possess a longer linker than prokaryotic forms, for instance 63 amino acids in human, ~ 56 amino acids in yeast and only 7 amino acids in *E.coli* (Shiau et al., 2006; Tsutsumi et al., 2012). Additionally, the CL of human Hsp90 possesses a higher negative charge than yeast Hsp90. Replacement of yeast CL by the human sequence results in reduced ATPase activity. However, an uncharged GS-linker of similar length also reduces yeast ATPase activity, except for a short 7 amino acids GS-linker (Tsutsumi et al., 2012).

1.4.2 Co-chaperones

Hsp90 does not act alone in chaperoning of its clients. Post-translational modifications as well as co-chaperone interactions are involved in modulation of Hsp90 structure and function and in client recruitment. Binding sites for co-chaperones have been identified within all three domains of Hsp90. The most prominent interaction site is the C-terminal MEEVD-peptide, required for binding of TPR-domain containing co-chaperones. The mode of action and role in the chaperone-cycle is diverse and interaction occurs in a sequential manner. For instance, some co-chaperones stabilize a specific conformation of Hsp90 which might be a prerequisite for binding of the next co-chaperone. A general model for client delivery and regulation of client maturation in the Hsp90 cycle is shown in Figure 1-2. The TPR-

co-chaperone Hop (yeast homologue Sti1) binds to the MEEVD-motif and stabilizes the open-conformation, thus inhibiting ATPase activity. Hop possesses three TPR-domains, facilitating simultaneous interaction with Hsp90 and co-chaperone Hsp70. Client protein has been loaded on Hsp70, mediated by Hsp40 prior to Hsp90-binding and can now be transferred to Hsp90. Progression to the closed-state conformation weakens Hop binding affinity and thus promotes its dissociation (Li et al., 2012). Client maturation is regulated and/or progressed by a large number of co-chaperones, for example TPR-containing PPIases (peptidyl-prolyl cis-trans isomerase) that might act as a folding-promoter by changing between cis- and trans-configuration of peptide bonds with the amino acid proline (e.g. activation of steroid hormone receptors). Phosphatases like PP5 also bind via the MEEVD-motif and dephosphorylate Hsp90. Sequential regulation of the Hsp90 and also co-chaperone phosphorylation state are important for efficient client maturation (Mayer and Le Breton, 2015). Aha1 (accelerator of Hsp90 ATPase activity) is the only known co-chaperone that substantially accelerates Hsp90 ATPase activity. It promotes formation of the closed-state conformation and thus might have an effect on the client-retention time (Röhl et al., 2013). Aha1 is displaced by p23 that interacts with the Hsp90-NTDs. p23 stabilizes the hydrolysis-competent closed-state conformation, but nonetheless inhibits Hsp90 ATPase activity, probably by slowing down product release (Graf et al., 2014). The first derived crystal structure of the closed-state conformation is from yeast Hsp90 in complex with two p23 bound to the NTDs and shows a symmetric structure. It is proposed that p23 promotes a symmetric structure, because in an asymmetric conformation only one p23 would be able to bind as there would be a sterical clash. The following crystal structure of the AMP-PNP-bound closed-state conformation of mitochondrial isoform TRAP1 shows an asymmetric conformation (Lavery et al., 2014). That the symmetric yeast-structure is promoted by p23 is also supported by NMR-data, revealing that p23 can influence MD conformation (Karagöz et al., 2011).

Hsp90 ATPase activity acceleration by Aha1 has been studied extensively, providing deeper insights into regulation points of Hsp90. Aha1 consists of two domains: the N-terminal domain (Aha1-N) binds to Hsp90 MD and the C-terminal domain (Aha1-C) interacts with the dimerized Hsp90 NTDs. Interaction is asymmetrically, as one Aha1-molecule is sufficient to fully accelerate ATPase activity

about 5-fold (Lotz et al., 2003). Aha1-N in isolation is also capable to stimulate ATPase activity, but to an about 10-times lesser extent than full-length Aha1 (Retzlaff et al., 2010). Upon binding of Aha1-N to Hsp90-MD the catalytic loop is modulated to a partially open state in apo Hsp90 and stabilizes the open active catalytic loop conformation that enables interaction of Arg-380 and γ-phosphate in ATP-bound Hsp90 (Prodromou, 2012). Catalytic loop reconfiguration seems to be involved in ATPase activity acceleration. This is supported by the fact that Aha1 binding rescues the effect of F349A mutation, which is thought to be incapable to correctly position the Arg-380 residue (Meyer et al., 2003).

Aha1-C is not able to stimulate ATPase activity in its isolated form, but substantially increases the stimulating effect of full-length Aha1 compared to Aha1-N. Its exact mode of action remains unclear. NMR-studies show chemical shift perturbations within the lid region and the first α-helix in ATP-bound Hsp90 upon addition of Aha1, but no significant changes in nucleotide-free Hsp90, suggesting that Aha1-C preferentially binds to the N-terminal dimerized state (Retzlaff et al., 2010). This is supported by a tighter binding to Δ8-Hsp90, which shifts the equilibrium stronger towards the closed state conformation in presence of ATP (Richter et al., 2002). Furthermore, a similar acceleration of ATPase activity as in heterodimers consisting of wild-type and lidless Hsp90 can be observed. It is proposed that Aha1 promotes lid-closure (Wolmarans et al., 2016).

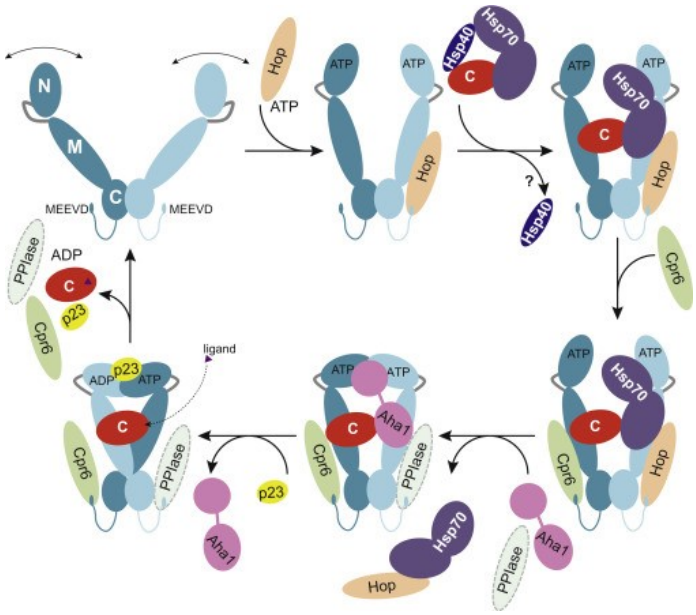

Figure 1-2: Chaperone cycle of Hsp90, modified by co-chaperone interactions. In the nucleotide unbound state, Hsp90 is highly flexible. Binding of TPR-co-chaperone Hop to the C-terminal MEEVD-motif stabilizes the open-state, preventing ATP-hydrolysis. Hop mediates interaction with the client-transferring co-chaperone Hsp70. Binding of Aha1 promotes NTD-dimerization, in which Hop-affinity is reduced and thus Hop-Hsp70 dissociates. Chaperone cycle and client maturation is further processed by different co-chaperone classes like PPIases, that promote folding, or p23 which slows product release and thus inhibits ATPase activity. Figure taken from (Mayer and Le Breton, 2015). Reuse permission has been granted.

1.4.3 Hsp90 inhibitors as potential cancer therapeutics

Hsp90 is an essential protein for the maintenance and survival of tumor cells, but it is not an oncogene by itself because it does not drive the carcinogenesis process. Many potent anti-cancer agents target selected oncoproteins that are associated with the development of a specific type of cancerous disease. However, due to uncontrolled mutations tumour cells are very fast evolving and often develop resistance to the agent. Therefore, a combination of multiple chemotherapeutic agents, that inhibit cell growth and proliferation, is often applied. Inhibiting multiple signalling pathways that are essential for tumor proliferation and survival by applying only one agent would be a very promising therapeutic approach. And this is the intention of many current studies that develop and investigate new compounds that target Hsp90. Most Hsp90 inhibitors target the nucleotide-binding pocket and possess a higher affinity to it than ATP or ADP (Whitesell and Lin,

2012). Much progress regarding affinity, retention time and toxicity has been achieved since identification of the natural Hsp90 inhibitors geldanamycin and radicicol almost 20 years ago (Neckers and Trepel, 2014). However, administration of Hsp90 inhibitors as single-agent induced no or only minor response, depending on the type of cancer. It was hypothesized that especially those kinds of cancer that are driven by highly Hsp90-dependent oncogenes could positively respond to Hsp90-inhibitor treatment. Indeed, some kinds of cancer like HER-2 associated breast cancer (HER-2 = onco-client of Hsp90) did show promising results in clinical trials. But, not all cancers that are associated to Hsp90-dependent clients respond to the treatment and sometimes one patient might response to the therapy while another does not. Furthermore, combination therapies of Hsp90 inhibitor with chemotherapeutic agents or oncogene targeting compounds could also increase the likelihood for a positive disease prognosis. For example, combination of an HER-2-targeting monoclonal antibody with Hsp90 inhibitors showed promising activity. It was suggested that Hsp90 inhibitors could delay or reverse the development of resistance to the agent (Whitesell and Lin, 2012; Jhaveri et al., 2014).

While most inhibitors target the nucleotide binding pocket, C-terminal inhibitors also show a high potential (Butler et al., 2015). N-terminal Hsp90 inhibitors induce activation of Hsf1, the central regulator of the heat shock response. Some tumor cells are not capable to upregulate the heat shock response and are more selective to Hsp90 inhibitors (Whitesell and Lindquist, 2005). But in other tumor types this might reduce the activity of Hsp90 inhibitors. C-terminal Hsp90 inhibitors were shown to activate Hsf1 much less (Butler et al., 2015). Another approach could be the development of client-specific Hsp90-inhibitors, facilitating a more disease specific treatment with less side-effects. Mutational studies reveal that distinct client proteins place different constraints on Hsp90 (Zuehlke and Neckers, 2016). For example, variable mutations within the NTD of Hsp90 had severe effects on the maturation of the kinase v-src, but not on the glucocorticoid receptor. Furthermore, other kinases were impacted to a lesser extent, indicating that even clients of the same class require distinct functional features of Hsp90 NTD (Mishra et al., 2016). Compounds targeting these functional sites could provide potential client-specific Hsp90-inhibitors.

1.5 Optical approaches to study protein structure and dynamics

Biomolecules adopt their function and activity by switching between a dynamic ensemble of conformational states. Interaction with binding partners or posttranslational modifications often changes the equilibrium towards a certain conformational state. To shed light on the fundamental processes in protein folding, on the role and mode of action of chaperones and other folding promoters and also on the role of conformational dynamics and transitions for protein function, it is key to visualize structural alterations. This knowledge might promote the development and/or improvement of specific modulators of protein function and thus would be highly valuable for disease treatment.

Knowing a protein's structure provides the basis for the mechanistic understanding of protein function and regulation. About 90 % of protein structures deposited in Protein Data Bank (PDB) have been determined by X-ray crystallography. The remaining were determined by nuclear magnetic resonance spectroscopy (NMR; ~ 9 %) and electron microscopy (EM; ~ 1 %). Since the establishment of PDB in 1971 with only seven entries, there are more than 130 000 protein structures available today (Shi, 2014). The prerequisite for X-ray structural analysis is the formation of protein crystals. This is a challenging task, as conditions need to be found that allow for nucleation and crystal growth. Very dynamic proteins that undergo large conformational changes between states are very hard to crystallize (Rupp, 2013). In Hsp90-crystallography experiments, this obstacle was solved by stabilizing Hsp90 in its closed state-conformation by co-crystallization with AMP-PNP and the co-chaperone p23 (Ali et al., 2006). However, dynamic, unstructured regions like the remains of the truncated charged linker are not resolved. And still, the highly dynamic full-length crystal structure of the open clamp of eukaryotic Hsp90 remains elusive. In this matter, electron microscopy is a very good complementary method to gain insights into the ensemble of different conformational states of Hsp90 and how the equilibrium between open and closed conformers shifts in presence of nucleotides (Southworth and Agard, 2008). Nonetheless, no information about conformational dynamics is provided. This information can be

revealed by applying NMR spectroscopy synergistically to X-ray crystallography. In NMR local structural changes can be studied in solution by interpreting several observables that provide information about dynamic regions and/or interaction sites. However, due to the need of isotopic labelled samples and a complex data interpretation, this is a costly technique in time and also financial terms, (Kleckner and Foster, 2011).

Application of fluorescent reporter systems that monitor on conformational transitions or binding events in solution is a fast, cheap and easy-to-use method. Prerequisite for the development of a reporter system to probe for a structural rearrangement or interaction with a binding partner, is to know the structure of the element or interaction site that is under investigation. A frequently applied, well known reporter system is based on fluorescence resonance energy transfer (FRET) from an excited donor to an acceptor fluorophore, resulting in a decrease of donor fluorescence emission and concomitant an increase of acceptor fluorescence. The efficiency of energy transfer is dependent on the förster radius R_0 and the distance between fluorophores. For most organic fluorophores, an effective transfer is permitted at a distance range of 2 to 10 nm. R_0 describes the distance at which FRET efficiency is 50 %. This value is dependent on several factors like the relative orientation of donor and acceptor transition dipole moment and spectral fluorophore characteristics (Grecco and Verveer, 2011). Binding of a macromolecule or structural changes can be transduced into a far-field detectable signal change by designing a suitable FRET-reporter system. In combination with time-resolved fluorescence spectroscopy, fluorescence correlation spectroscopy (FCS), stopped-flow spectroscopy and single-molecule microscopy techniques, biological reactions can be investigated on a wide span of timescales. However, FRET is limited to spatial dimensions of several nanometers. Intramolecular conformational transitions and dynamics, occurring on spatial scales of only a few nanometer to sub-nanometer, cannot be monitored by FRET.

1.5.1 Photoinduced electron transfer (PET) based reporter systems

Electron transfer from an excited donor to an acceptor molecule or vice versa, resulting in charge separation, plays a fundamental role in many natural and technical processes, like photosynthesis or photovoltaic systems. If the redox potentials

of for instance a chromophore, excited by the absorption of light and an interaction partner match, an electron can be transferred from donor to acceptor, resulting in a charge separated radical ion. Excited state energy will dissipate non-radiative via charge recombination to the ground state. Excitation of a molecule changes its redox properties. An electron transfer reaction might occur in this state via two possible processes. Either the excited state electron is donated to an electron acceptor (oxidative electron transfer) or the unoccupied ground state accepts an electron from an electron donor (reductive electron transfer). A reaction scheme is shown in Figure 1-3.

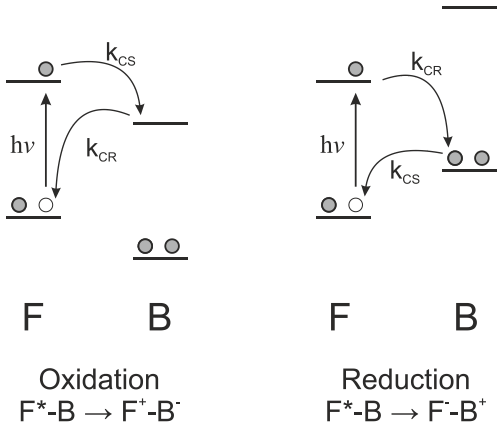

Figure 1-3: Simplified PET-reaction scheme. In the excited state of the fluorophore F^* an electron is either transferred from the higher energy level of the excited state to the electron accepting interactor B (oxidation, left) or from the ground state of B to the ground state vacancy of F^* (reduction, right), resulting in charge separation with the rate k_{CS}. The charge separated system relaxes to the ground state via charge recombination with rate k_{CR}.

The efficiency as well as the pathway of electron transfer is dependent on the change in free energy upon charge separation ΔG_{cs}, and can be estimated by the Rehm-Weller equation:

Oxidative transfer
$$\Delta G_{CS} = E(F^+/F) - E(B/B^-) - E_{0,0} + C \qquad (1\text{-}1)$$

Reductive transfer
$$\Delta G_{CS} = E(B^+/B) - E(F/F^-) - E_{0,0} + C \qquad (1\text{-}2)$$

E (X^+/X) describes the oxidation potential and E(X/X^-) the reduction potential of either the fluorophore F or the interactor B. $E_{0,0}$ is the energy difference between ground state and excited state and C the coulombic interaction energy between two charged molecules. The latter is dependent on distance d between molecules

and the solvent polarity, described by the dielectric constant ε according to following equation:

$$C = \frac{-e^2}{d \cdot \varepsilon} \tag{1-3}$$

The natural amino acid Trp is unique in its ability to serve as potent electron donor when it is in contact to oxazine or rhodamine dyes (Doose et al., 2009). Photoinduced electron transfer between Trp and the excited fluorophore results in fluorescence quenching. A prerequisite for a PET-reaction is that the fluorophore and the interactor are in van der Waals contact, meaning a distance of ≤ 1nm. As this process is reversible, it can report on distance changes at the sub-nanometer level and provides a perfect complement to FRET-based reporter systems (Haenni et al., 2013).

Different quenching mechanisms contribute to the reduction of fluorophore quantum yield (QY), which describes the ratio of the number of photons emitted to the number of photons absorbed. Collision of freely diffusing excited fluorophores and Trp can cause a non-radiative relaxation to the ground state, a process termed dynamic quenching. QY and fluorescence lifetime is transiently reduced. Another quenching process, that does not influence fluorescence lifetime but reduces QY, is called static quenching. Stably formed fluorophore-quencher complexes that last for several excitation-emission cycles efficiently supress fluorescence emission, such that on-off switches can be well detected by fluorescence spectroscopy techniques (Doose et al., 2009). The organic fluorophores Atto655 and MR121 were shown to be efficiently quenched by Trp mainly due to static quenching (Doose et al., 2005). AttoOxa11, a derivative of Atto655, has proven to be a well-suited dye for monitoring contact-based dynamics within biomolecules. PET in combination with fluorescence correlation spectroscopy (PET-FCS), is a powerful tool to measure the kinetics of chain motions in folding intermediates, loop-closure and chain motion modulations in intrinsically disordered proteins for example (Neuweiler et al., 2010; Teufel et al., 2011; Lum et al., 2012). PET-FCS provides a method by which fluorescence fluctuations, caused by fluorophore-Trp interaction of a PET-reporter labelled molecule, can be detected with a temporal resolution of

nanoseconds to milliseconds, only limited by the molecules diffusion time through a confocal excitation volume (Sauer and Neuweiler, 2014).

1.5.2 Single-molecule versus bulk studies

Classical biochemical assays are performed in bulk. A signal, for example light absorption or fluorescence emission, is averaged over a vast ensemble of molecules. Conformational changes in the biomolecular system due to biochemical reactions or interactions, are only observable if they cause a clear shift in the systems equilibrium state. Otherwise, in case that the conformational change is only transient, no change in ensemble averaged signal will be visible. One example: first studies of the overall clamp-closure kinetics of Hsp90, applying FRET-reporter systems, were performed in bulk. ATP-hydrolysis is a fast reaction compared to the long-range, slow conformational kinetics of clamp-closure and the closed state conformation seems to be rather short-lived, too (Mickler et al., 2009; Zierer et al., 2016). Upon addition of ATP to the system, the individual molecules will pass into the closed-clamp conformation with different transition kinetics. While some are still in the process of clamp-closure, others have already started the next ATPase cycle. Thus, FRET will only be a short, transient event and will be hidden in the ensemble averaged signal, because proteins do not switch synchronously into the closed conformation. Triggering clamp-closure by addition of the non-hydrolysable ATP-derivative AMP-PNP instead of ATP, traps the clamp in the closed-state configuration. This open-closed state shift of the equilibrium resulted in an ensemble detectable change in FRET-signal, providing information about clamp-closure kinetics (Hessling et al., 2009). However, multi-exponential kinetics raised the question of their origin.

Single-molecule techniques provide a platform by which rare events - subpopulations as well as intermediate, transient states – that are hidden in ensemble measurements, become observable and provide new mechanistic insights in biomolecular reactions. A number of questions might be answered: How does a protein progress along an energy landscape to its native state? Are specific conformational states selective for client-chaperone interaction? How is the hydrolysis of ATP related to conformational changes of the chaperone as well as to binding and

release of the client? Does the chaperone promote folding passively via suppressing and reversing aggregation through repeated cycles of binding and release or actively by directly guiding the folding pathway? (Avellaneda et al., 2017)

In recent years, several techniques have been employed to study biomolecules at the single-molecule level. Very common are force-based methods that determine the force needed for elongation and thus denaturation of a protein, whose ends are tethered between two surfaces that move apart (Borgia et al., 2008). Refolding of the polypeptide is permitted by releasing the force. Information about the folding mechanisms and the occupation of intermediate states or misfolded states, which slow folding kinetics, can be gained (Zoldák and Rief, 2013; Jahn et al., 2015). Furthermore, folding promotion can be investigated by comparing pulling and relaxation experiments in absence and presence of folding promoters (Avellaneda et al., 2017). Long-range dynamics within proteins occurring at time-scales of nanoseconds to milliseconds can be detected by investigation of FRET-based fluorescence fluctuations in diffusion based FCS-experiments (Schuler and Hofmann, 2013). Very low concentrated solutions (pM to nM) of the labelled biomolecule are applied in FCS, such that only a few molecules are detected at a time in the confocal excitation volume. Therefore, FCS is considered as a single-molecule technique (Sauer and Neuweiler, 2014). But as folding transitions often occur on longer timescales of seconds to minutes, such kinetics can't be determined in freely-diffusing molecules. Immobilization of biomolecules to a surface facilitate prolonged observation times, only limited by photobleaching. Different surface passivation techniques have been developed to diminish non-specific interactions of the biomolecules with the surface (Roy et al., 2008; Jeyachandran et al., 2010; Hua et al., 2014). Ever improving fluorophore properties in terms of photostability and brightness further contribute to the applicability of FRET to monitor conformational transitions in single molecule microscopy (Borgia et al., 2008). Oxygen scavenger systems have been developed to reduce photobleaching caused by reactive oxygen species (Benesch and Benesch, 1953; Aitken et al., 2008). However, this might cause increased fluorescence intermittency, also described as photoblinking. If a fluorophore is excited, an electron is lifted from its singlet ground state (S0) into the first excited state (S1) and can relax by emission of a photon. A fluorophore's excited state lifetime is in general in the range of a few nanoseconds. It is also possible that

a triplet state is entered via intersystem crossing, possessing a lifetime of milliseconds to seconds. Relaxation occurs non-radiatively or via emission of a phosphorescent photon (Lakowicz, op. 2006; Sauer et al., op. 2011). Molecular oxygen is a very effective triplet state quencher and its removal results in prolonged residence times in the triplet state, causing higher fluorescence intermittency (Hübner et al., 2001). The triplet state can readily react with a reductant e.g. ß-mercaptoethanol, producing stable dark-state radical ions. This effect is exploited in super-resolution microscopy techniques, for example *d*STORM (direct stochastic optical reconstruction microscopy). In this approach, only a few fluorophores return from a stable dark state into the excitable, fluorescent state at a time, such that individual fluorophores are temporally separable (van de Linde et al., 2011).The position of a single fluorophore can be localized with nanometer precision by fitting a two-dimensional Gaussian function to the emitters point spread function (Heilemann et al., 2008). In contrast, long-lasting emission and reduced photoblinking is needed for single-molecule studies of biomolecular reactions. The vitamin E analogue Trolox is an efficient triplet-state quencher, often applied together with an oxygen scavenger system to achieve stable fluorophore emission, reduced blinking and prolonged observation times (Roy et al., 2008; Cordes et al., 2009).

Due to the low concentration of biomolecules that have to be applied to obtain a low molecule density, single-molecule interaction experiments are limited to strong interacting partners. Furthermore, photophysical fluctuations of the dye might interfere with biological events monitored by FRET. Because of the antagonistic behaviour of donor and acceptor fluorescence in FRET-experiments, detection of the signal change in both channels is a good determinant to distinguish between a FRET-originating signal change and photophysics.

So far, local conformational dynamics are only accessible at fast time-scales of nanoseconds to milliseconds, using PET-FCS. Observing PET events on prolonged timescales at the single molecule level might be challenging, owing to the fact that a PET quenching event would be hard to distinguish from photophysical events like photoblinking or bleaching.

1.6 Goals of this work

Binding of ATP to the Hsp90 molecular chaperone machinery triggers global conformational changes, essential for ATP-hydrolysis. Kinetics of clamp-closure were determined by application of FRET-reporter systems and are in agreement with the slow ATP-hydrolysis rate, indicating that transition into the N-terminal dimerized state is rate-limiting (Hessling et al., 2009; Mickler et al., 2009). Structural and mutational studies reveal that global changes are coordinated by a network of local structural rearrangements. An ATP-lid folds over the nucleotide binding pocket, exposing a hydrophobic surface forming the N-terminal dimerization interface. This is accompanied by motion of an N-terminal ß-strand that swaps subunits and by association of the NTD and MD. Lidless-Hsp90 as well as a Δ8-mutant, lacking the N-terminal ß-strand, revealed that these structural elements regulate clamp-closure kinetics and concomitantly ATPase activity. Although all residues needed for ATP-binding and hydrolysis are present in the NTD, association with the MD is essential, as shown by C-terminal dimerized NTD-constructs, incapable of ATP-hydrolysis.

Kinetics of local structural rearrangements remain elusive, hampered by the spatial and temporal resolution limit of available techniques. To shed light on the mechanism and regulation of the Hsp90 molecular chaperone machinery, photoinduced electron transfer based reporter systems that report on Lid-closure, ß-strand swap and N- and M-domain association shall be designed within the scope of this doctoral thesis project. Kinetics of local motions and the impact of functional mutations and co-chaperones on these kinetics shall thus be examined. That way, we might come closer to the puzzle's solution about which elements in the Hsp90 chaperone cause the extremely slow clamp-closure kinetics and ATPase rates of Hsp90. By lifting the whole system to the single-molecule level, it shall be investigated if it is possible to detect PET-events on the single-molecule level. Furthermore, the question shall be answered if is feasible to distinguish between PET and photophysical events. Assuming that this is the case, directionality in the network of local motions shall be revealed by the development of a two-colour single-molecule PET microscopy method, to detect local motions simultaneously and in real-time

2 Materials and Methods

In this section all Materials and Methods used within this work are listed. It is to mention that all buffers and media were prepared and diluted in Millipore H_2O. If not autoclaved, they were filtered through a 0.2 µm pore-size cellulose acetate filter (Sartorius).

2.1 Molecularbiology

2.1.1 Transformation and cultivation of bacterial cells

Buffers:

2x TY-Media, 1l (pH 7.4):	16 g Tryptone, 10 g yeast extract, 5 g NaCl
TY-Agar-Plates, 1l:	15 g Bacterial Agar, 8 g NaCl, 10 g Tryptone, 5 g yeast extract

Media for bacterial cultivation were sterilised by autoclaving (15 min, 121 °C). Bacterial agar plates were prepared by cooling down the TY-Agar Media to <50°C under gentle shaking, addition of antibiotics and pouring into petri-discs. Ampicillin (Melford Laboratories) was added at a final concentration of 0.1 mg/ml.

For bacterial transformation, a stock of chemically competent *E.coli* cells, stored at -80 °C, was placed on ice for 10 min. For plasmids from QuikChange Mutagenesis, 3 µl of the PCR-reaction were incubated on ice for 2 minutes in a sterile 1.5 ml reaction tube. 40 µl of *E.coli* cells were added, followed by 5 minutes incubation on ice. The reaction mixture was streaked on ampicillin-containing bacterial agar plates and incubated at 37 °C overnight. In case of plasmid-DNA from Miniprep purification, only 1 µl of plasmid-DNA (~ 200 ng/µl) were incubated with 20 µl *E.coli* cells. 4 µl of the reaction mixture were streaked on agar plates.

For bacterial start cultures 2x TY-Media was inoculated with a bacterial colony, picked with a sterile pipette tip and incubated overnight at 37 °C in a shaking incubator.

2.1.2 Preparation of chemically competent cells

This standard protocol for the preparation of chemically competent *E.coli* cells with a very high transformation efficiency was taken from (Inoue et al., 1990). Chemically competent XL1-Blue and C41 (DE3) *E.coli* strains were prepared according to this protocol.

Buffers, solvents and materials to prepare:

Transformation buffer (TB): 10 mM PIPES, 15 mM $CaCl_2$*$2H_2O$, 250 mM KCl, 7.5 % Glucose, fill up to 980 ml with H_2O - adjust pH to 6.7 with KOH, add 55 mM $MnCl_2$*$4H_2O$ - adjust volume to 1 l. Sterilise by applying a single-use sterile filtration unit (0.45 µm pore size). Precool in fridge.

14 % DMSO in TB: 3.5 ml DMSO, 21.5 ml TB. Chill on ice

Ethanol and dry ice

8 ml bacterial start culture were prepared by inoculation of TY-media free from antibiotics with a bacterial stock of chemically competent *E.coli* cells. 800 ml TY-Media were then inoculated with 8 ml of the overnight-culture and grown at 37 °C up to an optical density (OD) of 0.5 at λ = 600 nm. The temperature was lowered to 4 °C for 30 min. Afterwards the cells were centrifuged at 4 000 rpm for 10 min at 4 °C. The bacterial pellet was resuspended in 100 ml of precooled TB and centrifuged at 4 000 rpm, 10 min, 4 °C. This was followed by a second resuspension step with 200 ml of precooled TB, incubation on ice for 30 min and centrifugation at 4 000 rpm, 10 min, 4 °C. In the last step, the bacterial pellet was resuspended in 25 ml of precooled TB and the suspension was transferred on 25 ml precooled 14 % DMSO. The suspension was split into 200 µl Aliquots in sterile 1.5 ml reaction tubes, frozen in an ethanol-dry ice bath and stored at -80 °C.

2.1.3 Primerdesign

All Primers listed in this section were ordered at Sigma Aldrich.

2.1.3.1 For QuikChange mutagenesis

QuikChange site directed-mutagenesis is a very simple and quick technique for mutation of single residues within proteins. In this technique, developed by Stratagene, two overlapping primer pairs are designed that contain the mutation to be inserted. Amplification of the plasmid will result in double-stranded linear DNA strands with overlapping single-stranded DNA of primer-sequence. These complementary overlaps will hybridise and will be ligated by *E.coli* host repair enzymes after transformation (Liu and Naismith, 2008). The mutational-site should be flanked by 10-15 bp of the non-modified surrounding DNA-sequence. Primers should be 25 to 45 bp long and have a GC-content of 40 – 60 %. To facilitate specific binding G or C should be present within the last 5 base pairs of 5′ and 3′ end. All primers used for exchange of single amino acids are listed in Table 2-1.

Table 2-1: Nucleotide-sequences of the Primers used for generation of point mutations. f = forward, r = reverse

Mutation	Nucleotide-sequence
A2C_f	5‘-CATCATCATGGTATGTGCAGCGAAACTTTTGAATTTCAAGC-3‘
A2C_r	5‘-GCTTGAAATTCAAAAGTTTCGCTGCACATACCATGATGATG-3‘
E162W_f	5‘-CACTGTTACTCTAGACTGGGTTAATGAAAGAATTGG-3‘
E162W_r	5‘-CCAATTCTTTCATTAACCCAGTCTAGAGTAACAGTG-3‘
A2W_f	5’-CATCATCATGGTATGTGGAGCGAAACTTTTGAATTTCAAGC-3’
A2W_r	5’-GCTTGAAATTCAAAAGTTTCGCTCCACATACCATGATGATG-3’
E162C_f	5’-CACTGTTACTCTAGACTGCGTTAATGAAAGAATTGG-3’
E162C_r	5’-CCAATTCTTTCATTAACGCAGTCTAGAGTAACAGTG-3’
S51C_f	5’-GGATAAAATTAGATACAAATCTTTGTGCGATCCAAAGCAATTGG-3’
S51C_r	5’-CCAATTGCTTTGGATCGCACAAAGATTTGTATCTAATTTTATCC-3’
A110W_f	5’-CCTTCATGGAAGCTCTATCTTGGGGTGCCGATGTATCC-3’
A110W_r	5’-GGATACATCGGCACCCCAAGATAGAGCTTCCATGAAGG-3’
S51W_f	5’-GGATAAAATTAGATACAAATCTTTGTGGGATCCAAAGCAATTGG-3’
S51W_r	5’-CCAATTGCTTTGGATCCCACAAAGATTTGTATCTAATTTTATCC-3’
A110C_f	5’-CCTTCATGGAAGCTCTATCTTGCGGTGCCGATGTATCC-3’

A110C_r	5’-GGATACATCGGCACCGCAAGATAGAGCTTCCATGAAGG-3’
E192C_f	5’-GGAAGAAAAGAGAATAAAGTGCGTTATCAAGAGACATTC-3’
E192C_r	5’-GAATGTCTCTTGATAACGCACTTTATTCTCTTTTCTTCC-3’
N298W_f	5’-CTATAAGTCTATTTCATGGGACTGGGAAGACCC-3’
N298W_r	5’-GGGTCTTCCCAGTCCCATGAAATAGACTTATAG-3’
T101I_f	5’-CCATTGCCAAGTCTGGTATTAAAGCCTTCATGGAAGC-3’
T101I_r	5’-GCTTCCATGAAGGCTTTAATACCAGACTTGGCAATGG-3’
R380A_f	5’-CCATTGAATTTGTCCGCGGAAATGTTACAACAAAATAAG-3’
R380A_r	5’-CTTATTTTGTTGTAACATTTCCGCGGACAAATTCAATGG-3’
L160W_f	5’-GGTTCTTCACTGTTACTTGGGACGAAGTTAATGAAAGAATTG-3
L160W_r	5’-CAATTCTTTCATTAACTTCGTCCCAAGTAACAGTGAAGAACC-3’
A107N_f	5’- CCAAAGCCTTCATGGAAAACCTATCTGCTGGTGCC-3’
A107N_r	5’- GGCACCAGCAGATAGGTTTTCCATGAAGGCTTTGG-3’
A107N-A110W_f	5’- CCAAAGCCTTCATGGAAAACCTATCTTGGGGTGCC-3’
A107N-A110W_r	5’- GGCACCCCAAGATAGGTTTTCCATGAAGGCTTTGG-3’
F349A_f	5’- GTACGTTCGTCGTGTTGCGATCACTGATGAAGCTGAAG-3’
F349A_r	5’- CTTCAGCTTCATCAGTGATCGCAACACGACGAACGTAC-3’
A2C_C-His_f	5’-GAAGGAGATATACATATGTGCAGCGAAACTTTTG-3’
A2C_C-His_r	5’-CAAAAGTTTCGCTGCACATATGTATATCTCCTTC-3’
D560C_f	5’- CCTTGAAAGAAATTTTGGGTTGCCAAGTGGAGAAAGTTG-3’
D560C_r	5’- CAACTTTCTCCACTTGGCAACCCAAAATTTCTTTCAAGG-3’

2.1.3.2 For cloning of DNA-fragments

One big challenge in the development of a single-molecule microscopy technique for the observation of motions within proteins is to immobilise the protein in its functional form. Hsp90 is only able to hydrolyse ATP in its homodimeric form. But binding affinities of the protomers are too low for dimer-formation at single-molecule concentration. All modifications of the Hsp90-protein made to meet the needs of an experiment at the single-molecule level are explained in detail in section 2.4.2. Here the cloning schemes are explained.

In a first step, the N-terminal His-tag was deleted and moved to the proteins C-terminus. The C-terminal His-tag was inserted by amplification of the insert using a

reverse primer extended by the His-tag and the HindIII restriction site flanked by six amino acids for efficient restriction close to the end of an oligonucleotide. NheI and HindIII served as restriction sites for the following digestion and ligation of the amplified vector and insert DNA fragments.

The coiled-coil (CC) sequence was too large for insertion by primer extension. Therefore an oligonucleotide of the WinZipA2 (WZA2) and WinZipB1 (WZB1) CC sequence including an eight amino acids GS-linker sequence, the C-terminal His-tag and Stop-Codon, flanked by a 5′ BamHI and 3′ HindIII restriction site, was ordered at GeneArt (Life Technologies). For cloning into the Hsp90 expression plasmid, a BamHI restriction site was inserted in 5′ direction of the HindIII restriction site, located 3′ of the Hsp90 Sequence Stop-Codon.

In a last step an Avitag was inserted. This was done in two steps. In the first step, the first half of the Avitag was attached to the 5′ end of the forward and reverse primer, respectively. As the two ends are complementary to each other, these will hybridise and the nick will be ligated within *E.coli* XL1-Blue cells by host enzymes. This step was repeated with primers containing the second half of the Avitag.

The nucleotide sequences of all primers and oligonucleotides are listed in Table 2-2.

Table 2-2: Nucleotide-sequences of the Primers used for insertion and deletion of DNA fragments. f = forward, r = reverse

Primer	Nucleotide-sequence	Purpose
NheI_f His6_r	5‘-GGTTCTCATCATCATCATCATGGTATGGCTAGC-3‘ 5’-CGGATCAAGCTTAATGATGATGATGATGATGATCTACC TCTTCCATTTCGGTGTC-3’	Amplification insert for C-His-tag insertion
HindIII_f NheI_r	5’-GTTCCAGCTGACACCGAAATGGAAGAGGTAG-3’ 5’-CCCGGCTAGCCATATGTATATCTCCTTCTTAAAGTTAA AC -3’	Amplification vector excluding N-terminal His-tag
WZA2 WZB1	5’-GGTAGATGGATCCACCTCCGGCTCCACCACCGTGGCG CAGCTGCGTGAACGTGTGAAAACCCTGCGTGCGCAGAAT TATGAACTGGAATCCGAAGTGCAGCGTCTGCGTGAACAG GTGGCGCAGCTGGCGTCCCATCATCATCATCATCATTAAG CTTCGACAC-3’ 5’-GGTAGATGGATCCACCTCCGGCTCCACCACCGTGGAT GAACTGCAGGCGGAAGTGGATCAGCTGCAGGATGAAAA TTATGCGCTGAAAACCAAAGTGGCGCAGCTGCGTAAAAA AGTGGAAAAACTGGCGTCCCATCATCATCATCATCATTAA GCTTCGACAC-3’	Oligonucleotides for insertion of CC sequences
HindIII_f BamHI_r	5‘-CATTAAGCTTGATCCGGCTGCT-3’ 5’-GATGGGATCCATCTACCTCTTCCATTTCGG-3’	Insertion of BamHI restriction site for CC insertion
AviWZA2_f1 AviWZA2_r1	5’-GGCCTGAACGATATTTTTGAAGCCATCATCATCACCA TCATTAAGCTTGATC-3’ 5’-GCTTCAAAAATATCGTTCAGGCCGCTTGCCAGCTGG GCAAC -3’	Insertion of first half of Avitag to WZA2 constructs
AviWZA2_f2 Avi_r2	5’-GCAGAAAATTGAATGGCATGAACATCATCATCACCAT CATTAAGCTTGATC-3’ 5’-TTCATGCCATTCAATTTTCTGCGCTTCAAAAATATCGT TCAGGC-3’	Insertion of second half of Avitag to WZA2 Insertion of second half of Avitag to both CC
AviWZB1_f1 AviWZB1_r1	5’-GGCCTGAACGATATTTTTGAAGCCATCATCACCATCA CCATTAAG-3’ 5’-GCTTCAAAAATATCGTTCAGGCCGCTTGCCAGTTTTT CAAC-3’	Insertion of first half of Avitag to WZB1 CC-constructs
AviWZB1_r2	5’-GCAGAAAATTGAATGGCATGAACATCATCACCATCACC ATTAAG-3’	Insertion of second half of Avitag to WZB1 constructs

2.1.4 PCR

The polymerase chain reaction is used for the amplification of a specific part of a DNA-sequence. Primers that are complementary to the start and end of the DNA-fragment serve as starting point for amplification of the sense and anti-sense DNA-strand by a DNA-polymerase.

The following reaction mixture was used for 50 µl PCR-reactions with Q5 High-Fidelity DNA-Polymerase (New England Biolabs)

5x Q5 reaction buffer	10 µl
25 mM dNTPs	1 µl
forward Primer (125 ng/µl)	1 µl
reverse Primer (125 ng/µl)	1 µl
template DNA	15 ng
Q5 HF-Polymerase (2U/µl)	1 µl
dH_2O	to 50 µl

A PCR-reaction consists of three steps. First the double-stranded DNA is denaturated by heat. Then the temperature is lowered such that the primer can anneal to the complementary DNA-sequence. In the last step the temperature is risen to the optimum working temperature of the DNA-polymerase and elongation takes place. This cycle is repeated 20 times. In case of insertion of a sequence by primer extension and amplification of DNA vector and DNA insert for molecular cloning, two different cycle schemes were used. In the first ten cycles, the annealing temperature was chosen according to the melting temperature of the complementary primer sequence. This was followed by 20 cycles where the annealing temperature was risen according to the melting temperature of the complete primer (but not higher than 68 °C). By using this method, the sequence to be inserted by primer extension would not produce single stranded overlaps. Both PCR-programmes are listed in Table 2-3. The success of a PCR-reaction was controlled by Agarose-Gel Electrophoresis.

Table 2-3: Thermocycling Conditions for amplification of complete plasmid (used for QuikChange and Avitag-insertion) and for insertions done by molecular cloning experiments

Cycle times		Reaction step	Temperature	Reaction time
Plasmid amplification	**Molecular cloning**			
1	1	Initial denaturation	98 °C	30 sec
20	10	Denaturation Annealing Elongation	98 °C 56 °C 72 °C	30 sec 30 sec 30 sec / kb
-	20	Denaturation Annealing Elongation	98 °C Primer dependent 72 °C	30 sec 30 sec 30 sec / kb
1	1	Final Extension	72 °C	2 min
1	1		4 °C	∞

2.1.5 Restriction endonuclease digestion

Before continuing to the next steps after a PCR-reaction, the template DNA should be removed from the reaction mixture. Methylation of DNA is used by all kinds of organisms for different purposes. In Bacteria DNA-methylation serves as a DNA-repair control mechanism. The newly synthesized DNA can be distinguished from the methylated template DNA. As the template plasmid DNA was always amplified by and isolated from bacterial cells this could be removed by DpnI digestion. This restriction endonuclease recognizes and cuts methylated DNA. Therefore 1 µl DpnI (20 U/µl; New England Biolabs) was added after the PCR-reaction took place and incubated for 90 min at 37 °C.

DNA resulting from QuikChange as well as Avitag insertion PCR-reaction was then transformed into *E.coli* XL1-Blue cells, selected by its Ampicillin resistance and plasmids were isolated from bacterial start cultures.

DNA-fragments resulting from PCR reactions for molecular cloning experiments were purified after DpnI digestion according to the protocol of the QIAquick PCR Purification Kit (Qiagen).

For moving of the N-terminal His-tag to the C-terminus of Hsp90 the restrictional sites NheI and HindIII were used for insertion of the C-terminal His-tagged Hsp90-insert into the pRSET A vector. For insertion of the synthesized coiled-coil oligonucleotides into the Hsp90 expression plasmid, the restriction sites BamHI (inserted by PCR reaction) and HindIII were used. The CC-oligonucleotides were digested in a 25 µl reaction volume, because of a low amount of DNA. All used restriction enzymes were purchased from New England Biolabs. The reaction mixture was as followed:

10x reaction buffer	5 µl	2.5 µl
DNA	1 µg	0.3 – 0.4 µg
restriction enzyme I (20 U/µl)	1 µl	0.5 µl
restriction enzyme II (20 U/µl)	1 µl	0.5 µl
dH_2O	to 50 µl	to 25 µl

The reaction mixture was incubated for 2 h at 37 °C. Digested DNA fragments were isolated by agarose gel electrophoresis and DNA extraction and purification using the QIAquick Gel Extraction Kit (Qiagen).

2.1.6 Agarose gelelectrophoresis

Buffers:

5x TBE, 0.5 l:	27 g Tris, 13.8 g boric acid,
	10 ml EDTA (0.5 M, pH 8.0)

An Agarose-Gel served as a matrix to separate linear nucleic acid strains within an electric field. Because of the negatively charged phosphate backbone nucleic acids are attracted by the positively charged anode and move through the gel according to their size. In this work 1 % Agarose-Gels in 0.5x TBE-Buffer were used. SafeView (Applied Biological Materials, Canada) was applied for nucleic acid stain. 0.5x TBE served as running buffer. 10 µl of PCR product were loaded with 2 µl of 6x DNA

gel loading dye (Thermo Scientific). A DNA ladder served as size reference. An electrical field of 10-15 V/cm was applied and the gel-bands were imaged by an UV-illuminator.

2.1.7 DNA-ligation

For covalent linkage of two nicked DNA-fragments the enzyme T4 DNA-ligase (New England Biolabs) was used. The insert was added in an at least 3-times molar excess to the vector and 1 µl ligase (400 U/µl) was used in a total reaction volume of 20 µl. Reaction took place over night at 16 °C.

The ligase was heat inactivated for 10 min at 65 °C and different volumes of the ligation reaction (2.5 µl and 5 µl) were transformed into *E.coli* XL1-Blue cells (same transformation protocol as for QuickChange PCR-reactions, section 2.1.1), selected by ampicillin resistance and plasmids were isolated from bacterial start cultures.

2.1.8 Isolation of plasmid DNA and DNA sequencing

Isolation of plasmid DNA from a 5 ml bacterial start culture of XL1-Blue cells was done according to the protocol of the High Pure Plasmid Isolation Kit (Roche). Elution was performed in 50 µl Elution buffer.

A sample of 20 µl of the purified plasmid DNA, diluted to a concentration of 30 – 100 ng/µl was send to GATC Biotech for sequencing analysis.

2.2 Protein preparative methods

The expression plasmid pRSET A (Invitrogen) encoding the N-terminal His-tagged wild-type sequence of either Hsp82 or Aha1, both from *Saccharomyces cerevisiae*, was kindly provided by Chrisostomos Prodromou (University of Sussex, Brighton). The expression and purification protocol for purification of Hsp82 was used for the wildtype as well as the Hsp82 protein that was modified for single-molecule experiments. All purifications were performed at room temperature. All solutions and lysates were filtered through a 0.22 µm pore size filter prior to loading on a chromatography column.

Buffers:

Buffer N1:	50 mM phosphate, 30 mM imidazole, pH 8.0
Buffer N2:	300 mM imidazole, pH 8.0
Buffer I1:	20 mM Tris/HCl, pH 8.0
Buffer I2:	20 mM Tris/HCl, pH 8.0, 1 M NaCl
Buffer S:	40 mM HEPES, 200 mM ionic strength (KCl), pH 7.5

2.2.1 Expression and purification of Hsp82 and Aha1

The protein expression plasmid was transformed into *E.coli* C41 (DE3) cells (GeneArt, Life Technologies). These cells encode a T7-RNA-polymerase, whose expression is controlled by a lac-operon. Expression of the pRSET A vector encoded gene is controlled by a T7-Promoter. Transcription is only possible by the T7-RNA-polymerase. Upon addition of the lactose-analogue IPTG the T7-RNA-polymerase will be expressed and so will the protein of interest.

800 ml 2xTY-media, 0.1 mg/ml Ampicillin were inoculated with 8 ml of a 100 ml bacterial start culture and grown at 37 °C up to an OD of 0.6 - 1.0 at λ = 600 nm. Expression was initiated by addition of 1 mM IPTG. The temperature was lowered to 20 °C and expression took place overnight.

The bacterial cells were pelleted by centrifugation at 5000 rpm, 10 min. The cells were resuspended in buffer N1. 100 µl DNAse I (4 mg/ml, Applichem) and Lysozyme (Sigma-Aldrich) were added and cell disruption was completed by ultrasonic homogenization (10 sec pulse, 30 sec break. Overall pulse duration: 2 min 30 sec).

For removal of cellular debris the homogenate was centrifuged for 1 hour at 15 000 rpm. His-tagged Hsp82- and Aha1 proteins were separated from bacterial proteins by Ni-NTA-chromatography (Ni Sepharose 6 Fast Flow; GE Healthcare). Buffers N1 and N2 were used for washing and elution of protein, respectively. The eluate was diluted 1:5 in milliQH_2O to lower the ionic strength of the elution buffer to facilitate binding to POROS HQ Anion Exchange column. In case of Hsp82 Cys-variants 10 mM DTT was added to the protein eluate and 1mM DTT to buffer I1 and I2. Elution was performed by setting a gradient of 0 to 100 % buffer I2 within 60 min. The eluate was concentrated to a volume of ≤ 10 ml applying

10-kDa MWCO (molecular weight cut-off) centrifugal concentrators (Sartorius). In case of Hsp82 Cys-variants 10 mM DTT were added. No DTT was added to Buffer S, because DTT would interfere in following maleimide labeling reactions. Instead buffer S was washed with argon gas. A Sephacryl S-400 column (GE Healthcare) was used for Hsp82 and a Superdex 75 column (GE Healthcare) for Aha1 size exclusion chromatography. Proteins were again concentrated applying 10-kDa MWCO centrifugal concentrators, flash frozen in liquid nitrogen and stored at -20 °C.

Protein purity was controlled by SDS-PAGE (sodium dodecyl sulfate polyacrylamide gel electrophoresis). Therefore precast NuPAGE Bis-Tris gels (Thermo Fisher Scientific) were used.

2.2.2 Dye conjugation of cysteine-side chains

Cysteine side chains were introduced by QuikChange Mutagenesis for conjugation of its thiol-group by a maleimide modified fluorescent dye. In combination with an introduced Trp amino acid, this system can be used as an fluorescent reporter for visualization of conformational changes and dynamics within a protein.

The reaction took place in Buffer S with a 10-fold molar excess of the reducing agent TCEP. Dye was added in a 5-fold molar excess to protein and the mixture was incubated for 2.5 h at room temperature. Non-conjugated dye was removed by gel-filtration using Sephadex G-25 resin (GE-Healthcare). Labelled protein was concentrated applying 10-kDa MWCO centrifugal concentrators.

2.2.3 Determination of protein and dye concentrations

The extinction coefficient ε is a characteristic parameter of a biomolecule. It defines how much light of a certain wavelength is adsorbed by this molecule. In absorption spectroscopy the intensity of light that can transmit through a solution before (I_0) and after (I) addition of a biomolecule is measured. If ε is known, the molecule-concentration can be determined applying the Lambert-Beer law:

$$A = -\log(\frac{I}{I_0}) = \varepsilon \cdot c \cdot d \qquad (2\text{-}1)$$

d is the path length of the cuvette. Absorption was measured applying a NanoPhotometer® (IMPLEN).

To determine the degree of labelling (DOL) after dye-conjugation, an absorption spectrum was measured to determine the absorption maxima of protein and dye. Knowing these the DOL could be calculated applying the following equation:

$$DOL = \frac{A_{\max} \cdot \varepsilon_{Protein}}{(A_{280} - (CF_{280} \cdot A_{\max})) \cdot \varepsilon_{\max}} \qquad (2\text{-}2)$$

A_{max}/A_{280} and $\varepsilon_{max}/\varepsilon_{Protein}$ are the absorption and extinction coefficient of the dye / protein at the wavelength of maximum absorption. CF_{280} is a dye-specific correction factor for dye absorbance at 280 nm.

2.2.4 Avitag-biotinylation

Buffers:

10x biotinylation buffer A: 0.5 M Bicine, pH 8.3 with NaOH

10x biotinylation buffer B: 100 mM ATP, 100 mM MgOAc, 500 μM d-biotin

The B-vitamin biotin possesses a very strong binding affinity to Streptavidin, a homo-tetrameric protein with four biotin-binding sites. This is one of the strongest known non-covalent binding interactions and is often used in many biotechnological areas for isolation or immobilisation of a molecule of interest. The BirA ligase (Avidity) is an enzyme from *E.coli* that recognizes a 15 amino-acid peptide of the sequence GLNDIFEAQKIEWHE and conjugates a biotin to the lysine residue. This so-called Avitag was fused to Hsp90's C-terminus for biotinylation to facilitate protein immobilisation in single-molecule experiments. Following reaction mixture was prepared:

10x biotinylation buffer A	20 µl
10x biotinylation buffer B	20 µl
fluorophore-labelled Hsp90	up to 10 nmol
BirA ligase (1 mg/ml)	5 µl
dH_2O	to 200 µl

The final concentration of fluorophore-labelled Hsp90 was in the range of 10 to 40 µM. The mixture was incubated for 1 h at 30 °C and for removal of non-conjugated biotin dialysed against 50 mM Phosphate, 200 mM ionic strength (KCl), pH 7.5 applying a 10-kDa MWCO Slide-A-Lyzer Dialysis Cassette (Thermo Fisher Scientific). Dialysis took place for at least 2 h at room temperature, followed by buffer refreshment and dialysis over night at 4 °C.

2.3 Bulk measurements

2.3.1 ATPase activity assay

Buffers:

ATPase assay buffer:	0.2 mM NADH, 2 mM phosphoenolpyruvat, 50 U/ml pyruvate kinase, 50 U/ml lactate dehydrogenase, 5 mM DTT, 10 mM $MgCl_2$, 2 mM ATP in 40 mM HEPES, 200 mM IS (KCl), pH 7.5

Hsp90 ATPase activity of purified proteins was checked applying a previously described ATPase assay (Panaretou et al., 1998). This assay is based on regeneration of the hydrolysed ATP (A6419, Sigma Aldrich) by an enzymatic reaction that is coupled to oxidation of NADH (N8129, Sigma Aldrich) to NAD^+. Pyruvate kinase (P7768, Sigma Aldrich) is phosphorylating ADP using phosphoenolpyruvate (P7127, Sigma Aldrich). The resulting pyruvate is then converted to lactate by a lactate dehydrogenase (L2625, Sigma Aldrich). This step is connected to the oxidation of NADH to NAD^+. NADH absorbs at λ = 340 nm and a decrease in absorbance is in direct stoichiometry to ATP-hydrolysis. The slope of the linear decrease in

absorbance was determined and ATPase activity was calculated using the following equation:

$$ATPase\left[\min^{-1}\right] = -\frac{dA_{340}}{dt}\left[OD/\min\right]\cdot d\cdot \varepsilon_{NADH}\cdot c_{ATPase} \qquad (2\text{-}3)$$

$\frac{dA_{340}}{dt}$ = slope of the change in absorbance

d = path length of cuvette

ε_{NADH} = extinction coefficient NADH of 6220 $\frac{l}{mol*cm}$

c_{ATPase} = concentration of ATPase

Measurements were performed at 25 °C or 37 °C in ATPase assay buffer. To measure the effect of the co-chaperone Aha1 on Hsp90 ATPase activity, 20 µM Aha1 were added to the assay buffer. 5 – 20 µM Hsp90 were added to start the reaction. The assay was checked for background ATPase activity by inhibition of Hsp90 using Geldanamycin (Cayman Chemical). Therefore 150 µM geldanamycin and 5 – 20 µM Hsp90 were preincubated for at least 30 min in assay buffer without ATP. 2 mM ATP were added to start the reaction. The decrease in absorbance at λ = 340 nm over time was detected using a V-650 spectrophotometer (Jasco).

2.3.2 Fluorescence spectroscopy

Fluorescence spectra and intensity changes over time were measured using a FP-6500 spectrofluorometer (Jasco). A 150 W Xenon Lamp served as light source. This lamp emits white light in a spectral range of 220 to 750 nm. The polychromatic light is focused by a mirror on an excitation monochromator. Monochromatic light is led by mirrors to the centre of the sample cell. The emission light is detected in a right angle to the excitation light to reduce detection of this. The emission light is led to an emission monochromator and the monochromatic light is detected by a photomultiplier tube. The temperature of the sample was regulated by a peltier thermocouple. Measurements were performed in a 500 µl quartz glass cuvette with a path length of 1 cm (Hellma Analytics).

2.3.2.1 PET-reporter systems

Different fluorophores were tested for PET-competence. Therefore the reactive group of the maleimide-modified fluorophore was first neutralized by addition of a 10-fold molar excess of cysteamin and incubation for 2 h at room temperature. A solution of the free fluorophore in buffer S and in buffer S containing 25 mM Trp was prepared. A fluorescence spectrum was measured. All fluorophores used within this work and and their specific properties are listed in Table 2-4

Table 2-4: List of dye-specifc properties. λ exc/ λ em are wavelengths of maximum absorption/emission. ε is the extinction coefficient at λ exc.

Dye	λ_{exc} (nm)	λ_{em} (nm)	ε ($\frac{l}{mol*cm}$)	Quantum yield	Manufacturer
Atto 495	498	526	80 000	0.2	Atto-Tec
Atto 514	511	532	115 000	0.85	Atto-Tec
Atto 520	517	538	110 000	0.9	Atto-Tec
Atto 542	542	562	120 000	0.93	Atto-Tec
Atto Oxa11	658	679	125 000	0.25	Atto-Tec
Alexa 488	493	516	72 000	0.92	Thermo Fisher Scientific
Alexa 594	588	612	96 000	0.66	Thermo Fisher Scientific

AttoOxa11 was used as PET-competent dye in bulk measurements. Fluorescence was excited at 620 nm and fluorescence changes over time were recorded at 678 nm. To detect kinetics of conformational changes visualized by PET-reporter systems, samples were prepared in Buffer S containing 10 mM $MgCl_2$ and 150 nM AttoOxa11 labelled Hsp90-constructs. To ensure heterodimeric constructs where only one subunit carries the fluorophore, the non-labelled wild-type or variant Hsp90 protein was added in a 33-fold excess at a concentration of 5 µM. Incubation

for at least 30 min at room temperature (1 h at 37 °C in case of CC-constructs) facilitated complete subunit exchange. Prior to start of the ATPase cycle, fluorescence signal was checked for stability over a time span of 10 min. The reaction was started by addition of 2 mM AMP-PNP (Sigma-Aldrich).

The measured data were fitted to a multi-exponential decay function using the software OriginPro 2016G.

$$I(t) = I_0 \sum_i a_i \exp(\frac{-t}{\tau_i}) \quad (2\text{-}4)$$

I(t) and I_0 are the fluorescence intensities at time point t and before start of the reaction. a_i is the amount that component i with the characteristic time constant τ_i adds to the complete fluorescence change.

2.3.2.2 FRET-reporter systems

To measure improvement of dimer stability by addition of a CC sequence C-terminal to Hsp90's natural dimerization site, chasing experiments were performed. Asp at position 560 was mutated to a Cys and served as labelling site for the FRET-competent dyes, as described previously (Ratzke et al., 2010) One monomer was labelled with the donor fluorophore Alexa 488 and the other with the acceptor Alexa 594. A solution of 100 nM donor-labelled Hsp90 with a 5-fold excess of acceptor-labelled Hsp90 in buffer S containing 10 mM $MgCl_2$ was prepared. The solution was incubated for 1 h at 37 °C to facilitate complete subunit exchange. Fluorescence spectra with excitation at 485 nm were measured. The stability of the dimer is detected by addition of 5 µM or 10 µM in case of CC- WZB1 of the respective non-labelled Hsp90 wild-type or CC-variant. Dissociation of a heterodimeric FRET-pair would result in re-association with a non-labelled Hsp90 subunit. Dissociation was observed by detection of a fluorescence decrease over time of the acceptor dye. The donor was excited at 485 nm and acceptor fluorescence was detected at 614 nm.

2.3.3 Stopped-flow spectroscopy

The stopped flow-technique is used to measure fast kinetics of chemical or biological reactions within the range of milliseconds. The reagents are filled within different syringes and are very fast injected into a mixing vessel, from which they get into a cuvette where the flow is rapidly stopped by a piston. The reaction can now be observed over time by a suitable method, e.g. fluorescence spectroscopy or CD-spectroscopy.

In the setup used within this work, up to three different solutions can be mixed (Bio-Logic SFM-300; Figure 2-1). There is a delay volume between mixer 1 and 2, such that it is important to add one of the reactants into syringe 3, to keep the dead time at a minimum. A 639 nm laser diode was used as excitation source. A photomultiplier tube served as detector and was arranged in a right angle relative to the laser diode to prevent detection of excitation light. Emission light was filtered using a long pass optical filter (RazorEdge 647RU, Semrock).

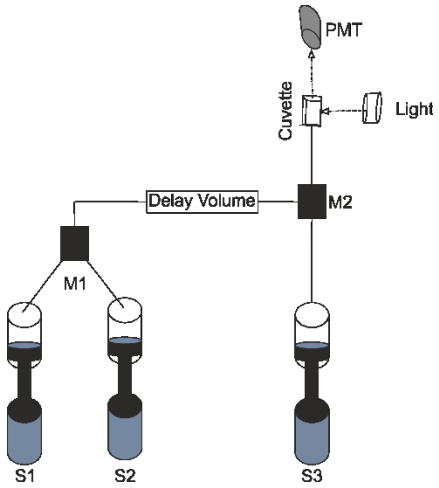

Figure 2-1: Scheme of the Stopped-Flow Setup. S1, S2 and S3 are the syringes, M1 and M2 the mixers and PMT the photomultiplier tube. Figure was modified from Bio-Logic SFM-300/400 user's manual.(Bio-Logic)

Buffer S containing 10 mM $MgCl_2$ was used for all stopped-flow measurements performed within this work. For determination of the kinetics of conformational rearrangements in presence of the co-chaperone Aha1, a solution of 200 nM AttoOxa11-labelled Hsp90 with 5 µM wild-type Hsp90 or variant E162W and 20

μM Aha1 was prepared. A second solution of 4 mM AMP-PNP was prepared and solutions were mixed in a 1:1 ratio.
For determination of rapid lid-dynamics, a solution of 400 nM AttoOxa11-labelled S51W-A110C was prepared with 5 μM wild-type Hsp90 and loaded into syringe 3. Syringe 1 and 2 were filled with a solution of ADP and buffer, respectively. Thus ADP could be premixed in M1 and be mixed with the Hsp90-construct in varying concentrations.
Data were fitted to an exponential decay function (2-4) using the software OriginPro 2016G.

2.4 Single-molecule microscopy

Buffers and Stock solutions:

T50-buffer:	20 mM Tris/HCl pH 8.0, 50 mM NaCl
Buffer M:	50 mM Phosphate, 200 mM ionic strength (KCl), 10 mM $MgCl_2$, pH 7.5
BSA-biotin:	1 mg/ml in T50-Buffer, flash frozen in liquid nitrogen, stored at -20 °C
Neutravidin:	10 mg/ml diluted in water. Further diluted to 1 mg/ml in PBS, flash frozen in liquid nitrogen, stored at –20 °C
Oxygen scavenging system:	25 mM KCl, 22 mM Tris/HCl pH 7.0, 2000 U/ml glucose oxidase, 40 000 U/ml catalase, 4 mM TCEP. Stored at -20 °C

2.4.1 Surface preparation

One of the biggest challenges in single-molecule microscopy is the surface preparation. There are two points to address. First the surface should be as clean as possible to avoid signal arising from fluorescent impurities. Second the surface should be sufficiently passivated. As many biomolecular interactions possess dissociation constants (K_D) in the range of nano- to micromolar, non-specific binding of biomolecules at this concentration range should be efficiently blocked. A DDS-

Tween-20 surface-passivation protocol, developed by Hua et al., fulfils these requirements. Additionally, this method is very inexpensive and achieves equal or even better blocking efficiencies than the most common covalent polyethylene glycole (PEG) coating or noncovalent protein blocking methods.(Hua et al., 2014).

2.4.1.1 Cleaning and modification of borosilicate cover slips

The following passivation protocol was slightly modified from the protocol described in (Hua et al., 2014). First the glass coverslips had to be rigorously cleaned. All washing steps mentioned in the following were performed by rinsing the slides three times with milliQ water. Coverslips were placed in a glass staining dish and sonicated in 2 % Hellmanex (Hellma Analytics) for 15 min, followed by washing, sonication in milliQ water for 15 min, washing and 15 min sonication in aceton. Coverslips were rinsed with absolute ethanol, washed and sonicated for 1 h in 1 M KOH. This time was used to prepare a second staining dish by sonicating once with hexane (Sigma-Aldrich, ≥97.0 %), moistening the surface once again with hexane and sealing the empty dish until use. The coverslips were washed, followed by 15 min sonication in milliQ water and washing.

The clean clover slips were then air-dried thoroughly in a nitrogen stream and transferred into the prepared staining dish. At this point the surface should be completely hydrophilic. Free surface hydroxyl groups are now ready for modification. First the cover slips are rinsed twice with hexane. Then 75 ml hexane are filled into the staining dish and 50 µl dichlorodimethylsilane (DDS, Merck, ≥98.0 %) are added using a 1 ml syringe. To prevent hydrolysis of chlorosilanes, air contact was avoided by direct injection into the hexane solution. Reaction took place for 1.5 h under gentle shaking at room temperature. Afterwards the cover slips were rinsed with hexane and sonicated for 1 min. Now the coverslips should be completely hydrophobic. Coverslips were air-dried in a nitrogen stream, placed in air-dried 50 ml falcon tubes, sealed with parafilm, put into a food saver bag and vacuum sealed. Stored at -20 °C, cover slips were usable for up to several month.

2.4.1.2 Assembly of flow-chambers

In house built flow chambers do consist of a reusable cover slide that is provided with two holes in a distance of 3 cm. An inlet pipette tip and an outlet luer lock plastic tip are attached to these. Furthermore a parafilm slide of the same size

then the coverslip is prepared and a mask was cut out which will serve as flow channel. For assembly the modified coverslips are removed from –20 °C and warmed up to room temperature. A heating plate is preheated to 70 °C. A sandwich of cover slide, parafilm and coverslip is assembled and warmed on the heating plate, until the parafilm melts. To ensure a good attachment between coverslip and cover slide, the sandwich was slightly pressed on the heating plate. The flow chamber was now connected via the luer-lock outlet tip to a polyethylene-tubing that was connected to a peristaltic pump (Ismatec sa, REGLO Analog MS-4/8).

After use, the flow chamber was first washed by flowing in milliQ water, 5 M KOH, absolute ethanol and milliQ water. Afterwards flow chambers were disassembled by melting of the parafilm at 70 °C on a heating plate and removal of parafilm and coverslip. The reusable cover slide was rinsed with milliQ water, ethanol and again milliQ water and remaining parafilm was scrubbed off using an acetone soaked tissue. After rinsing once again with milliQ water, ethanol and milliQ water the cover slides were dried in an oven at 50 °C and stored in a box until use.

2.4.2 Protein immobilisation.

2.4.2.1 Surface passivation

The DDS-coated surface was next passivated by self-assembly of a layer of Tween 20 molecules. Before blocking the surface from non-specific binding of biomolecules, BSA-biotin had to be adsorbed. Thus a site for specific binding of biotinylated biomolecules was provided. 250 µl of 0.2 mg/ml of BSA-biotin (A8549, Sigma Aldrich) in T50-Buffer were flown into the flow chamber and incubated for 10 min. After washing with 250 µl T50, 500 µl 0.2 % Tween 20 in buffer T50 were flown in and incubated for 10 min, followed by washing with 500 µl T50 and 500 µl Buffer M. To check for specificity of binding, a low concentration (~ 1 nM) of labelled Hsp90 molecule is flown in. If non-specific binding events are negligible, surface modification is continued. 250 µl of 0.2 mg/ml neutravidin (Thermo Fisher Scientific) were added, incubated for 10 min and washed with 750 µl Buffer M to ensure that the surface is free from unbound neutravidin. Now the surface is ready for specific immobilisation of biotinylated biomolecules. The surface passivation protocol is shown schematically in Figure 2-2.

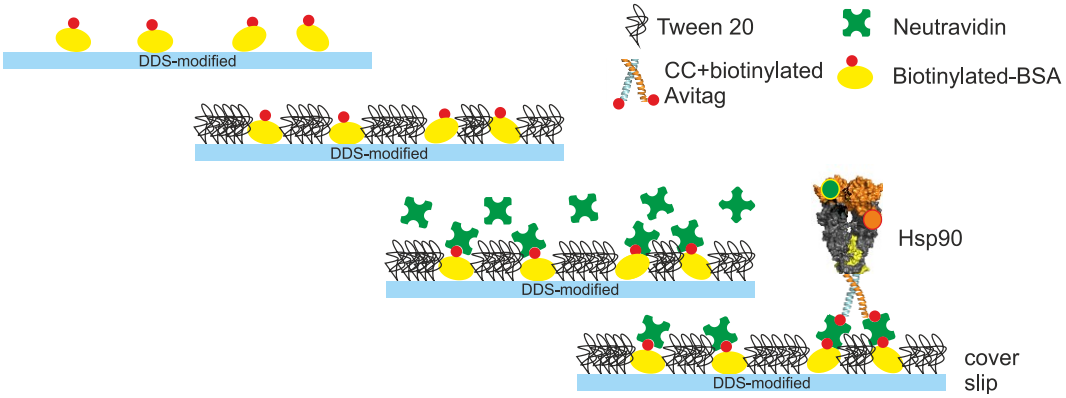

Figure 2-2: Passivation of DDS-coated coverslips. Upper picture shows the first step and lower picture the last step in the protocol. First BSA-biotin is added, followed by Tween 20. Neutravidin is added and finally serves as attachment site for the biotinylated Hsp90-molecule, added in the last step.

2.4.2.2 Hsp90 construct for single-molecule microscopy

For immobilisation of dimeric Hsp90-constructs on a single-molecule surface, modifications of Hsp90 protein had to be taken. The cloning scheme is explained in 2.1.3.2. An Avitag (GLNDIFEAQKIEWHE) was introduced to facilitate immobilisation by Biotin-Neutravidin interaction. To ensure immobilisation of stable dimeric Hsp90 constructs at concentrations needed to get clearly separable single-molecules (~ 100 pM), Hsp90's dissociation constant K_D=60 nM had to be improved (Richter et al., 2001). For two-colour single-molecule microscopy it was important to get heterodimeric Hsp90 constructs containing two different PET-reporter systems. Therefore a coiled-coil (CC) motif was introduced which facilitates formation of stable heterodimeric constructs, while homodimers are unfavoured. The applied CC construct, named WinZip-A2B1, was identified by Arndt et al., 2002 using a library vs. library strategy in which the sequences of the leucine zipper pair c-fos/c-jun served as template (Pelletier et al., 1999). It possesses a very high heterodimer stability with a K_D of 4.5 nM, while homodimers of WinZipA2 (WZA2: VAQLRERVKTLRAQNYELESEVQRLREQVAQLAS) and WinZipB1 (WZB1: VDELQAEVDQLQDENYALKTKVAQLRKKVEKLAS) are formed with a low K_D of 17 nM and 70 µM, respectively (Arndt et al., 2002). An eight amino acid linker N-terminal to the CC sequence, consisting of Gly and Ser residues (GSTSGSTT), facilitated free movability of the natural Hsp90 dimerization site.

Modifications taken are shown in Figure 2-3. Additionally, in case of ß-strand reporter construct A2C, efficient fluorophore conjugation to the cysteine side-chain was only possible in presence of an N-terminal His-tag. Therefore, the His-tag was moved to the N-terminus in A2C single-molecule constructs, reporting on ß-strand swap.

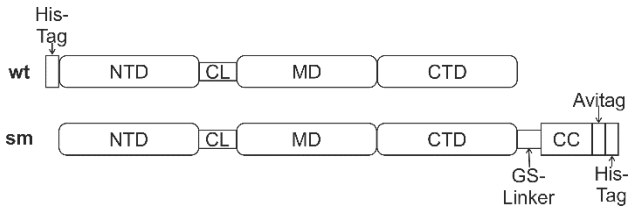

Figure 2-3: Scheme of N-terminal His-tagged wild-type (wt, upper) and modified Hsp90 protein for single-molecule microscopy (sm, lower). N-terminal domain (NTD) and middle domain (MD) are connected by a charged linker. Coiled-coil (CC), Avitag and His-tag are fused to the C-terminal domain (CTD), together with a GS-linker that facilitates free movability of the natural dimerization site in the sm construct.

2.4.2.3 Protein immobilisation for one-colour experiments

In one-colour-experiments only the dye-labelled Hsp90 was biotinylated and specifically immobilised on the surface. The complementary, non-labelled and non-biotinylated Hsp90 construct was added in excess at a concentration of 1 µM to the labelled Hsp90-construct and to all buffers and solutions applied after immobilisation. Thus labelled, immobilised Hsp90 molecules should mainly form heterodimers on the surface, as concentrations applied are far above the K_d. Solutions of 100 pM, 500 pM and 1 nM dye-labelled Hsp90 in Buffer M containing 1 µM non-labelled Hsp90 of the complementary CC construct were incubated for 1 h at 37 °C to allow for subunit exchange. Beginning with the lowest prepared concentration of labelled-Hsp90, the solutions were added to the surface until a sufficient amount of single-molecules was visible. Unbound fluorophore-labelled molecules were removed by washing with 1 µM Hsp90 in buffer M.

2.4.2.4 Protein immobilisation for two-colour experiments

In two colour-measurements, both of the differently labelled Hsp90 PET-reporter constructs were biotinylated. This way it was more likely that immobilised heterodimers would not dissociate, because they are kept in close proximity by the bound neutravidin protein. CC WZA2 possesses a quite high homodimer

stability (K_D=17 nM). To ensure formation of heterodimeric constructs it was necessary to incubate 1:1 mixtures of WZA2 and WZB1 modified Hsp90 protein at elevated temperature. Thus the dissociation rate of WZA2 is increased and association with WZB1 is possible. A solution of 100 nM WZA2-Hsp90 and 100 nM WZB1-Hsp90 in buffer M was incubated for 1 h at 37 °C. The solution was diluted to 100 pM in buffer M containing 1 % glucose. 1 µl oxygen scavenger system was added to 250 µl protein-solution and immediately flown in to prevent dissociation of Hsp90 dimers. If the density of molecules on the surface was too low, the concentration was increased until sufficient single-molecules were visible. Unbound molecules were removed by washing with oxygen scavenger system in buffer M containing 1 % glucose.

2.4.3 Setup configuration

For single-molecule microscopy experiments a custom-built objective-type total internal reflection fluorescence (TIRF) microscope was used, placed on a vibration damped optical table (Linos). The Olympus IX71 inverted microscope was equipped with an oil-immersion objective (APON 60x, NA 1.49, Olympus) and a nosepiece stage (IX2-NPS, Olympus) for drift-reduction. Four different lasers of the multicolour-setup were applied, listed in Table 2-5. The excitation light was spectrally cleaned by a clean-up filter and all laser lines are overlaid on one pathway by mirrors and a combination of dichroic mirrors. Laser power could be further adjusted by a circular, variable neutral density filter wheel.

Table 2-5: Lasers and the respective clean-up filters used for excitation.

Laser	**Designation**	**Manufacturer**	**Clean-Up Filter**	**Manufacturer**
488 nm	Diode iBeam smart-488-S	Toptica Photonics	BrightLine HC 488/10	Semrock
514 nm	OPSLaser Diode System Genesis MX514-STM	Coherent	ZET 514/10	Chroma
558 nm	OPSLaser Diode System Genesis MX561-STM	Coherent	BrightLine HC 561/14	Semrock
640 nm	OPSLaser Diode System Genesis MX639-STM	Coherent	BrightLine HC 642/10	Semrock

The laser beam was widened by a 15 mm focal length achromatic lens and focused by a second lens on the back focal plane of the objective. A mirror that is installed together with the lens-system on a linear translational stage, enables a switch between TIRF, HILO and Epi illumination. The excitation light is reflected into the objective by a dichroic mirror. The emission light is collected by the same objective and transmits through the dichroic mirror. In two-colour measurements the emission light is spectrally separated by a dichroic beam splitter (Edge Basic 635 LP, Semrock) and filtered by dichroic bandpass filters before detection by two EMCCD cameras (iXon Ultra 897, Andor), installed on a two-camera adapter (TuCam, Andor). All filters used are listed in Table 2-6.

Table 2-6: Filters applied for filtering of excitation and emission light

Filter	**Manufacturer**
Dichroic mirrors	
HC Tripleband 403/497/574	Semrock
zt405/514/635rpc	Chroma
HC Tripleband 425/532/656	Semrock
Bandpass filters	
HQ 610/75	Chroma
ET 525/50	Chroma
BrightLine HC 582/75	Semrock
BrightLine 679/41	Semrock
Longpass filters	
Edge Basic 514 LP	Semrock

2.4.4 smPET measurements

Flow chambers were mounted on the microscope setup. A box was placed over the flow chamber to shield the probe from ambient light. For reduction of background signal, all measurements were done in TIRF-illumination mode. Signal intensity was amplified by an electron multiplying gain of 100 and a 1x1 CCD binning was applied. For reduction of thermal noise the CCD was cooled to -50 °C. The area of the CCD to be readout was reduced to pixels that showed homogenous

illumination. All single-molecule measurements were performed at room temperature.

2.4.4.1 One-colour smPET

Hsp90 possesses a very low inherent ATPase activity of only 0.2 ATP/min. Therefore, very long measurement times of at least 10 min were necessary to observe the main number of events. A very low laser-excitation power of 0.005 kW/cm^2, measured at Epi illumination directly after leaving the objective, was applied to prevent photobleaching. Applying a blend, the field of illumination was set as small as the chosen field of view of the camera chip. This prevented photobleaching in close proximity to the field of view. Frame rates of 1 frame per second with exposure times of 1 sec were applied. First, we measured the fluorophore stability at the chosen conditions. Measurements over a time frame of 600 sec were performed in buffer M containing 1 % Glucose and Oxygen Scavenger System. After switching to another field of view, measurements were performed in the same buffer with 4 mM AMP-PNP. After data collection of 600 frames, excitation was stopped promptly by closing of a shutter. Flow chamber was washed with 750 µl Buffer M without oxygen scavenger system, added carefully such that x,y,z-drift was kept at a minimum. The shutter was opened again and the measurement over a time frame of 600 sec was started immediately at exactly the same field of view.

The Oxygen Scavenger System served to remove oxygen from solutions by a coupled enzymatic reaction (Benesch and Benesch, 1953). Molecular oxygen is a potent quencher of an excited dye in its singlet and triplet state, the latter responsible for blinking (Hübner et al., 2001). Excitation energy is transferred to the oxygen molecule. This results in the formation of a higher energy species known as singlet oxygen that readily reacts with organic dyes and amino acid residues such as Cys, Met, His, Tyr and Trp, causing oxidative damage of dyes and amino acids (Aitken et al., 2008; Gracanin et al., 2009). Removal of molecular oxygen served to prevent photobleaching and also destruction of the Trp-molecule in a PET-reactive complex. For distinction between dyes that are quenched due to formation of a PET-reactive complex from dyes switched off by photobleaching, we applied this phenomenon vice versa. After the AMP-PNP triggered ATPase cycle was observed for

600 frames, the chamber was washed with buffer without oxygen scavenger system. Trp molecules within a PET-reactive state are readily oxidized. Thus the PET-complex is destroyed and the excited dye can recover into its ground state by photon emission.

2.4.4.2 Channel registration for two-colour measurements

Prior to and following every two-colour experiment, a registration sample is measured to allow for alignment of both detection channels. Therefore fluorescent microspheres of a size of 0.5 µm (TetraSpeck™, Thermo Fisher Scientific) were applied. Every microsphere is stained with four fluorescent dyes that are spectrally separable. Thus the same pattern of microspheres can be detected within both acquisition channels and is used for the generation of a transformation file for channel alignment (explained in 2.4.5.3). The TetraSpeck probe was mounted on the microscope sample holder. The setup configuration had to be exactly the same as used in the two-colour experiments. 200 frames with an exposure time of 20 msec were acquainted simultaneously. Laser power was adjusted such that a similar signal to noise ratio was reached in both channels, avoiding oversaturation of the CCD chip. Data acquisition was repeated at different regions within the sample, such that a reconstruction image with sufficient marker molecules in all areas of the image can be reached.

2.4.4.3 Two-colour smPET

Two-colour measurements were performed to observe conformational rearrangements simultaneously and in real-time. If there is directionality in the network of conformational rearrangements within Hsp90, the sequence of different motions might happen within a very tiny time lapse. Due to this it was important to choose the exposure times as low as possible to achieve a high temporal resolution. Because of the long measurement times needed to observe PET-events, very low excitation intensities were needed to prevent photobleaching. For the applied fluorophores AttoOxa11 and Atto542 the lowest excitation times with the best signal to noise ratio were reached at a laser power of 0.017 kW/cm² for excitation at 514 nm and 0.032 kW/cm² at 641 nm and an exposure time of 0.3 sec. Measurements were started simultaneously by setting the green camera in slave mode. Data acquisition was thus triggered by starting of the red camera. A negligible time

offset of ~ 20 msec was still present due to camera specific parameters. The dichroic mirror zt405/514/635rpc was used and emission light was filtered applying band-pass filters 679/41 (red camera) and 582/75 (green camera). Measurements were performed in buffer M containing 1 % Glucose and Oxygen Scavenger System with and without 4 mM of ATP or AMP-PNP nucleotide. In case of measurements performed in presence of AMP-PNP we used the same strategy as in one-color smPET measurements to distinguish between photobleached and PET-reactive dyes.

2.4.5 Data analysis

In this section all software-tools applied for localization and analysis of single-molecule PET trajectories are described.

2.4.5.1 Single-molecule localization analysis using rapidSTORM

The exact positions of single-molecules were determined applying the rapi*d*STORM software. A user manual and a detailed description of the applied single-molecule localization algorithms is given in (Wolter et al., 2014) and (Wolter et al., 2010). In short, an emitter's image is fitted to a two-dimensional Gaussian algorithm with the same full-width half maximum (FWHM) as given by the emitter's optical point spread function (360 nm and 300 nm for AttoOxa11 and Atto542, respectively). All identified localizations are reconstructed in an image by accumulation of data from each single frame. Image resolution in x- and y-position was set to 50 nm/pixel. A constant colour coding was chosen for display. Localizations within the red channel were displayed in red and in green within the green channel. A fluorophore-specific and laser power dependent threshold was set to filter noise. The x- and y-positions of each localization and in which frame they were detected are listed in an ASCII-text file. The open-source software rapidSTORM is free for download at the homepage of the department of biotechnology & biophysics, University of Würzburg (http://www.super-resolution.biozentrum.uni-wuerzburg.de/)

2.4.5.2 Analysis of one-colour smPET trajectories

To perform data analysis, a very stable microscope setup free of drift was crucial. The two image sequences recorded to identify molecules that were switched

into a PET-reactive complex, were concatenated in one video using FiJi. Only localizations identified within the first frame of the AMP-PNP measurement were considered for further analysis. This served to proof that signal changes are only arising from fluorophores that are specifically immobilised on the surface (non-specifically bound fluorophores could change position on surface, such that they could lead to new localizations during measurement). The x- and y-positions, listed in the rapidSTORM localizations file of frame 1, were displayed in the concatenated raw image sequence as an overlay in square form (5x5 pixel) applying the FiJi plugin RSView, kindly provided by Dr. Patrick Zessin (former PhD student at institute of physical and theoretical chemistry, Goethe University, Frankfurt). Overlays were added to the ROI-manager and minimum and maximum gray values of each frame within the ROI were analysed using the multi-measure tool.

Maximum gray values were further analysed for PET-reaction using an in-house written data-analysis software in Python language (Python 2.7), kindly provided by Sebastian Letschert. This script filters for smPET-traces that turn off during the AMP-PNP measurement and switch on again after washing with oxygen scavenger free buffer. Therefore a minimal gray value threshold was set to distinguish between on and off-state. A maximum gray value threshold was set to avoid collection of data arising from homodimers of dye-labelled subunits. Gray value fluctuations over time of filtered traces are displayed as an image and stored as png and txt files. The latter were further analysed for the time point at which the fluorophore turns off using Origin and listed in a table. These data represent the transition time of a single molecule into the PET-compatible conformation.

2.4.5.3 Alignment of two-colour smPET reconstructed images

Localizations identified in image sequences taken from different areas within the registration sample (2.4.4.2) were combined and reconstructed in an image using rapidSTORM. Reconstructed images of localizations within the two different camera channels were opened in Fiji. Alignment of the 2D images was performed using the Fiji plugin bUnwarpJ. This plugin performs elastic deformations based on B-splines of the source image until it represents the target image as precise as possible (Arganda-Carreras et al., 2006). Registration mode was set to mono, such that only the source image is being transformed to fit the fixed target image. A

sufficient number of landmarks (~50) was placed on TetraSpeck localizations identified in both channels. An elastic transformation matrix was calculated and saved. Reconstructed images of two-color smPET image sequences were opened in Fiji and aligned by loading the elastic transformation matrix in the bUnwarpJ plugin. It was crucial to choose the same channel as source image as was done in image registration.

2.4.5.4 Analysis of two-colour smPET trajectories

Aligned two-colour images were overlaid using Fiji. Co-localizations of green and red spots could be identified as yellow spots. These spots were selected for further analysis by placing an overlay in square form and adding it to the ROI manager. Raw image sequences were enlarged by increasing the total number of pixels to fit the size of reconstructed images. That way the selected ROIs identified in the reconstructed image matched to the raw data. Nonetheless the selected ROIs did not fit to the untransformed raw image sequence of the source image channel. Therefore, the untransformed source image was opened and ROIs were manually shifted to exactly the same spot within the untransformed image.

Minimum and maximum gray values of each frame within the ROI were analysed using the multi-measure tool. Maximum gray values within the two channels were further analysed and compared for PET-reactions applying an in-house written script in Python language, kindly provided by Sebastian Letschert. This data analysis software can detect steps within a 1-dimensional data array. A first order derivative of Gaussian wavelet convolution (dG) was applied. Briefly explained, this method estimates gradients after smoothing with a Gaussian function (Sadler and Swami, 1998). A standard deviation of 5 frames was set as default for the Gaussian kernel (sigma). This value efficiently filtered gradients caused by blinking events. Higher sigma values caused a low temporal resolution, such that events with a short residence time got lost. Estimated gradients were normalized by dividing gradient values with the maximum absolute value within each channel. This facilitated comparability of data from both channels despite vastly varying magnitudes.

Next steps were detected by application of 5 different filters, displayed schematically in Figure 2-4.

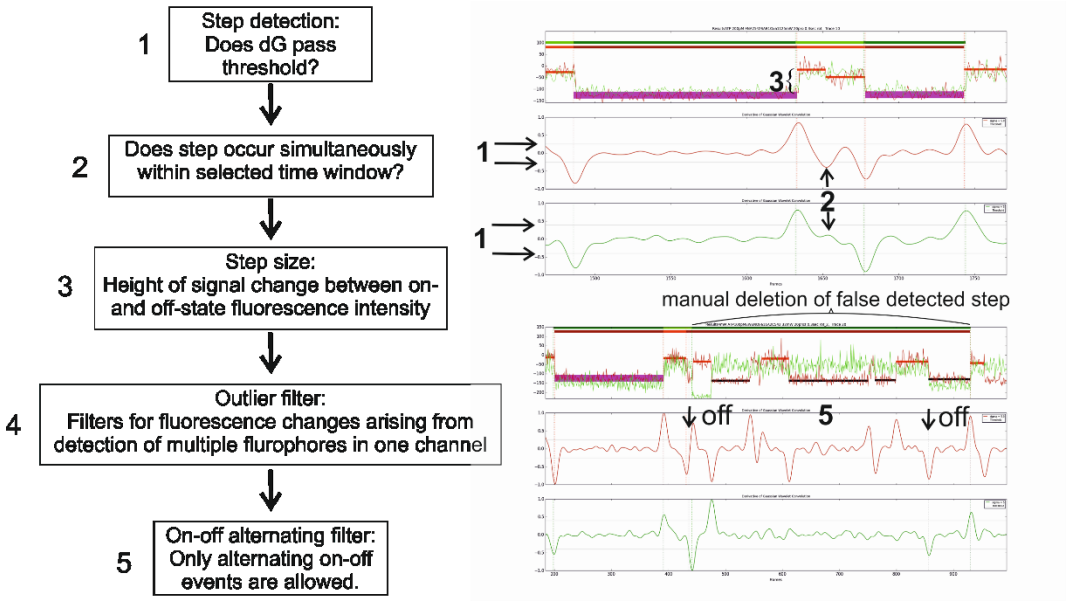

Figure 2-4: Schematic explanation of the two-colour smPET step detection script. The workflow for detection of steps by application of different filters is shown on the left. The figure on the right shows the analysed output figure of an analysed trace. Arrows indicate events at which the different filters got active. The lower figure shows an example for a false detected step. Therefore a manual deletion option was integrated in the python script. The detected steps are displayed by red and green bars (light colour = on state; dark colours = off state). The calculated mean fluorescence intensity of an identified PET-complexed state (magenta bars, dimmed off state) and of a blinking or photobleached state (black bars) within the red channel is indicated. The red bar shows the mean fluorescence intensity of the on-state.

In a first step, gradients passing a defined threshold are detected. The same kind of event must have been detected at a similar time point (±15 frames) in the second channel. Next the step size of an event, defined as the signal change between the two states, was estimated. Therefore, the mean fluorescence intensity of the two states was calculated out of 10 frames prior to and after the event. This was only done for the green channel, as the red fluorophore showed too strong fluctuations. The difference between the mean values had to be higher than a defined threshold. An outlier filter was implemented to prevent detection of gradients arising from detection of a second fluorophore within the same channel. Only if one event is followed by the opposite kind of event, the time in between those events is estimated as the residence time within one of the two different states (on-state and PET-complexed off-state). All detected steps within filtered traces were displayed

in a figure and had to be validated by the operator. Completely false filtered traces could be discarded. A built-in option allowed for manual adjustment of the default filter parameters, to delete or include events mistaken by the program. A text-file was generated that listed following information about detected events: the residence time within the on and off state of the respective fluorophore, the time offset between red channel and green channel (positive value = the event occurred first within the red channel, negative value = the event occurred first within the green channel) and the dim level of the PET-complexed stated. The latter was calculated by estimating the mean intensity of dye in on-state (set as 100 % intensity), in off-state (bleaching or blinking events, set as 0 % intensity) and in PET-complexed state. The dimmed state was only estimated for the red fluorophores, because blinking or photobleaching events were rarely detectable in the green channel. The dimmed state of green fluorophores was calculated manually applying the software Origin.

3 Results

3.1 Design of PET-reporter systems

3.1.1 Identification of suitable labelling site

PET-reporter systems for visualization of lid-closure, NM-domain association and ß-strand swap kinetics have been designed and implemented within the scope of my master thesis (Schulze, 2013). Suitable labelling sites were identified at positions that facilitate formation of a contact-induced PET-complex in the closed clamp conformation, while in the open clamp conformation dye and Trp are too far apart. PET only occurs at van-der Waals contact between fluorophore and Trp, requiring a distance at the subnanometer level. Therefore the crystal structures of the isolated NTD (PDB ID: 1AM1), resembling the open-clamp structure and of the full-length Hsp90 closed clamp conformation (PDB ID: 2CG9) were compared. Only solvent-exposed positions were considered as suitable labelling sites. Designed PET-reporter systems as well as amino acid positions mutated to alter Hsp90 function are shown in Figure 3-1.

Engineered Cys side chains were utilized as attachment site for maleimide-modified dyes. Lid-closure was probed by reporter system S51C/A110W. For visualization of a fast lid remodelling kinetic, positions were swapped (A110C/S51W), such that the fluorophore was placed on the moving lid element. ß-strand swap was monitored by placing fluorophore on the N-terminal ß-strand (A2C) of one subunit and Trp in waiting-position (E162W) on the second subunit. For visualization of NM-domain association, the fluorophore was attached to the NTD and Trp was placed in the MD (E192C/N298W).

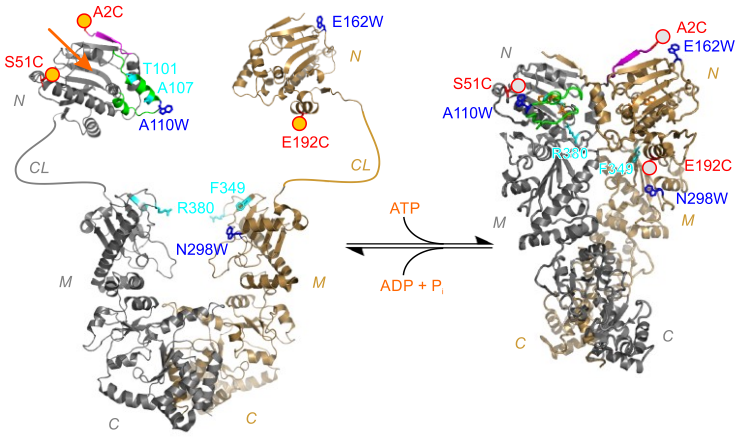

Figure 3-1: Illustration of Hsp90 in its nucleotide-unbound apo form (left), based on crystal structures of isolated NTD (PDB ID: 1AM1) and MC-domains (PDB ID: 2CGE) and in its AMP-PNP bound closed clamp conformation (PDB ID: 2CG9; right). Fluorophores are displayed as red spheres (orange filling = bright state; gray = dark state) and Trp by blue sticks. Lid structure and N-terminal ß-strand are shown in green and magenta, respectively. NTD (N), M-domain (M), CTD (C) and Charged Linker (CL) are marked. Positions of amino acids that were mutated to alter Hsp90 function are shown in cyan. Adapted from (Schulze et al., 2016)

3.1.2 Functionality tests of AttoOxa11-conjugated constructs

Designed PET-reporter systems were checked for functionality by determination of their ATPase activity. All reporter systems showed a similar or even higher ATPase activity compared to wt Hsp90 (Figure 3-2). It should be noticed that measurements reflect the ATPase activity of homodimeric AttoOxa11-conjugated constructs. In ensemble measurements the kinetics of heterodimeric Hsp90 constructs, consisting of a dye-labelled and non-labelled Hsp90 subunit (wt or E162W), were investigated.

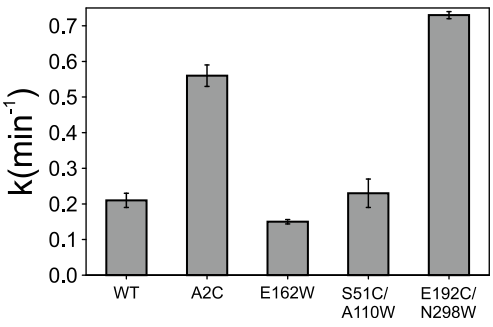

Figure 3-2: ATPase activities of AttoOxa11-conjugated reporter constructs and wild-type Hyp90 (WT), measured at 25 °C. Data represent mean values of three measurements ± s.d.

3.2 Kinetics of local motions measured in bulk

Part of the results of measurements performed in bulk and stated within this chapter have been published (Schulze et al., 2016). Figures and tables are partly adapted from this publication. A part of the results listed in Chapter 3.2.1 and 3.2.2 have already been obtained and discussed within my master thesis (Schulze, 2013).

3.2.1 Nucleotide induced conformational changes

Hsp90 is a slow ATPase with a hydrolysis rate of only 0.2 ATP/min at 25 °C under the buffer conditions used within this work (Figure 3-2). As the ATP-hydrolysis reaction itself is much faster than closure of the clamp (clamp closure is suggested to be the rate-limiting step in hydrolysis (Hessling et al., 2009; Krukenberg et al., 2011)), the closed-clamp conformation is short-lived and transient. In bulk measurements this state would be invisible due to the averaged signal over an ensemble of molecules in different states of the ATPase cycle (shown in Figure 3-3).

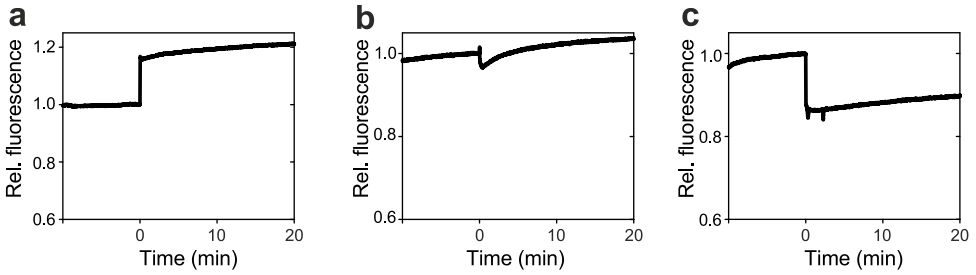

Figure 3-3: ATP-induced fluorescence changes over time measured for ß-strand-swap (a), Lid-closure (b) and NM-domain association (c). 2 mM ATP were added at t = 0 min.

Therefore the non-hydrolysable ATP-derivate AMP-PNP was used, to trap the clamp in its closed clamp conformation. Fluorescence changes over time triggered by the addition of 2 mM AMP-PNP to heterodimers of labelled PET-reporter constructs with non-labelled wt or E162W Hsp90 protein are shown in Figure 3-4.

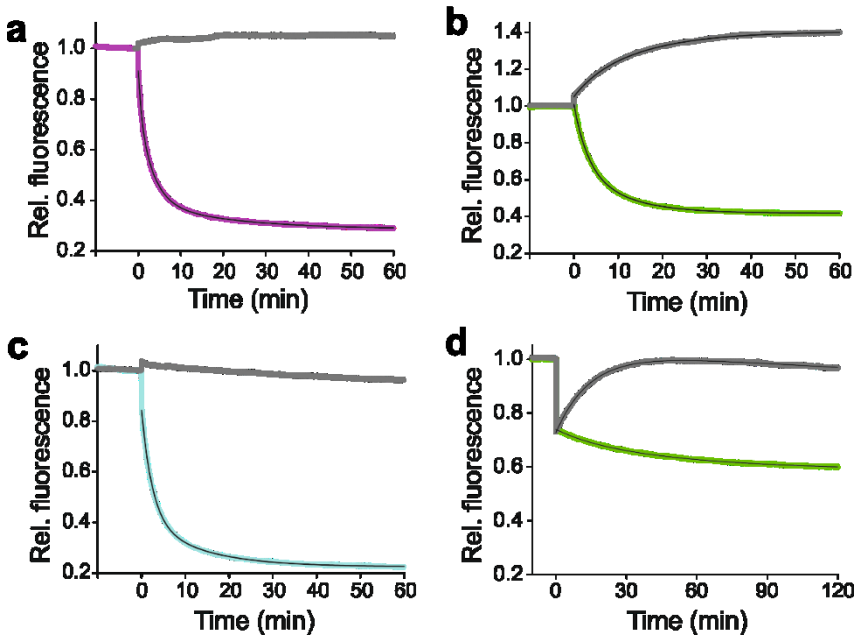

Figure 3-4: AMP-PNP induced fluorescence changes over time observed for PET-reporter constructs of ß-strand swap (A2C+E162W, magenta; a), Lid-closure (S51C/A110W, green; b), NM-domain association (E192C/N298W, cyan, c) and the reporter-construct for lid closure with swapped dye-quencher positions S51W/A110C (d) performed at 25 °C. 2 mM AMP-PNP were added at t = 0 min. Control measurements lacking the quenching Trp residue are shown in gray. Black curves show multi-exponential fits to the data (bi-exponential function applied in b and c, three-exponential in a). Adapted from (Schulze et al., 2016)

A strong decrease of fluorescence could be observed for the three reporter systems in Figure 3-4; a – c. To proof that fluorescence changes arose from PET-reactions between the introduced fluorophore and Trp-residue, control measurements were performed using dye-labelled constructs without the Trp-mutation. A constant fluorescence intensity was observed after addition of AMP-PNP for the ß-strand-swap and NM-association controls. However, a fluorescence increase could be observed for the Lid-reporter in b, probably due to a change in polarity in close proximity to the fluorophore. In d a very fast drop of fluorescence about 30 % could be observed within the dead time of the experiment, followed by a slow decay of fluorescence resulting from closure of the lid. This so called burst phase was also visible for the control-measurement, indicating that quenching is not caused by PET-complex formation. It is more likely caused by a fast lid-remodel-

ling kinetic of the dye-labelled lid-element resulting in a change within the fluorophores microenvironment. This burst-phase kinetic was further investigated in Chapter 3.2.4

Data were fitted using bi-exponential (Lid-closure and NM-reporter) or three exponential functions in case of the ß-strand swap reporter. Kinetic parameters are listed in Table 3-1.

While the multi-exponential behaviour of conformational switch raises the question to its origin (further investigated in Chapter 3.3), the overall mean rate constant of each local motion, calculated by the inverse of the sum of each time constant weighted by its amplitude, was similar and in good agreement with the ATPase rate (~ 0.2 ATP/min, Figure 3-2). This result suggests that the switch into the closed clamp conformation is controlled by local motions, acting cooperatively (see Chapter 3.2.2).

Furthermore it was checked whether ADP does also induce conformational changes. Therefore the measurements were repeated with 4 mM ADP, shown in Figure 3-5.

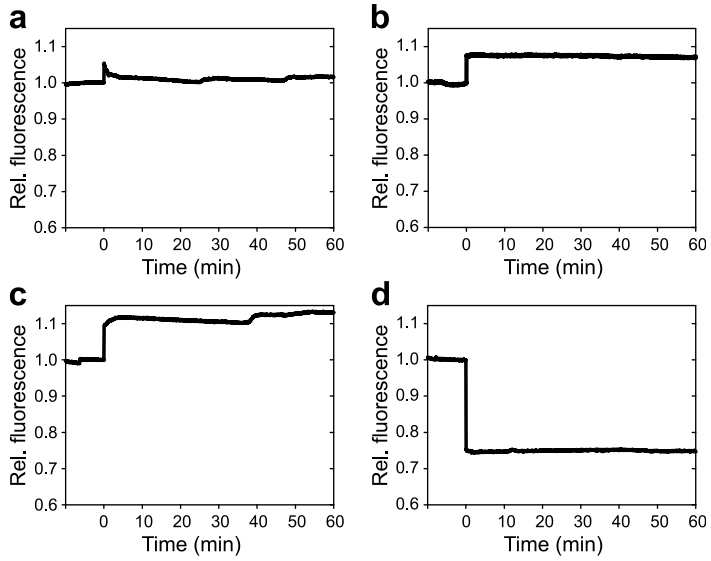

Figure 3-5: ADP induced fluorescence changes over time measured for ß-strand swap (a), NM-domain association (b), Lid-closure reporter S51C/A110W (c) and S51W/A110C (d). 4 mM ADP were added at t = 0 min. Adapted from (Schulze et al., 2016)

Only minor changes of fluorescence could be observed within the dead time of the experiments after addition of ADP. These might be explained by fast rearranging subpopulations of the different Hsp90 open-state conformers, causing a change to the fluorophores microenvironment. But no kinetics of local motions were detectable, proofing that the presence of γ-phosphate is a crucial trigger for conformational switch. Data show that the burst phase kinetic of the fast-remodelling lid element is not dependent on the presence of γ-phosphate (Figure 3-5, d).

3.2.2 Cooperation of local motions

Allosteric communication and cooperation of local motions was investigated by introducing single-point mutations in Hsp90 that cause a change in functionality and/or kinetics of conformational rearrangements.

It is proposed that the inhibiting mutation T101I stabilizes the lid in its open conformation via a hydrophobic interaction, while the mutation A107N has been shown to stimulate ATPase activity, probably due to an accelerated lid closure (Prodromou et al., 2000; Vaughan et al., 2009).

A highly conserved Arg at postion 380 is interacting with the γ-phosphate of bound ATP and thus provides a connector between the N-terminal and middle-domain. Mutation to Ala results in substantially reduced ATPase activity and is lethal in yeast (Cunningham et al., 2012). N- and M-domain association is very likely impaired by mutation R380A.

The N-terminal ß-strand was stabilized in its apo-state conformation. This was done by introduction of a so called Tryptophan-Zipper (TrpZip). Two Trp-side chains were placed on the N-terminal ß-strand (A2W) and on the neighbouring ß-strand (L160W, see Figure 3-6), leading to a substantial stabilization of the ß-hairpin fold (Cochran et al., 2001).

These mutations were introduced into Hsp90 PET-reporter system containing constructs and their effect on the respective local motion as well as on structural changes at remote positions was observed. Mutations were present within both subunits of heterodimers consisting of dye-labelled reporter constructs and non-labelled Hsp90. To measure the effect of the TrpZip-motif on ß-strand swap, heterodimers of A2W/L160W and dye-labelled E612C Hsp90 protein were formed. For mutants T101I and R380A we applied the reporter S51W/A110C, reporting on

the fast lid remodelling and slow lid-closure event. The observed time-dependent fluorescence changes of PET-reporter constructs on mutant Hsp90 protein are displayed in Figure 3-6. Fluorescence curves from wild-type measurements (Figure 3-4) are included for a better visualization of altered kinetics.

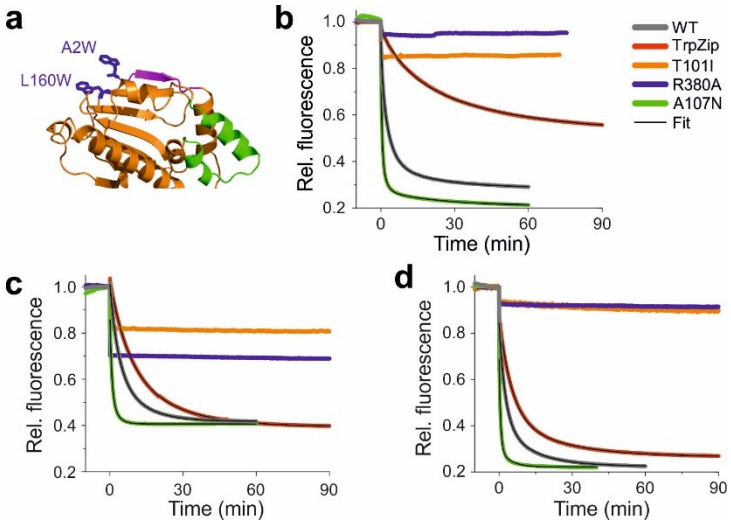

Figure 3-6: Influence of functional mutations on local motions at remote positions. The TrpZip-motif, introduced for stabilization of the N-terminal ß-strand in apo-conformation, is shown within the crystal structure of Hsp90 NTD (PDB ID: 1AM1, a). Time-dependent fluorescence changes of PET-reporter constructs on wildtype (WT, gray) and mutant Hsp90 protein (colour code depicted in legend) are shown for ß-strand swap (b), lid-closure (c) and NM-domain association(d). AMP-PNP was added at t = 0 min and measurement were performed at 25 °C. Adapted from (Schulze et al., 2016)

As expected, mutation R380A and T101I did abolish NM-domain association and lid-closure, but also all other investigated structural rearrangements. However, the fast lid-remodelling kinetic was still present in both mutants, even though less pronounced in T101I. ATPase activity stimulating mutation A107N showed accelerated kinetics and the TrpZip-motif decelerated kinetics of local motions. Bi- or three-exponential functions were applied to fit the data accurately. Fitting parameters of the individual reporter systems introduced in wild-type and mutant Hsp90 protein are listed in Table 3-1.

Table 3-1: Fitting parameters representing kinetics of conformational changes of Hsp90 measured at 25 °C

Mutant	Reporter	a_1[a]	k_1[a]	a_2[a]	k_2[a]	a_3[a]	k_3[a]	mean k[b]
wild-type	ß-strand swap	0.59 ±0.07	0.31 ±0.02	0.19 ±0.02	0.05 ±0.005	0.22 ±0.03	1.47 ±0.24	0.18 ±0.01
wild-type	NM association	0.68 ±0.05	0.41 ±0.03	0.32 ±0.008	0.08 ±0.007			0.18 ±0.02
wild-type	Lid closure	0.55 ±0.01	0.33 ±0.01	0.45 ±0.007	0.10 ±0.002			0.16 ±0.003
A2W-L160W	ß-strand swap[c]	0.35 ±0.07	0.10 ±0.01	0.65 ±0.04	0.02 ±0.001			0.03 ±0,0005
A2W-L160W	N/M association	0.72 ±0.04	0.20 ±0.01	0.28 ±0.04	0.04 ±0.004			0.10 ± 0.01
A2W-L160W	Lid closure	0.5 ±0.03	0.14 ±0.01	0.5 ±0.07	0.05 ±0.002			0.07 ±0.0005
A107N	ß-strand swap	0.61 ±0.05	2.47 ±0.37	0.27 ±0.05	0.62 ±0.10	0.12 ±0.03	0.05 ±0.01	0.34 ±0.03
A107N	NM association	0.84 ±0.02	1.63 ±0.05	0.16 ±0.02	0.20 ±0.04			0.78 ±0.06
A107N	Lid closure	0.32 ±0.09	0.40 ±0.08	0.68 ±0.14	1.37 ±0.21			0.79 ±0.08

[a] Rate constants $k_{1\text{-}3}$ ($1/\tau_n$ in min^{-1}) and the corresponding relative amplitudes $a_{1\text{-}3}$ of the individual phases contributing to the overall conformational change. Data represent mean values ± s.d. of three measurements.

[b] mean rate constant $k = \frac{1}{\sum_n a_n \tau_n}$

[c] A heterodimer of TrpZip mutant A2W/L160W and AttoOxa11 labelled E162C was formed

While in wild-type Hsp90 kinetics of local motions seemed to occur on a similar timescale, mutational studies show that the ß-strand swap seems to be weakly coupled to NM-association and Lid-closure. The latter are influenced equally by a slowed ß-strand swap (A2W/L160W) or accelerated lid-closure (A107N). However, motions of ß-strand swap seemed to occur subsequently on slower timescales.

To examine if changes in ß-strand kinetics or in Lid-closure and NM-association are directly expressed in an altered ATP hydrolysis rate, ATPase activity assays of

wild-type and mutant Hsp90 protein were performed. The relative increase or decrease in ATPase activity and kinetics of mutant compared to wild-type protein was calculated and is displayed together with the complementary relative change in rate constants (Figure 3-7).

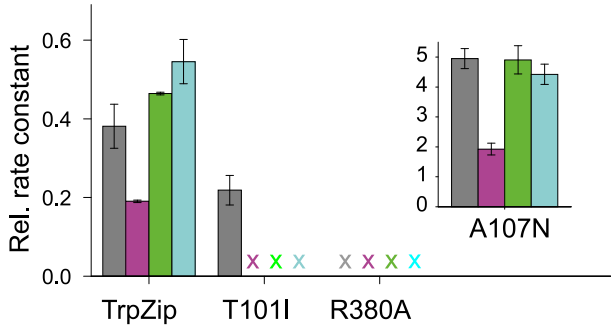

Figure 3-7: Relative rate constants of ATPase activity (gray bars) and local motions of the respective mutant compared to wild-type Hsp90. The colored bars show kinetics of ß-strand swap (magenta), lid-closure (green) and NM-domain association (cyan). ATPase assays of deactivating mutations TrpZip, T101I and R380A were performed at 37 °C and assays of accelerating mutant A107N were performed at 25 °C. Crosses mark non-detectable kinetics. Data represent mean values ± s.d of three measurements. Adapted from (Schulze et al., 2016).

Data show a clear connection between change in ATPase activity and kinetics of lid-closure and NM-domain association. ß-strand swap shows a lower influence on ATPase activity. Nonetheless it does possess a regulatory role, indicated by a lowered ATPase activity due to the TrpZip mutation.

The role of the middle domain catalytic loop was further investigated. The catalytic loop (F375 - I388 in yeast) interacts with a conserved, surface exposed hydrophobic patch (residues 342-352 in yeast) in the open state conformation. Upon binding of ATP, this interaction is loosened and the catalytic loop reconfigures to enable interaction with the ATP γ-Phosphate (Cunningham et al., 2012). Mutation of Phe-349 to an Ala shows decelerating effects on ATPase activity (Meyer et al., 2003). This residue might be involved in the right positioning of the catalytic loop in the closed but also in the open state conformation (Siligardi et al., 2004). The effect of this mutation on ATPase activity as well as on kinetics of local motions was investigated. Motions were slowed to a high extend (Figure 3-8b). But the mutation caused a severe decrease in AttoOxa11 quantum yield for the NM-reporter E192C/N298W (~ 50% reduced fluorescence intensity compared to NM-reporter without F349A mutation) further analysed within the next chapter.

3.2.3 Influence of co-chaperone Aha1 on local motions

The co-chaperone Aha1 is a stimulator of Hsp90 ATPase activity. This protein consists of an N-terminal domain that interacts with Hsp90 MD and a C-terminal domain that binds to Hsp90 NTD within the closed state-conformation. It is proposed that Aha1 binding induces remodelling of the catalytic loop and of the lid (Meyer et al., 2004; Wolmarans et al., 2016).

The influence of Aha1 on local motions was investigated. Motions were accelerated to such an extent that most of the kinetic events got lost within the dead time of the experiment. Therefore stopped-flow spectroscopy was utilized that covers events happening on fast time-scales in the order of milliseconds. Additionally, ATPase activity assays of Hsp90 with 20 µM Aha1 were performed and rate constants were compared with kinetics of local motions. These experiments were also performed on mutant F349A (described in former chapter), as Aha1 is capable of restoring the mutational effect on Hsp90 ATPase activity up to wild-type levels (Siligardi et al., 2004). Time-resolved fluorescence spectroscopy was sufficient to detect kinetics of F349A with Aha1. Data are shown in Figure 3-8.

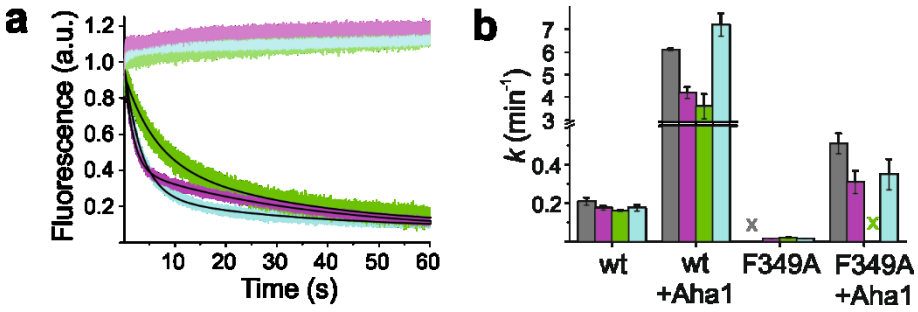

Figure 3-8: Co-chaperone Aha1 induced changes in kinetics of local motions. (a) Fast kinetics of lid-closure (green), ß-strand swap (magenta) and NM-association (cyan) of Hsp90 preincubated with Aha1. Control measurements of reporter-constructs lacking the quenching Trp residue are displayed in light colours. Reactions were started by rapid-mixing with AMP-PNP applying stopped-flow spectroscopy. Black curves show multi-exponential fits to the data. (b) Rate constants of wild-type (wt) and mutant F349A ATPase activity (gray bars) and local motions with and without Aha1. Crosses mark non-detectable kinetics. Colour code is consistent with a. Data represent mean values of three measurements ± s.d. Adapted from (Schulze et al., 2016).

AMP-PNP induced fluorescence decays behaved multi-exponential, consistent with measurements performed in absence of Aha1. Control measurements with constructs lacking the engineered Trp stayed constant, proofing specificity of the

detected kinetics. The increase in ATPase activity by Aha1 is again reflected in kinetics of local motions. An about 40-fold accelerated NM-domain association is in good agreement with the ATPase activity (6.1 ± 0.04 ATP/min for wt Hsp90). Lid-closure and ß-strand swap were accelerated to a lesser extent of ~20 fold. The faster kinetics of NM-domain association might be caused by the proposed Aha1 induced remodelling of the catalytic loop, which could induce a more closed conformation in which NTD and MD are preassociated.

The mutant F349A was ATPase-deficient and detected kinetics were negligible. This severe effect could be completely recovered by Aha1. Nonetheless, kinetics of Lid-Closure were non-detectable as addition of Aha1 caused a significant decrease in fluorescence of the Lid-reporter system. The amplitude of AMP-PNP induced fluorescence decays was thus too low to be fitted accurately.

To gain more insights into conformational changes caused by Aha1 binding to apo-Hsp90, a closer look was taken on changes in equilibrium fluorescence intensities of the investigated reporter systems upon addition of Aha1 (Figure 3-9).

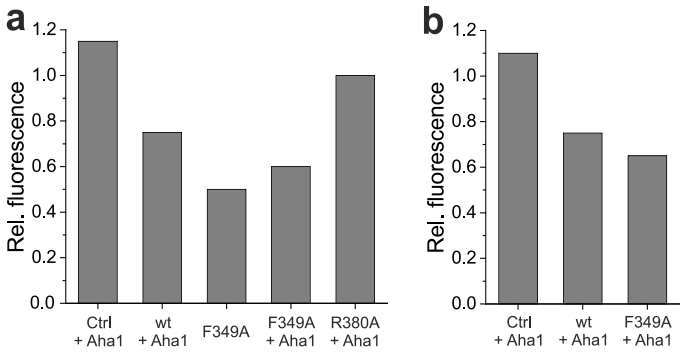

Figure 3-9: Effect of Aha1 on Fluorescence intensity of NM-association reporter E192C/N298W (a) and Lid-closure reporter S51C/A110W (b) on wild-type (wt) and mutant Hsp90 protein. Controls (Ctrl) were performed with constructs lacking the engineered Trp-residue. Data show the relative fluorescence compared to fluorescence intensity prior to addition of Aha1. Fluorescence of F349A on NM-reporter is compared to the average fluorescence intensity of NM-reporter on wt-Hsp90. Modified from (Schulze et al., 2016).

Like described in the former chapter, F349A caused a substantial decrease in QY of NM-domain association reporter (Figure 3-9, a). A possible explanation is a destabilization of the open conformation, such that a more frequent contact between NTD and MD might occur, reflected in higher PET-quenching events. Aha1 partially restored the loss in QY. As the control E192C did not-show a change in

fluorescence upon addition of Aha1, this change is not caused by a change in fluorophore microenvironment by Aha1. It is likely that Aha1 binding stabilizes an Aha1-bound specific open-conformation. This conformation might be directed towards a more closed clamp, as addition of Aha1 to wt-Hsp90 causes a decrease in QY in E192C/N298W reporter constructs. No fluorescence change was visible for the R380A mutant on NM-reporter system, indicating that Aha1 can't induce conformational change within this mutant.

Aha1 binding did also cause a fluorescence decay of ~ 25% (wt) and ~ 35% (F349A) within Lid-closure reporter S51C/A110W (Figure 3-9, b). This might again report on a more closed apo-conformation in the Aha1 bound state, as the control construct S51C, lacking the engineered Trp, did not show a decrease in fluorescence.

3.2.4 Two-state lid-closure kinetics

Fast burst phase kinetics of lid-closure reporter A110C/S51W were resolved using stopped-flow spectroscopy (Figure 3-10).

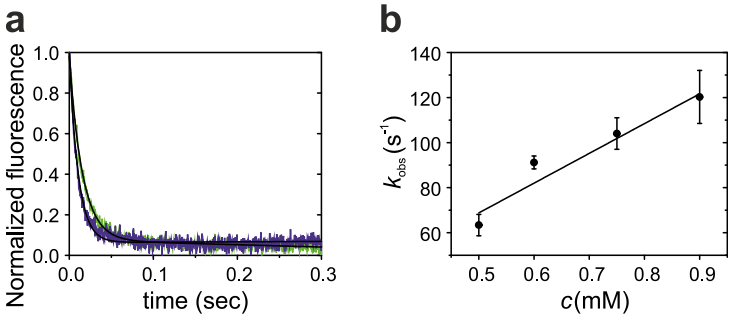

Figure 3-10: Fast lid-remodelling kinetics in dependence of nucleotide concentration. (a) Exemplary fluorescence decay curves of reporter S51W/A110C triggered by binding of 0.5 mM ADP (green) and 0.75 mM ADP (blue). Data were acquainted using stopped-flow spectroscopy. Each curve represents an average over three individual shots. Black curves describe a mono-exponential fit to the data. (b) Observed rate constants of lid-remodelling (black dots) show a linear dependence of ADP concentration (black line). The slope of the linear fit yields a bi-molecular rate-constant of $1.3 \pm 0.2 \times 10^5$ M^{-1} s^{-1}. Data represent mean values ± s.d of three measurements (performed at 25 °C). Adapted from (Schulze et al., 2016).

Fluorescence decay curves showed a dependence on nucleotide concentration. Data could be described accurately applying a mono-exponential fit function. The observed rate constant of lid-remodelling (k_{obs}) plotted versus ADP concentration showed a linear relationship with a bi-molecular rate constant of

$1.3 \pm 0.2 \times 10^5\ M^{-1}\ s^{-1}$. This value is in perfect agreement with the nucleotide association rate determined previously (Richter et al., 2002).

3.3 Single-molecule measurements

In the previous chapter, kinetics of local motions were discovered for the first time in bulk experiments. Local motions seemed to occur on similar timescales. But as kinetic traces represent average values over a vast ensemble of molecules, it is not possible to derive information about several conceivable scenarios: Local motions occur in a specific time order or local motions occur simultaneously or they occur just randomly. Furthermore, multi-exponential kinetics raised the question to about its origin. To address these questions, a single-molecule microscopy method was developed. First on the one-colour level in order to discover if it is in principle possible to detect PET-reactions using single-molecule microscopy.

3.3.1 Blocking efficiency of the surface

Every cleaned and DDS-Tween coated surface was tested for impurities prior to immobilisation of biotinylated and labelled Hsp90 constructs on the surface. Specificity of the Biotin-Neutravidin interaction could be granted by adding the biotinylated Hsp90 constructs (100 – 500 pM) to the surface before and after incubation with Neutravidin. Without Neutravidin no binding events should occur while in presence of Neutravidin homogenously distributed single-molecules should be visible. An exemplary specific binding test is shown in Figure 3-11.

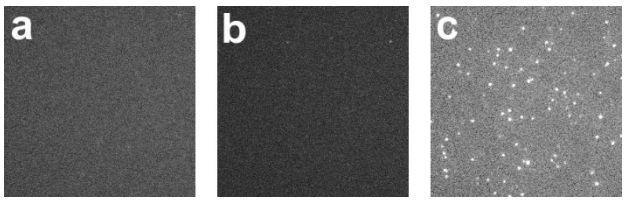

Figure 3-11: Specific immobilisation of biotinylated Hsp90 molecules on DDS-Tween20 passivated surface. Excitation at 641 nm, 0.06 kW/cm^{-2}, 0.5 sec integration time. Each picture shows a CCD-section of 35 x 35 μM in size. Autofluorescent impurities visible prior to addition of protein (a) Surface after incubation with 0.5 nM AttoOxa11 labelled, biotinylated Hsp90 protein before (b) and after (only 250 pM Hsp90, c) modification with Neutravidin.

The surface cleaning protocol successfully eliminates autofluorescent impurities on the glass surface. Also non-specific binding of Hsp90 was efficiently blocked at applied concentrations. It is to mention that phosphate buffer was applied in single-molecule measurements, while in bulk-measurements HEPES-buffer was used. This was done because the best blocking efficiencies were achieved in phosphate buffer.

3.3.2 Improved dimer stability of coiled-coil constructs

3.3.2.1 Functionality tests

To enable immobilisation of dimeric Hsp90 constructs on a single-molecule surface, modifications were carried out. The His-tag was switched to Hsp90's C-terminus, because prior to the avitag immobilisation strategy, it was tried to immobilise Hsp90 through the His-Tag, using Biotin-NTA. However, this method did not prove as feasible as no stable immobilisation was reached. Furthermore, an avitag and CC sequence was added to the C-terminus. Bulk experiments were repeated with these constructs in buffer M to check for an influence of modifications on local motions. As WZA2-CC possesses a decreased K_d of 17 nM, reaction mixtures of 150 nM dye-labelled Hsp90-CC with 5 µM of the non-labelled complementary CC were incubated for 1 h at elevated temperature (37 °C) to facilitate subunit exchange. These measurements were performed by Jonathan Schubert within the scope of his master thesis. Time-resolved fluorescence decay curves showed 10 to 20 % less overall change in fluorescence intensity (e.g. fluorescence intensity of NM-reporter was lowered about 80 % in wt but only about 60 % in CC-constructs after completion of the AMP-PNP triggered PET-reaction). Furthermore kinetics of local motions were slowed. To address the question if altered local motions are caused either by the CC or by the switch of the His-tag from N- to C-terminus, kinetics of local motions in C-terminal His-tagged Hsp90 constructs without CC and avitag were determined. Data are compared with N-terminal His-tagged constructs (derived from Table 3-1) and are listed in Table 3-2.

A switch in amplitudes was observed for ß-strand swap kinetics. While in N-terminal His-tagged constructs, the middle fast kinetic showed the main amplitude (0.31 min^{-1}), the fastest kinetic contributed to the main fluorescence change in

C-terminal His-tagged constructs (wt and CC). NM-association kinetics showed similar amplitudes, but a reduced mean rate constant for C-terminal His-tagged wild-type and CC constructs. Lid-closure amplitudes of C-His wt constructs did deviate highly. Except for ß-strand swap in C-His wt constructs, CC and C-His wt proteins showed slowed kinetics of local motions. But C-His kinetics were comparable to N-His kinetics with regard to the s.d. Kinetics of CC constructs were slowed to a higher extent, but as no complete PET-quenching efficiency could be achieved compared to wt Hsp90, it can be assumed that no complete subunit exchange was reached.

Even though changes in amplitude and rates of bulk kinetics of local motions were detected in modified Hsp90 proteins, local motions were still observable. If there is directionality within the network of functional conformational motions, C-terminal modifications shouldn't be able to alter this mechanism. Thus these constructs are applicable for use in single-molecule experiments to decipher if there is directionality within the Hsp90 ATPase cycle.

Table 3-2: Influence of CC sequence and His-tag position on kinetics of local motions at 25 °C. Measurements were performed in buffer S (N-term His) or buffer M (CC, C-term His)

Mutant	Reporter	a_1[a]	k_1[a]	a_2[a]	k_2[a]	a_3[a]	k_3[a]	mean k[b]
N-term His wild-type	**ß-strand swap**	0.59 ±0.07	0.31 ±0.02	0.19 ±0.02	0.05 ±0.005	0.22 ±0.03	1.47 ±0.24	0.18 ±0.01
WZA2-Oxa11 + WZB1		0.62	1.13	0.13	0.02	0.25	0.17	0.11
C-term His wild-type		0.53 ±0.09	1.32 ±0.22	0.12 ±0.03	0.07 ±0.01	0.36 ±0.06	0.33 ±0.05	0.30 ±0.04
N-term His wild-type	**NM association**	0.68 ±0.05	0.41 ±0.03	0.32 ±0.008	0.08 ±0.007			0.18 ±0.02
WZA2-Oxa11 + WZB1		0.70	0.19	0.30	0.03			0.08
C-term His wild-type		0.64 ±0.04	0.28 ±0.03	0.36 ±0.04	0.08 ±0.02			0.14 ±0.02
N-term His wild-type	**Lid closure**	0.55 ±0.01	0.33 ±0.01	0.45 ±0.007	0.10 ±0.002			0.16 ±0.003
WZB1-Oxa11 + WZA2		0.63	0.12	0.37	0.03			0.06
C-term His wild-type		0.43 ±0.11	0.19 ±0.03	0.57 ±0.09	0.07 ±0.007			0.11 ±0.03

[a] Rate constants $k_{1\text{-}3}$ ($1/\tau_n$ in min^{-1}) and the corresponding relative amplitudes $a_{1\text{-}3}$ of the individual phases contributing to the overall conformational change. Data represent mean values ± s.d. of three measurements, except for CC constructs, where only one measurement was performed.

[b] mean rate constant $k = \frac{1}{\sum_n a_n \tau_n}$

3.3.2.2 Dimer stability tests

The CC sequence was introduced to enable immobilisation of dimeric Hsp90 proteins at single-molecule concentrations (0.1 – 1 nM). Dimer stability improvement was checked by utilisation of a FRET reporter system, described in (Ratzke et al., 2010). Hsp90 D560C was labelled with Alexa488 (Donor) or Alexa594 (Acceptor). To ensure that most donor-labelled Hsp90 form a dimer with acceptor labelled Hsp90, the latter was added in a 5x excess in case of CC constructs (1:1 Stoichiometry in wt Hsp90) and heterodimer formation was facilitated by incubation

for 1 h at 37 °C. To eliminate cross-talk from acceptor excitation, an excitation wavelength of 485 nm was chosen. Emission spectra prior to and after chasing FRET-reporter constructs with an excess of non-labelled Hsp90 protein and time-resolved fluorescence decays of acceptor fluorescence are shown in Figure 3-12.

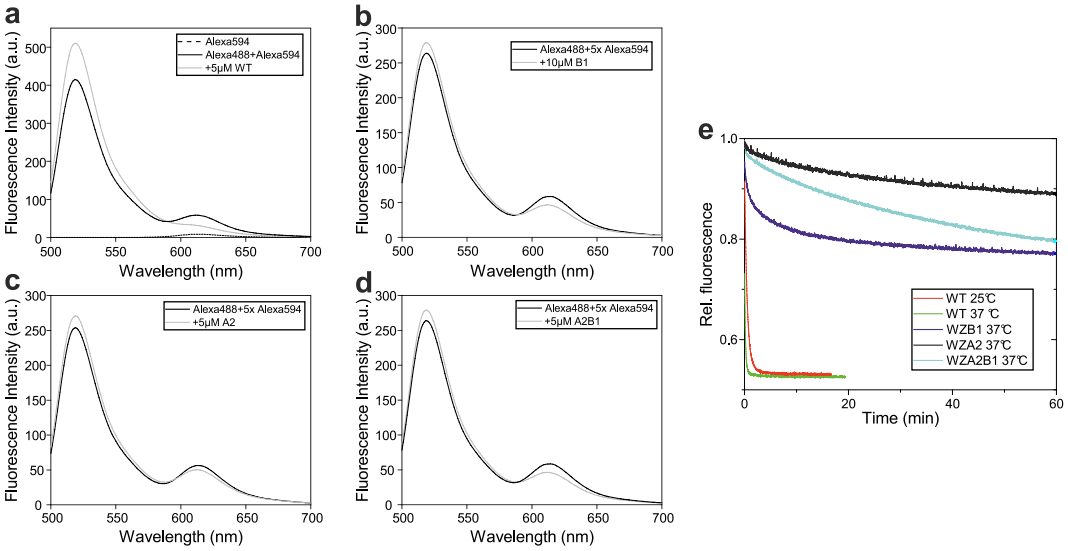

Figure 3-12: Dimer-stability tested by FRET-reporter systems. (a-d) Emission spectra of FRET reporter systems prior to (black lines) and after chasing with an excess of 5 or 10 µM non-labelled protein (gray lines) and 1 h incubation at 37 °C on wildtype (a), WZB1 (b), WZA2 (c) and WZA2B1 heterodimers (d). A cross-talk control of 100 nM Alexa594 labelled protein excited at 485 nm is shown in (a). Fluorescence decay curves over time are shown in (e).

The emission spectra of Alexa594 excited at 485 nm shows, that emission arising from cross-talk is negligible. FRET-spectra of wt-heterodimers show a complete subunit exchange of Alexa488-Hsp90 with non-labelled Hsp90. This can't be observed for homo- as well as heterodimeric forms of CC constructs after 1h incubation at 37 °C. Furthermore, acceptor fluorescence decay curves show that complete subunit exchange of wt Hsp90 occurs within a few minutes, while for CC constructs subunit exchange is highly slowed and after one hour incubation no saturation of fluorescence signal is reached, indicating no complete subunit exchange. WZB1 homodimers are less stabilised, which was expectable due to the low homodimer affinity with a K_D of 70 µM. Still WZB1 constructs seem to be more stable than wild-type Hsp90, maybe due to an antagonistic stabilisation effect of the native and artificial dimerization site. WZA2 and WZA2B1 heterodimers show an

extremely low subunit exchange and thus dissociation rate, well suited for single-molecule immobilisation experiments.

3.3.3 One-colour single-molecule PET

One of the biggest challenges in the detection of PET-events on a single-molecule level was to find a way to discriminate between fluorescence quenching by PET and photobleaching. First experiments were performed in an oxygen-including environment. The change of the number of fluorescence localizations over time was analysed in AMP-PNP free and AMP-PNP containing buffer. Unexpectedly, no differences were observable, indicating that either no PET-complexes were formed on the sm-level or that PET-quenched complexes were for some reason only transient. Experiments in an O_2 depleted environment gave the first hint that the last assumption is true. A faster decay and an overall higher change in number of localizations over time was observed in the presence of AMP-PNP if the buffer contained oxygen scavenger systems. Exchange with buffer lacking the scavenger system resulted in an increase of the number of localizations over time (Figure 3-13).

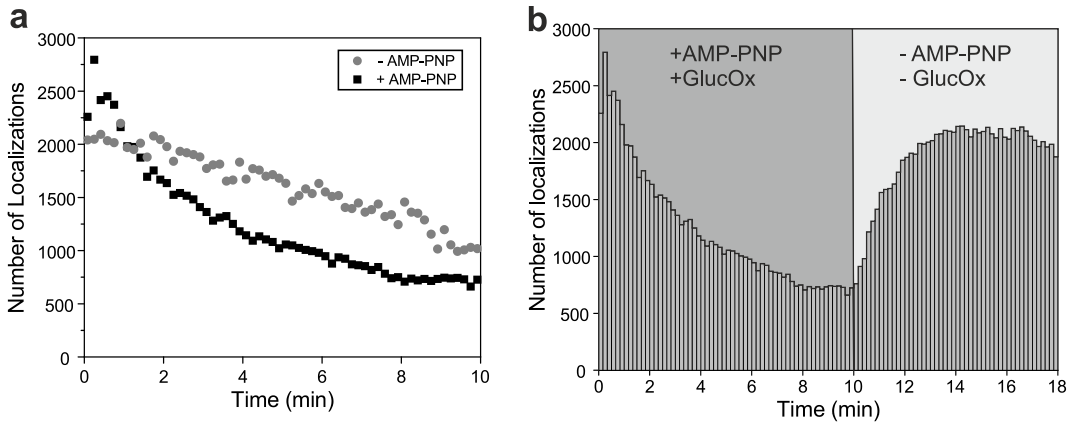

Figure 3-13: Changes in number of localizations over time for AttoOxa11 labelled NM-reporter constructs. (a) An exemplary bleaching curve (gray dots) and an AMP-PNP triggered PET-curve (black squares) are shown, measured in oxygen-depleted buffer. (b) The change in localizations measured at PET-reactive conditions (t = 0-10 min) and at the same field of view after buffer exchange in presence of oxygen (t = 10-18 min). GlucOx = oxygen scavenger system. Bin size = 10 sec.

The increasing number of localizations in presence of oxygen is an indication that the PET-quenched state is disrupted and the excited fluorophore can relax into its ground state by photon emission.

Disruption of PET-reactive complexes by oxygen was further examined as a potential tool for discrimination between PET and photobleaching events. Therefore, intensity changes over time of spots identified within the first frame of a measurement were analysed using FiJi. Indeed, the increasing number of localizations at oxygen conditions arose from recovery of fluorophores from a quenched off-state into a fluorescent on state.

Because of the high number of spots identified for evaluation on a single-molecule surface (~ 200 to 300 localized spots on ~50x50 μm field of view), an automated data pre-filtering algorithm had to be implemented. An in-house written software tool filtered for spots that fall beyond a certain threshold (defining the off-state) at PET-reactive conditions. These spots were further analysed for passing an on-state specific threshold after buffer exchange. In Figure 3-14 an example is given for spots that were identified as PET-reactive by the filtering software. False positives were filtered out by further manual data processing.

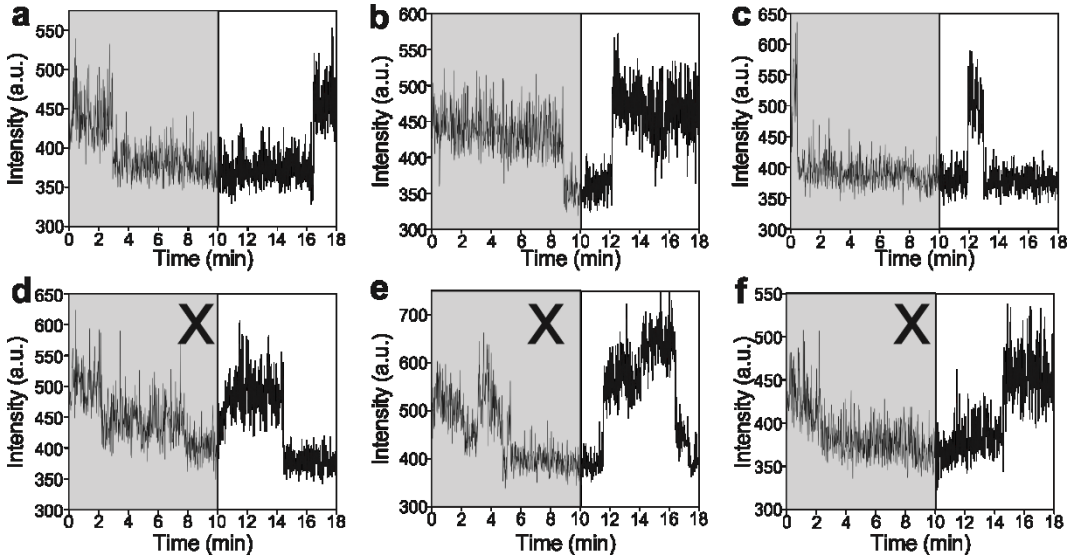

Figure 3-14: Exemplary traces filtered as PET-reactive candidates by the software tool. a – c shows correct filtered traces. d – f shows examples for false positives, discarded by manual data evaluation. Reasons were a too high fluctuation of on-state intensity (d and e) and not clearly distinguishable switch between on- and off (f)

All correct filtered traces were further evaluated for the length of time the molecule stays in the open state (on-state). Dwell-times in the open state were collected for the NM-domain association reporter system (heterodimer of Oxa11-labelled E192C-N298W-WZA2 and WZB1). A statistical pool of 274 PET events was gained. The individual dwell times were combined in a histogram and further analysed for the existence of subpopulations. Kinetic analysis of dwell time distributions has to be performed with care. Low bin width allow for a good time resolution, but the shape of the histogram becomes rougher, making it difficult to identify individual peaks. Larger bin width serve to smooth the histogram. Nonetheless, rare events might be hidden (Antonik et al., 2006). Figure 3-15, a shows a histogram calculated using a bin width of 20 sec. Data indicated the presence of at least three peaks. A Gaussian distribution model described the data well and was used to identify the centre of each individual peak. This method is valuable for the identification of subpopulations, which might switch into the closed clamp conformation via different reaction pathways. But as the breadth of the distribution and the individual rate constants might vary dependent on binning size and a sufficiently large statistical pool, this method is too liable to errors and was therefore not applied for analysis of the average rate constant (Brujic et al., 2007). A more robust analysis is provided applying a binning-independent data representation (Gebhardt et al., 2006). Cumulative sum plots of dwell time values were therefore fitted by an exponential function to identify the rate constant of NM-domain association (Figure 3-15, b).

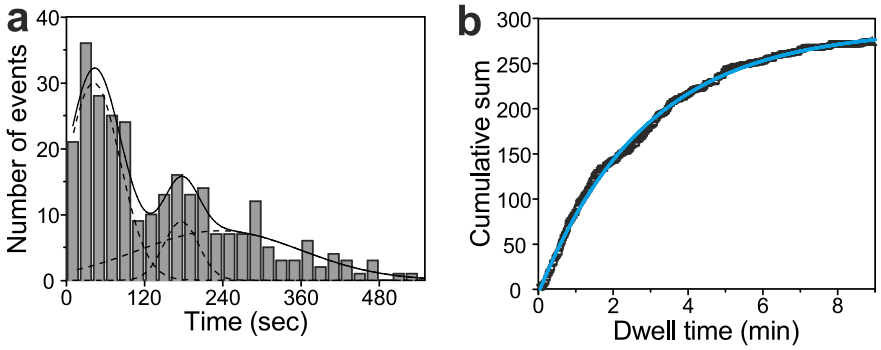

Figure 3-15: Dwell time distribution analysis. (a) Frequency distribution of dwell times. Binning size = 20 sec. Black curves show gaussian distribution fit to three identified peaks (dashed lines = fit to each individual peak, solid line = cumulative Gaussian distribution). (b) Cumulative sum plot of dwell time values. Blue curve shows a mono-exponential fit to the data.

Three gaussian distributed dwell time peaks were identified. The peak centres and the percentage of data spreading around this value are at 42 sec with 46%, 176 sec with 11% and 235 sec with 43%. Histogram indicated subpopulations are hidden in the cumulative sum plot of dwell time which could be well described by a single-exponential fit. A mean rate constant of 171 sec was estimated.

One-colour single-molecule measurements were continued on Lid-reporter and ß-strand swap reporter by Jonathan Schubert and are described in his master thesis (Schubert, 2017).

3.3.4 Two-colour single molecule-PET

Experiments on the one-colour level using AttoOxa11 as PET-quenchable dye confirmed that it is in principle possible to detect PET-events at the single-molecule level. The obtained data is a proof of the heterogeneity of local conformational motions detected in bulk measurements. Nonetheless, the results do not provide new information about a direct coupling or a specific sequence in which local motions occur. This information could be obtained by simultaneous observation of two individual local motion reporter systems within a single dimeric Hsp90 molecule. Therefore, several rhodamine dyes that are spectrally separable from AttoOxa11 were examined for their PET-quenching efficiency and their photostability. Prerequisites for applicability of a dye in single-molecule experiments are a high extinction coefficient ($\varepsilon > 50000\ M^{-1} cm^{-1}$) and a high quantum yield ($QY > 0.1$) (Roy et al., 2008). Thus a good signal to noise ratio can be gained.

Several fluorophores were examined for their single-molecule PET microscopy competence. This involves a good PET-quenching efficiency (Figure 3-16).

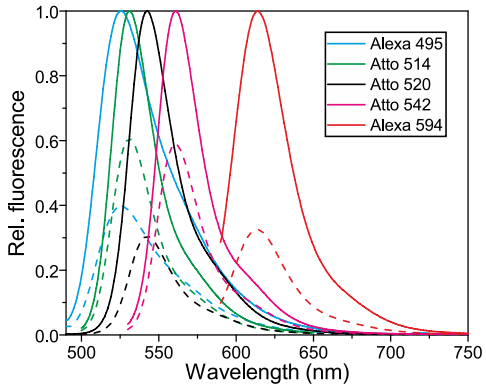

Figure 3-16: PET quenching efficiency of different dyes. Fluorescence emission spectra in absence (solid lines) and presence (dashed lines) of 25 mM Trp in buffer M.

Examined fluorophores are capable of contact-induced PET-quenching by Trp. A 40 - 70 % reduced emission intensity was reached in presence of 25 mM Trp. AttoOxa11 shows 80 % and Alexa488 50% reduced emission (personal communication with Dr. Hannes Neuweiler).

It could be assumed that a 40 % reduction in QY is too low to clearly distinguish between fluorescent and PET-quenched states within single molecules. However, measurements were performed under steady state conditions applying freely diffusing fluorophore and Trp. Differently high reduction in steady-state quantum yield could account for deviating affinities between Trp and the respective fluorophore and thus less efficiently or transient, unstable formed fluorophore-Trp complexes (Doose et al., 2009). In PET-reporter systems the quenching-reaction is not diffusion controlled. Depending on the contribution of static and dynamic quenching processes, the change in QY could be higher within PET-reporter systems. Therefore, all fluorophores were examined for single-molecule microscopy application.

NM-reporter systems were labelled with the respective fluorophore and immobilized on the single-molecule surface. Atto495 was not suitable for single-molecule experiments. Different laser power and acquisition time settings were tried, but either the signal was too weak or the fluorophore photobleached immediately. For each of the remaining fluorophores conditions were found at which a good signal to noise ratio required for single-molecule detection is reached. The changes in localizations over time were analysed in oxygen-depleted buffer in absence

(photobleaching curves) and presence of AMP-PNP. For better comparability, bleaching and AMP-PNP curves are displayed within one plot in Figure 3-17.

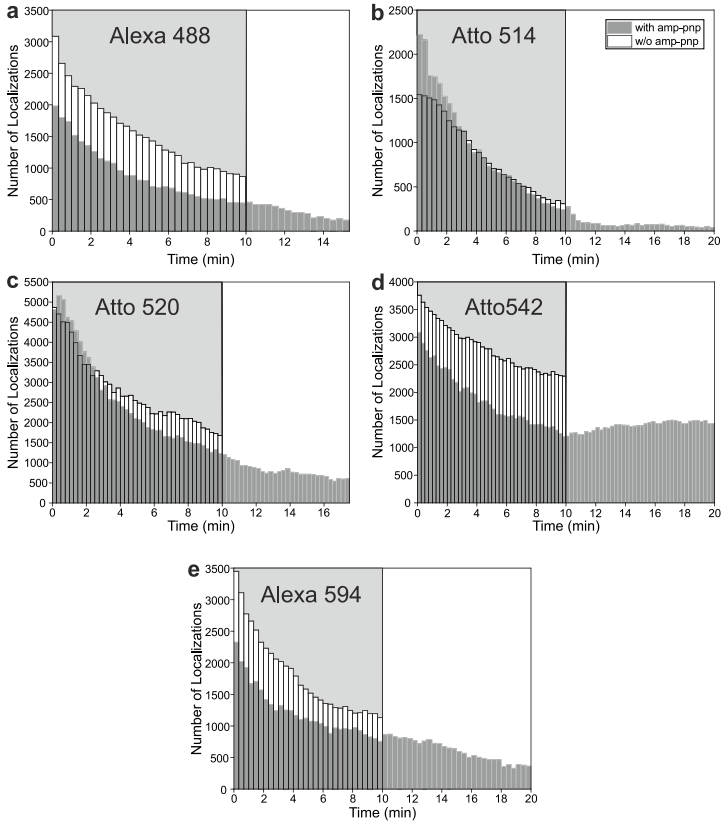

Figure 3-17: Changes in localizations over time for immobilised Hsp90 protein labelled with Alexa 488 (a), Atto514 (b), Atto520 (c), Atto542 (d) and Alexa594 (e). Histograms are calculated with a binning size of 10 sec. Measurements performed in the presence of AMP-PNP (gray filled bars) and absence of AMP-PNP (unfilled bars) in buffer M with oxygen scavenger system are represented at t = 0 – 10 min. At t > 10 min the change in localizations after washing with buffer M (oxygen including) was detected at exactly the same field of view measured at AMP-PNP conditions.

Measurements performed at AMP-PNP conditions were washed with buffer M without Oxygen Scavenger system and checked for an increase in localizations over time, indicative for destruction of PET-reactive complexes (compare with Section 3.3.3). No obvious difference was to assign for photobleaching and AMP-PNP curves of Alexa488 and Alexa594. Atto514, Atto520 and Atto542 do show a slightly different behaviour between PET-reactive and photobleaching conditions. However, Atto514 photostability was highly sensitive to oxygen represented by almost complete loss of localizations after washing with buffer M. Atto520 showed no change in the continuous reduction of localizations at oxygen conditions. But out

of the five analysed fluorophores, one promising candidate was identified. Atto542 showed a slight increase in the number of localizations at oxygen conditions, allowing for destruction of the PET-reactive complex. Furthermore, the slow and low decrease of localizations over time at AMP-PNP free conditions indicates that this fluorophore is very photostable and thus well suited for single-molecule applications.

In a first attempt, one-colour single-molecule experiments were repeated using Atto542 labelled NM-reporter systems. Indeed, traces were identified that switched off at AMP-PNP conditions and switched on after washing with buffer M. Bulk experiments were performed to check if Atto542 is able to report on kinetics of local motions. Fluorescence decay curves were recorded and compared to AttoOxa11 decay curves performed on CC-constructs (Figure 3-18).

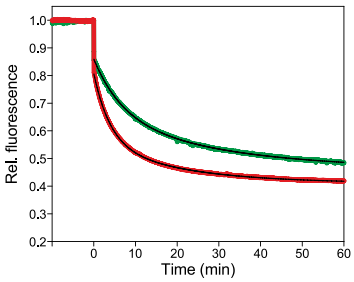

Figure 3-18: AMP-PNP triggered fluorescence changes over time detected for NM-reporter constructs on CC-reporter constructs labelled with AttoOxa11 (red) or Atto542 (green). Red lines represent a bi-exponential fit to the data.

Kinetics of NM-domain association were slowed in Atto542 labelled Hsp90-CC protein compared to AttoOxa11 labelled constructs (mean rate constant of ~ 0.06 min^{-1} compared to ~0.1 min^{-1}) . Nonetheless, this should not be of concern. The aim of two-colour experiments is to find out, if there is directionality within the network of local motions. If this is the case, altered kinetics due to Atto542-labelling would be reflected within the AttoOxa11 labelled subunit of heterodimeric two-colour constructs.

In one-colour experiments, kinetics of local motions could be evaluated from 10 to 15 % of molecules localized on the surface. This low amount is caused for example by interference of photobleaching events as well as presence of monomeric or double labelled homodimeric Hsp90 constructs.

In two-colour experiments there is one-more point to consider: the degree of labelling. If for example a DOL of 0.5 is reached for each fluorophore and efficient subunit exchange in a 1:1 stoichiometry is expected, only 25 % of dimeric Hsp90 would carry two fluorophores. Therefore, only reporter constructs with a DOL > 0.5 were used in two-colour experiments.

In one-colour experiments, only fluorophore-labelled Hsp90 proteins were biotinylated and immobilised, while the unlabelled and non-biotinylated protein was always present at a concentration of 1 µM, far above the K_D. In that way the equilibrium should be on the dimeric Hsp90 form.

In two-colour experiments it is not possible to add one dye-labelled subunit in excess to the buffers. The background would increase due to freely diffusing dye-labelled proteins, even at TIRF-illumination mode. Furthermore, efficient blocking of non-specific binding is only granted at protein concentrations at the x·10 nM range. For this reason, the CC was introduced. The purpose of this structure was improvement of the K_D mainly due to a lower dissociation rate, such that a formed dimer is stable over long timescales. To facilitate a homogenously distributed single-molecule surface with a low protein density, 1:1 mixtures of biotinylated AttoOxa11- and Atto542-labelled Hsp90 had to be diluted to a concentration of 100 pM (K_D WZA2B1 = 1.4 nM) prior to application to the single-molecule surface. At a sufficiently high dimer stability, dissociation of the preformed heterodimers should be prevented within the time span between dilution and loading into the flow chamber. CC-constructs do dissociate much slower compared to wild-type Hsp90, as shown in Figure 3-12. After binding to Neutravidin, the two subunits within the dimer are kept in close proximity, such that each dissociation event would result in fast re-association with the same subunit.

Immobilisation of heterodimeric two-colour constructs was successful. An example overlay of a red and green channel localizations stack is shown in Figure 3-19.

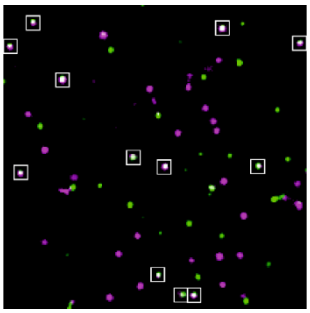

Figure 3-19: Colocalizations identified on a 10.7 x 10.7 µm section. Overlay of AttoOxa11 (magenta) and Atto542 (green) labelled Hsp90 molecules. Colocalizations are identified as white spots and are marked by white boxes. The image represents a stack of localizations identified in a 1200 frames image sequence (acquisition time 0.3 sec /frame).

First each channel was screened separately for occurrence of AMP-PNP induced PET-reactions, followed by analysis if positive spots can be assigned to co-localizing molecules. The yield was very low. One reason for this is that both dyes within a co-localizing molecule should not bleach within the 10 min acquisition time span. The few identified spots showed a simultaneous switch into the off-state, but the number of events was too low to be statistical relevant.

Because of the low yield of co-localizing AMP-PNP triggered PET-reactive spots, these measurements were not further pursued. Instead, it was tried to examine the complete ATPase cycle consisting of clamp-closure and clamp-opening processes by application of ATP instead of AMP-PNP. This was not possible in one-colour experiments, as differentiation between PET and bleaching was only possible by oxidation of Trp in the closed-clamp PET-reactive complex. In two-colour experiments, a clear difference between intensity fluctuations in absence and presence of ATP was recognized. In absence of ATP, fluctuations in the two channels were completely random while in presence of ATP intensity fluctuations were occurring simultaneously. However, AttoOxa11 exhibits a very strong blinking behaviour in two-colour measurements, while the green fluorophore shows very constant emission levels. Fluorescence intermittency of AttoOxa11 was not caused by the respective PET-reporter system, as shown by a swap of fluorophore positions (Figure 3-20).

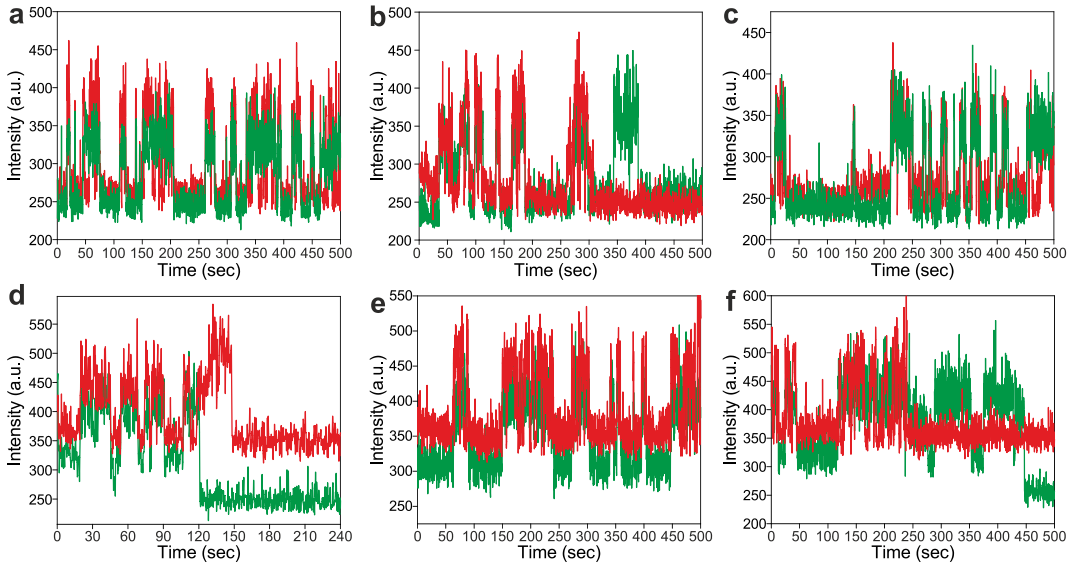

Figure 3-20: ATP-triggered fluorescence fluctuations over time observed within co-localizing single-molecule traces. (a-c) Heterodimers of E192C/N298W/E162W-WZA2-Atto542 (NM-reporter, green) and A2C-WZB1-AttoOxa11 (DS-reporter, red). (d-f) Fluorophore positions are switched (red = AttoOxa11 labelled NM-reporter, green = Atto542 labelled DS-reporter).

Atto542 showed very stable fluorescence emission when attached to NM-reporter as well as DS-reporter systems. Every switch into the off-state was accompanied by a simultaneous off-switch of AttoOxa11. However, AttoOxa11 did show additional very fast fluorescence fluctuations as well as some longer lasting off-states (for example in Figure 3-20, a at t ~ 50 sec and in f at t = 150 – 250 sec). Because fast, non-simultaneous fluctuations were not detectable when Atto542 was labelled to exactly the same PET-reporter systems, these fluctuations are rather of photophysical than of biological nature.

Furthermore, in d and f two clearly distinguishable intensity states are visible in the green channel: a dimmed state (0.39 ± 0.07 rest fluorescence, assigned to PET-complex) and a completely switched off state (bleached). This was not observable when Atto542 reported on NM-domain association (Figure 3-20, a – c).

Atto542 reported very reliably on PET-events and these were in almost all cases accompanied by the same kind of event (off- or on-switch) of AttoOxa11-labelled reporter. Therefore, only simultaneously occurring AttoOxa11 fluorescence fluctuations were considered as PET event.

Dimmed fluorescence in PET-reactive complexes was also observable for AttoOxa11 (0.17 ± 0.05 rest fluorescence) as well as Atto542 (0.18 ± 0.09 rest fluorescence) labelled to lid-closure reporter system (Figure 3-21). But no clear difference between PET-reactive state and background was to assign for both fluorophores on NM-reporter systems (Figure 3-20, d-f; Figure 3-21, a-b) and AttoOxa11 labelled to DS-reporter systems (Figure 3-21, c-d; Figure 3-20, a-c).

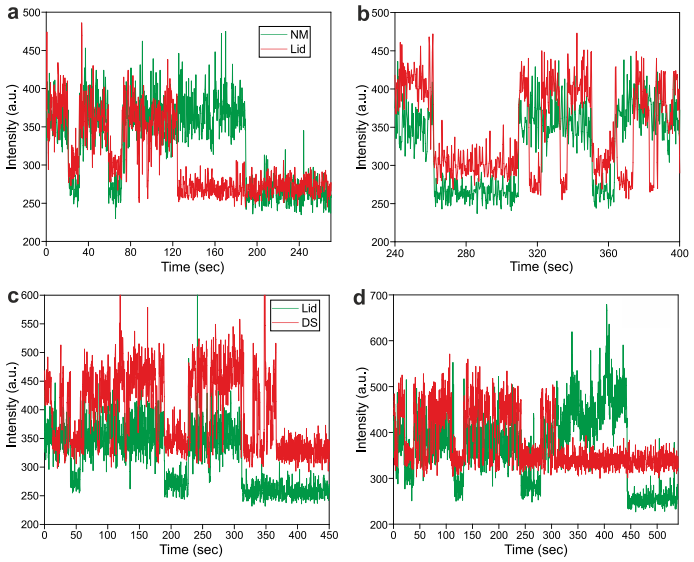

Figure 3-21: Identification of dimmed states in PET-reactive complexes. ATP triggered fluorescence fluctuations for Atto542 labelled NM-reporter (green, E192C/N298W-WZA2) and AttoOxa11 labelled Lid-reporter (red, S51C/A110W-WZB1) (a-b) and for Atto542 on lid-closure reporter (green, S51C/A110W/E162W-WZB1) and AttoOxa11 on DS-reporter (red, A2C-WZB1) (c-d).

The reason for the strong fluorescence fluctuations of AttoOxa11 were further investigated. AttoOxa11 was not prone to such strong photophysical events in one-colour experiments. In two-colour experiments, both fluorophores are excited simultaneously at a wavelength of 514 nm and 641 nm. Furthermore, a higher 641 nm laser power was used compared to one-colour experiments, to achieve a higher time-resolution (0.3 sec instead of 1 sec). Therefore, stronger blinking is either caused by a higher excitation power or by the presence of two-fluorophores within one Hsp90-dimer or by simultaneous excitation with 514 nm laser light. Last case was examined by switching off the 514 nm laser in two-colour experiments (Figure

3-22, d – f). The same strong blinking behaviour was observed as upon simultaneous green light illumination (a – c). Additionally, in very rare cases an energy transfer from green to red dye (FRET) was observed (b).

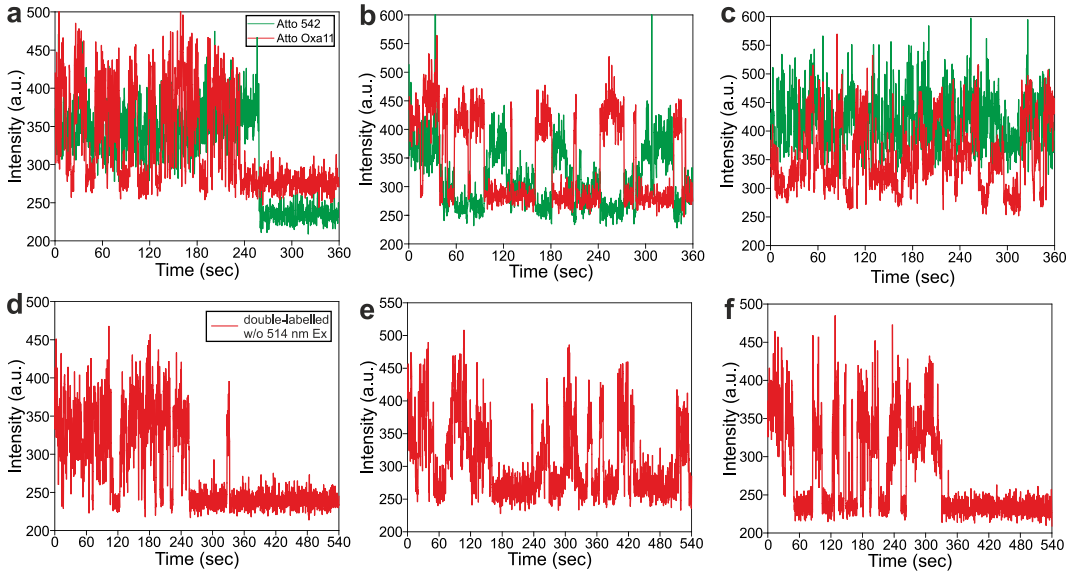

Figure 3-22: Example single-molecule traces representing the photophysical behaviour of AttoOxa11 in oxygen-depleted buffer in absence of nucleotide. In a – c single-molecule traces of co-localizing Lid-Atto542 and DS-AttoOxa11 labelled constructs are shown. Simultaneous excitation with laser light of λ = 514 nm and λ = 641 nm was applied. In d – f the same probe was analysed, the 514 nm laser was switched off and only the emission behaviour of AttoOxa11 was detected.

Two-colour single-molecule traces were examined for the existence of a specific time order, in which motions occur. Therefore, the potential time offset between an event happening in the green channel and the same kind of event (on- or off-switch) happening within a time window of ± 15 frames in the red channel was examined (acquisition time of 0.3 sec/frame). The chosen time window was set as threshold, to prevent analysis of false positive PET-events that are very likely caused by AttoOxa11-fluctuations. Because the switch between states sometimes happens gradually within two frames, only offsets of more than ± 1 frame are reliable. This gradual switch is very likely caused by an event happening within the middle of the acquisition time of a frame. Histograms of closure and opening offsets of all combinations of reporter systems examined within this work are represented in Figure 3-23.

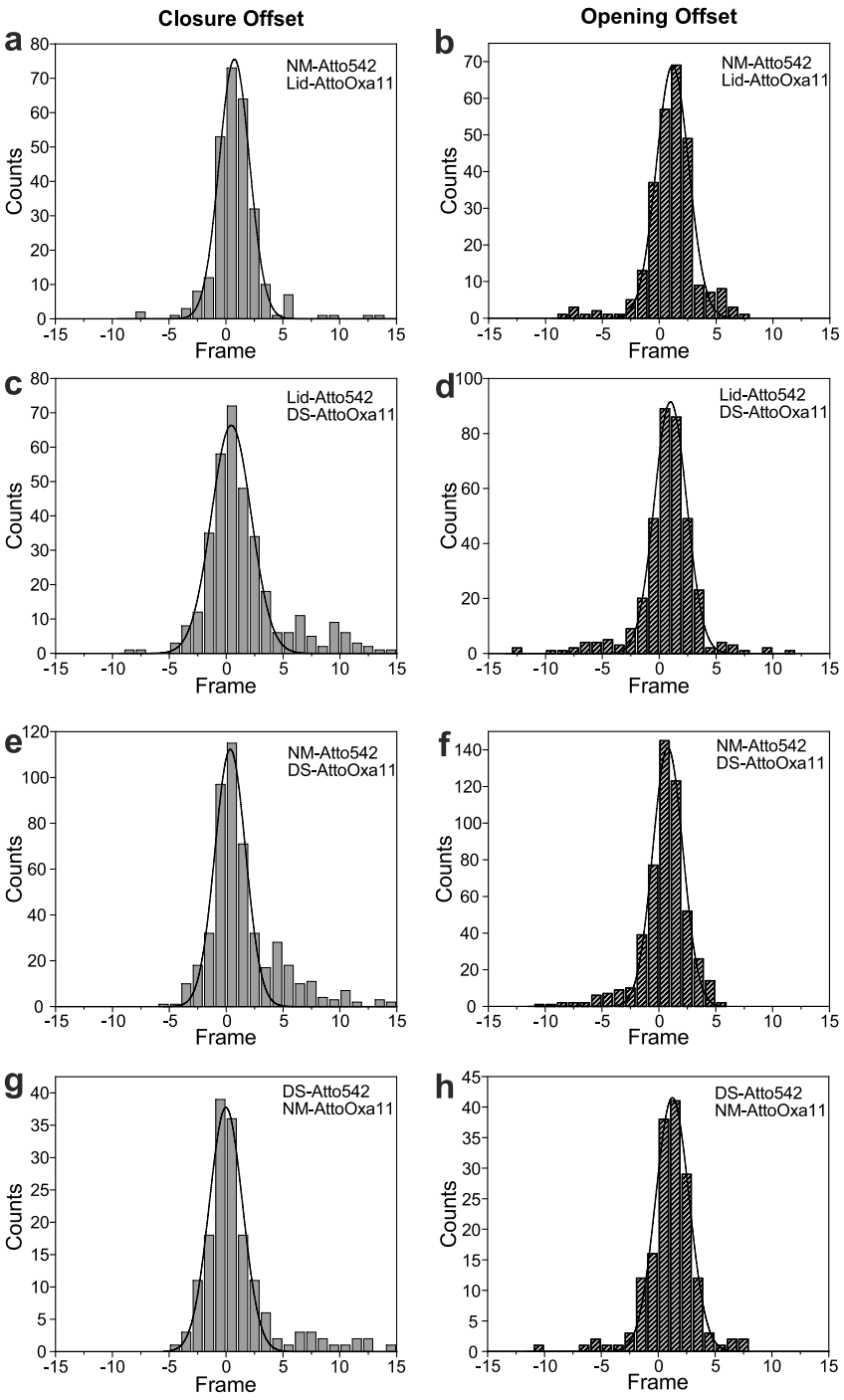

Figure 3-23: Closure- and Opening Offset of Atto542-labelled reporter in relation to Atto Oxa11-labelled reporter systems. Histograms are calculated with a binning size of 1 frame (0.3 sec/frame). A positive value means a delayed transition and a negative value an earlier transition of the Atto542-labelled construct. The closure offsets (off-switch) are shown on the left and the opening offsets (on-switch) on the right. Black lines represent a Gaussian distribution fit to the data.

Opening and Closure Offsets were Gaussian distributed with a centre located around frame 0. The exact peak-centres of each fit are listed in Table 3-3. A slight tendency to positive values can be noticed, which would be representative for an earlier switch of the red-labelled reporter into the closed or open state. However, this tendency is independent of the reporter-systems under investigation. For example e/f and g/h show exactly the same reporter-combination, but with switched dye-positions. If NM-domain association and domain swap would happen in a specific order, histograms should behave inversely.

Table 3-3: Opening and Closure Offset of the green relating to red-labelled reporter systems. Data represent the peak-centre of a Gaussian distribution fit ± s.e. of the fit.

Reporter	Offset green compared to red (in number of frames)	
	Opening	Closure
NM-WZA2-Atto542 / Lid-WZB1-AttoOxa11	1.16 ±0.07	0.74 ±0.03
Lid-WZB1-Atto542 / DS-WZA2-AttoOxa11	0.99 ±0.04	0.45 ±0.08
NM-WZA2-Atto542 / DS-WZB1-AttoOxa11	0.79 ±0.06	0.36 ±0.11
DS-WZB1-Atto542 / NM-WZA2-AttoOxa11	1.24 ±0.06	-0.02 ±0.08

The time the fluorophore resides in on- or off-state (dwell time in open- or closed state conformation) was further analysed. Data was handled on the same way as in one-colour experiments (compare with Figure 3-15). Histograms with a bin size of 20 sec were calculated. This data representation model is valuable for the identification of subpopulations. For a more robust analysis of opening- and closing kinetics, binning independent cumulative sum plots were fitted by mono- or bi-exponential functions. In one-colour experiments the ATPase cycle was analysed in the presence of AMP-PNP, trapping the chaperone in its closed clamp conformation. Only information about dwell-times of the open-state conformation could be derived. In two-colour-experiments the ATPase cycle was analysed in the presence of ATP. Thus it was possible to gain additional information about the closed-state dwell time. In Figure 3-24 histograms and cumulative sum plots of the three

different reporter combinations (DS/Lid; DS/NM; Lid/NM) are shown. Because events occurred simultaneously in the majority of cases (compare to Figure 3-23), graphs taken from Atto542 and AttoOxa11 labelled reporter system in the two-colour heterodimer were identical. Therefore, only one histogram and cumulative sum plot is shown for each state within the respective heterodimeric construct (Figure 3-24).

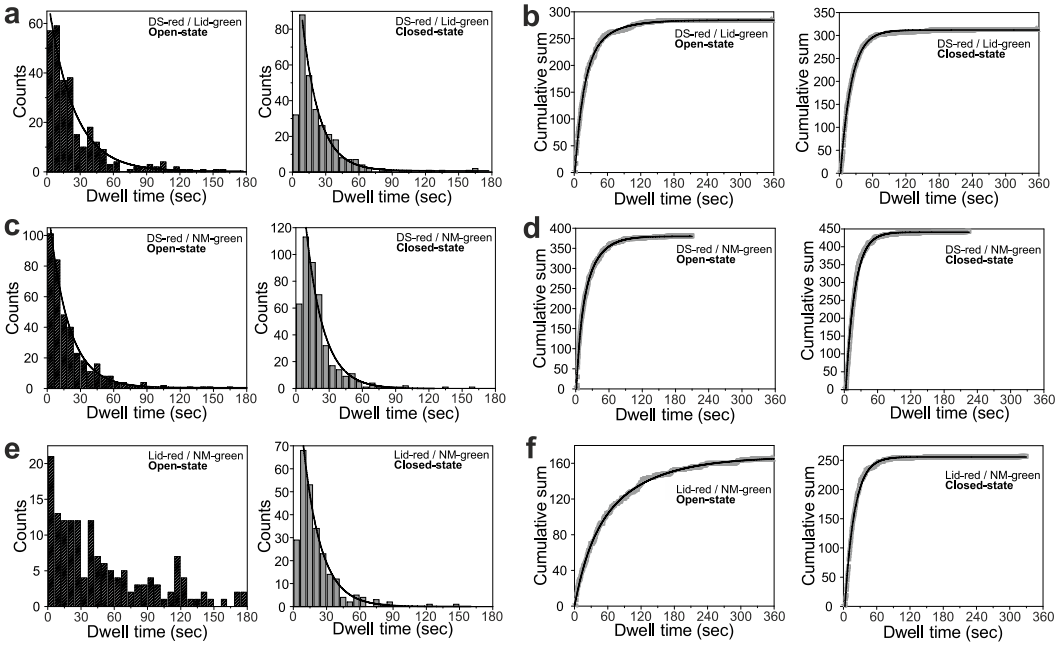

Figure 3-24: Dwell-time analysis of open- and closed-state conformations of different reporter-system combinations. Histograms were calculated with a bin size of 20 sec (a, c, e). Histogram data could be described by a mono-exponential fit function (solid line), except for the open-state histogram in e. In b, d and f the data is represented as a cumulative sum plot (grey boxes). Mono- or bi-exponential fits were used to describe the data accurately (solid line).

The largest statistical pool of open- (> 370) and closed-state (> 440) dwell-time data has been accumulated in DS/NM reporter combination (c and d). The histograms show a mono-exponential decaying dwell-time distribution. In DS/Lid reporter combination, a smaller statistical pool was gained and the open-state dwell times are less-well exponentially decaying (left graph in a). In Lid/NM reporter combinations the lowest number of open- (< 170) and closed-state (< 260) dwell-times was collected. Open-state dwell-time distribution can't be described by an exponential function and could lead to the assumption of subpopulations.

All analysed reporter combinations indicated that local motions occur simultaneously at a temporal resolution of 0.3 sec. Keeping this in mind, exactly the same kinetics and distributions of open- and closed state dwell-times can be expected. This was not the case because differently large statistical pools were analysed. The larger the statistical pool the more evenly the data were distributed. Therefore, c and d most likely represents the most reliable information about kinetics and subpopulations in clamp – closure and opening events. Fitting parameters, derived from cumulative sum plots, are listed in Table 3-4.

Table 3-4: Fitting parameters representing kinetics of clamp-closure (open-state dwell-time) and clamp-opening (closed-state dwell-time).

	Reporter	N[a]	a_1[b]	τ_1[b]	a_2[b]	τ_2[b]	mean τ[c]
Open	NM-WZA2-Atto542 / Lid-WZB1-AttoOxa11	167	0.67 ±0.02	92.2 ±2.2	0.33 ±0.02	26.3 ±1.4	70.5 ±3.2
	Lid-WZB1-Atto542 / DS-WZA2-AttoOxa11	285	0.70 ±0.02	15.2 ±0.3	0.30 ±0.02	45.4 ±1.4	24.3 ±1.2
	NM-WZA2-Atto542 / DS-WZB1-AttoOxa11	381	0.61 ±0.02	26.0 ±0.3	0.39 ±0.02	7.5 ±0.3	18.8 ±0.7
Closed	NM-WZA2-Atto542 / Lid-WZB1-AttoOxa11	257	1.0	17.4 ±0.1			17.4 ±0.1
	Lid-WZB1-Atto542 / DS-WZA2-AttoOxa11	314	1.0	19.5 ±0.1			19.5 ±0.1
	NM-WZA2-Atto542 / DS-WZB1-AttoOxa11	444	1.0	16.4 ±0.1			16.4 ±0.1

[a] N = Number of dwell-times collected

[b] Time constants $\tau_{1\text{-}2}$ (in sec) and the corresponding relative amplitudes $a_{1\text{-}3}$ of the individual phases contributing to the overall conformational change. Fitting parameters are given ± s.e. of the fit.

[c] mean time constant $\tau = \sum_n a_n \tau_n$

4 Discussion

4.1 Kinetics of local motions

Global conformational motions of the molecular chaperone Hsp90, leading to the catalytically active closed state conformation, are coordinated by a network of local conformational motions. FRET-reporter systems revealed kinetics of clamp-closure, agreeing with the ATP-hydrolysis rate (Hessling et al., 2009). Because of the multi-exponential behavior of clamp-closure, it was suggested that Hsp90 progresses through intermediate states into its hydrolysis-competent state. According to the proposed model, the fast process of ATP-binding is followed by slow transition into intermediate state 1, in which the N-terminal domains are still not dimerized. It was suggested that this intermediate represents the closed lid-configuration, accompanied by release of the N-terminal ß-strand. This step is followed by dimerization of the NTDs and ß-strand swap, representing the intermediate state 2. This is followed by a rearrangement of N-M-domain contacts, representing the active closed state. Upon ATP-hydrolysis and ADP-release, the clamp opens and is ready for the next ATPase cycle (Figure 4-1).

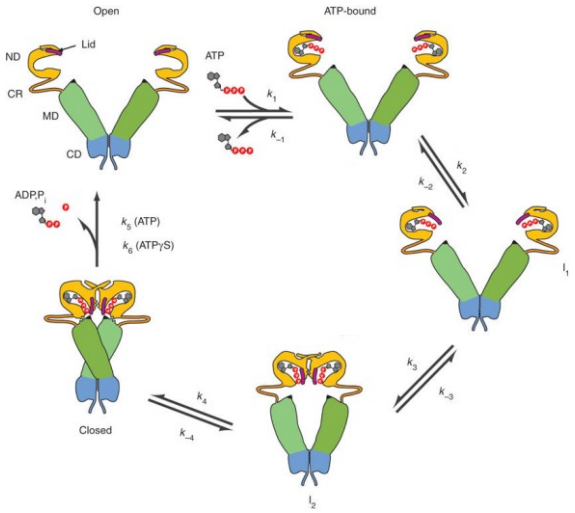

Figure 4-1: Model of the Hsp90 ATP-hydrolysis cycle, based on analysis of bulk FRET-measurements reporting on N-terminal dimerization. Fast binding of ATP leads to slow occupation of an intermediate state I1, in which the ATP-lid has folded over the binding pocket. This is followed by N-terminal dimerization and ß-strand swap (I2) and finally reconfiguration of the NM-orientation, resulting in the hydrolysis competent closed state. Modified from (Hessling et al., 2009). Reuse permission has been granted.

The depicted model suggests that local motions occur in a specific sequence. However, this assumption has so far not been approved, due to a lack of suitable methods that can detect local motions. PET-reporter systems that monitor on ß-strand swap, lid-closure and NM-association were designed within the scope of this doctoral thesis project. For the first time, AMP-PNP triggered kinetics of local motions were determined. Even though some of the designed reporter systems showed an accelerated ATPase activity in homodimeric form (see section 3.1.2), ATPase activity of heterodimers with wild-type Hsp90 should be accelerated to a lesser extent, as the slower wild-type kinetics will probably be reflected in the reporter-containing subunit. Therefore, measured kinetics should be comparable. In contrast to the proposed model, all investigated local motions occured on a similar time-scale (compare Table 3-1), agreeing with the ATP hydrolysis rate, thus suggesting cooperation of conformational switches upon formation of the closed clamp configuration. The effect of both, accelerating (A107N) and decelerating (TrpZip) mutations on lid-closure and NM-association kinetics was in both cases in good agreement with ATPase activity, in contrast to the lower accelerated and stronger decelerated ß-strand swap kinetics, respectively (compare Figure 3-7).

Furthermore, the open-lid stabilizing mutation T101I as well as mutation of the catalytic loop Arg-380 (R380A), which is essential for middle and NTD interaction, completely abolished local motions at remote positions. This finding reveals inter-dependence of local motions.

The first eight amino acids of yeast Hsp90 (N-terminal ß-strand) were shown to be not essential for ATP-hydrolysis, but to have an inhibitory effect on ATPase activity (Richter et al., 2002). This was proven by stabilization of the ß-strand on its own domain through introduction of a TrpZip-motif (see Figure 3-6). Although the kinetics of ß-strand swap were stronger decelerated than lid-closure and NM-association (see Figure 3-6 and Figure 3-7), the regulatory effect of this structure became evident. However, the TrpZip-motif reduces the dissociation rate of the ß-strand from its own domain. The designed reporter system does not monitor the ß-strand detachment kinetics, but instead the overall strand swapping kinetics, which is the time until the structure is completely swapped on the opposing subunit. It would have been also interesting to visualize the detachment process of the ß-strand from its own domain. Maybe lid-closure is controlled by the detachment kinetics of the N-terminal ß-strand, rather than by the overall swapping kinetics. This is supported by the observation that removal of the first 24 amino acids confers increased flexibility of the lid-structure (Richter et al., 2006). In a first attempt fluorophore and quencher were placed within the same subunit (A2C/E162W) to monitor ß-strand detachment kinetics (Schulze, 2013). However, fluorophore-Trp complex formation stabilized the structure, resulting in slowed kinetics. Thus, it was only possible to place fluorophore and Trp on opposing subunits, so that the stabilizing PET-complex is formed at the end of the closing cycle, reporting on the overall swapping kinetics.

4.2 Early events in the chaperone cycle

The mobility of the N-terminal ß-strand and the open-lid structure was investigated by Gerti Beliu and Dominic Helmerich within the scope of their master and bachelor thesis, respectively (Beliu, 2015; Helmerich, 2015). Dynamics of the N-terminal ß-strand were examined by PET-FCS reporter Q14C/A2W, in which fluorophore and Trp are in a distance of 3 nm in the folded strand, too far apart for PET-

complex formation. Detachment of the ß-strand facilitates PET-interaction through formation of a mobile coil. Mobility of the lid was investigated by reporter A112C/S25W, in which Trp and fluorophore are in PET-distance in the open-state configuration. Transient release of the lid into a less open conformation would result in fluorescence fluctuations that can be detected in FCS experiments. Measurements were performed on isolated NTD and NM constructs, incapable of ATP-hydrolysis and also lid closure (Beliu, 2013; Helmerich, 2015; Schulze et al., 2016). Results showed that both elements are highly mobile, although they appear well ordered in crystal structures. High mobility of the lid primes it for fast reconfiguration upon binding of ATP, which leads to a more open conformation, as observed in PET-FCS measurements in presence of ATP. In contrast, the ß-strand mobility does not change in presence of ATP. As already described before, it would have been interesting to investigate the influence of ß-strand dissociation kinetics on lid-mobility. The TrpZip-motif was shown to stabilize the ß-strand folded on its own domain, in PET-FCS experiments. However, the effect of the rigidified ß-strand structure on lid-mobility could not be examined, as a mutant consisting of the lid PET-FCS reporter with TrpZip was prone to aggregation (Beliu, 2015).

PET-FCS measurements already indicate that the lid directly responds to ATP-binding by changing into a partly closed conformation, independent of the presence of MD or CT-dimerization domain. Rapid lid remodelling in response to nucleotide binding was further proven in stopped-flow experiments at varying concentrations of nucleotide. Remodelling kinetics in dependence of nucleotide concentration were in perfect agreement with nucleotide association rate. Furthermore, the reaction is not dependent on presence of the ATP γ-Phosphate, as ADP also induced remodelling (compare Section 3.2.4).

4.3 Aha1 acts at specific steps in the ATPase cycle

PET-FCS experiments of lid-reporter in presence of cochaperone Aha1 also induced a more open configuration of the ATP-lid within isolated NM-constructs. This shows that binding of Aha1 already induces conformational changes within the lid element, prior to start of the hydrolysis cycle. Results are consistent with previous findings that report on a similar acceleration of the ATPase cycle, which

is due to addition of Aha1 or due to removal of the lid in one subunit (Hsp90 - lidless Hsp90 heterodimers). It is suggested that Aha1 promotes release of the lid (Wolmarans et al., 2016). This is supported by a decrease in fluorescence when Aha1 was added to lid-closure reporter S51C/A110W (see Figure 3-9).

But this does not seem to be the only regulation point, at which Aha1 acts. Addition of Aha1 to heterodimers of lidless Hsp90 and wt further accelerate ATPase activity, indicating that Aha1 not only promotes lid closure (Wolmarans et al., 2016). Furthermore, Aha1-N domain interacts with Hsp90 middle domain and can stimulate ATP-hydrolysis even in constructs lacking Aha1-C. In contrast, Aha1-C domain in isolation, which interacts with Hsp90 NTD, can't stimulate. Crystal structures of Hsp90-MD in complex with Aha1-N showed a partially open configuration of the catalytic loop (Prodromou, 2012). Fluorescence changes in NM-association reporter upon addition of Aha1 suggests that Aha1 stabilizes Hsp90 in a NM-domain pre-associated conformation (see Figure 3-9). This seems to be facilitated through interaction with the catalytic loop, which is indicated by the restoring effect of Aha1 on F349A mutation. This mutant is thought to be impaired in orienting the catalytic loop towards the NTD. Furthermore, F349A mutants showed reduced QY in NM-reporter systems, indicating that this mutation also destabilizes a preferentially open apo-state conformation. Addition of Aha1 leads to an increase of F349A fluorescence intensity, probably via re-orientation of the catalytic loop and stabilization in a partially open configuration and thus stabilization of a partly NM-associated state.

4.4 Model of the Hsp90 ATPase cycle

Multi-exponential kinetics of global conformational transitions into the closed clamp configuration were proposed to originate from intermediate states. Transition into the first intermediate state was suggested to be a slow event. Results obtained from bulk measurements within this work show that indeed binding of ATP induces occupation of an intermediate state, represented by a partly closed lid conformation. However, lid-reconfiguration occurs fast, in direct response to nucleotide binding. Complete closure of the lid appeared to occur slow and simultane-

ously with NM-domain association. Kinetics are in agreement with ATPase activity, while ß-strand swap showed slower kinetics in mutants that affect hydrolysis, revealing that hydrolysis is not dependent on complete subunit swap of the ß-strands. But maybe on ß-strand detachment from its own domain, which was not detectable with the designed reporter systems.

In agreement with global transition kinetics, local motions also behaved multi-exponential, questioning the idea of slowly occupied intermediate states, represented by local conformational switches. Another explanation of multi-exponential kinetics could be ground-state heterogeneity of Hsp90 in the apo state. This is supported by EM-data of apo Hsp90, showing an ensemble of open-state conformers (Southworth and Agard, 2008). Transition from different open-clamp conformations with different free energy would be connected to different energy barriers along parallel pathways to the closed state and hence deviating kinetics. Furthermore, different transition pathways with different free energy barriers from a specific open-clamp conformation to the closed clamp could also explain multi-exponential kinetics.

New findings from bulk measurements are integrated into the proposed Hsp90 ATPase cycle, shown in Figure 4-2.

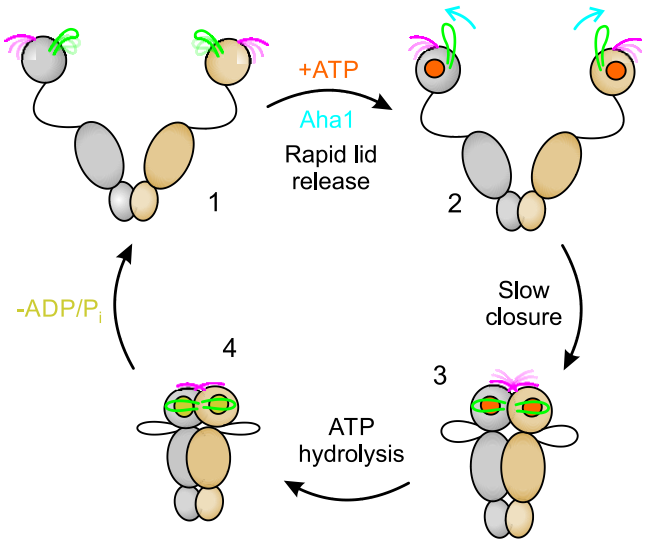

Figure 4-2: Model of the Hsp90 ATPase cycle, based on new findings from PET-reporter studies on local motions. The N-terminal ß-strand and the ATP-lid are highly mobile structures in the nucleotide unbound apo-state (1). Flexibility primes the lid for rapid release in response to nucleotide binding, leading to a more open conformation. Aha1 accelerates the ATPase cycle by remodelling of the lid-structure as well as pre-association on NTD and MD (latter not depicted) (2). Slow closure of the lid is accompanied by NM-association, leading to the hydrolysis competent closed state conformation (2). ß-strand swap is only weakly coupled and complete swap is not necessary for hydrolysis to take place (4). Upon ADP-release, the clamp opens and is ready for the next cycle. Adapted from (Schulze et al., 2016)

4.5 Single-molecule microscopy of conformational transitions

Most molecular systems behave ergodic. This means that the average measured over an ensemble of molecules simultaneously provides the same information than the average measured separately from a number of single-molecules. Single-molecule FRET studies of Hsp90 clamp-closure actually provided similar results as obtained in ensemble FRET measurements, with regard to multi-exponential behaviour of clamp-closure (Hessling et al., 2009; Mickler et al., 2009). However, the advantage of single-molecule microscopy is that also transient events, like for example the closed-state conformation, become visible. In ensemble measurements only reactions can be visualized that result in a clear shift in the equilibrium between states. In contrast, single-molecule microscopy enables the observation of a biomolecular system that continuously switches between conformational states.

Thus, Hsp90's ATPase cycle can be observed in presence of ATP, as no shift to the closed state by AMP-PNP is needed. smFRET measurements provided information about the dwell-time in open as well as closed state configuration (Mickler et al., 2009). Furthermore, Hsp90 also switches stochastically between open and closed state conformations in absence of nucleotide. Applying smFRET in nucleotide-free and ATP-conditions, it was possible to delineate if ATP-binding directs the ensemble of conformers towards occupation of the closed clamp conformation. Results suggested that little directionality is induced by ATP binding. Stochastic, thermal fluctuations of Hsp90 conformers were proposed to be the dominating mechanism (Mickler et al., 2009). smFRET can also provide information about a sequence of events when applied in combination with other techniques, like force microscopy, that can for instance report on local reconfigurations prior to long-range interactions upon folding of a polypeptide chain (Mashaghi et al., 2013). Furthermore, multi-colour FRET revealed the sequence of states of Hsp90 conformational change, p23 interaction and ATP-binding (Ratzke et al., 2014).

The aim of this work was to decipher coupling and directionality within the network of local conformational changes, coordinating transition into the catalytically active state of the Hsp90 molecular chaperone ATPase cycle. Bulk measurements show interdependence of local motions and reveal that conformational transitions occur on similar time-scales. But no information can be gained, if motions occur in a specific sequence. This was the motivation for development of a two-colour single-molecule technique, to observe local motions simultaneously and in real-time.

In a first attempt, a one-colour single-molecule PET technique was developed. This method should deliver similar results as obtained in ensemble measurements, when performed with AMP-PNP. That way, only transition kinetics into the closed clamp configuration are obtained. Using ATP was not possible, as at that time the only way for distinguishing between PET and bleaching event was oxidation of Trp in PET-reactive complexes by oxygen, which abolishes PET such that the excited dye can recover into its ground state via photon emission (on-switch, Figure 3-13). One-colour smPET microscopy of AMP-PNP triggered switches emerged as quite time-consuming. One flow-chamber can only be used for one-measurement, as the AMP-PNP triggered clamp-closure is non-reversible. From one field of view

about 40 positive traces were identified on average. For example, the statistical pool of 274 positive PET-traces, analysed in Figure 3-15, resulted from seven flow chambers. At least three individual peaks could be identified in histograms calculated with a bin width of 20 sec. However, binning-free cumulative sum plots were well described by a mono-exponential fit. Distribution analysis of histograms is to handle with care. A very large statistical pool is needed for reliable identification of subpopulations, as demonstrated in Figure 3-24, e. The larger the number of events, the smoother becomes the shape of the histogram, such that peaks identified in a smaller data set might vanish. Additionally, the shape of a histogram is dependent on the binning size. Too small bins would lead to a rugged distribution, such that individual peaks cannot be identified. Larger bins smoothen the data, but small subpopulations might be hidden by too large bins. The width of a histogram distribution provides information about the extent of heterogeneity in the investigated system. The shape of histograms calculated from one-colour smPET data of local motions, described in Jonathan Schubert's master thesis, deviated vastly among the individual reporter systems (Figure 4-3; (Schubert, 2017). While the NM and ß-strand reporter system histograms are skewed right, so that most events occurred at fast time-scales, the lid showed a plateau shaped histogram, distributed equally over the complete observation time of the experiment. When compared to ensemble measured kinetic data of C-His constructs, listed in Table 3-2, varying distributions might reflect the distinct amplitudes of kinetic phases, by which the individual reporter systems transit into the closed configuration. Bi- or three exponential functions were needed to describe ensemble measured AMP-PNP triggered fluorescence changes accurately. All three reporter systems showed one slow kinetic phase at a timescale > 10 min. Most of the events, which account to this slow kinetic phase, are lost in single-molecule experiments, due to a short observation time window. In NM-reporter systems, a kinetic phase of about three minutes presents the main component (> 60 %). Most switching events were registered at t < 200 sec (Figure 4-3, a). In lid-reporter systems, both kinetic phases of ~ 5 min and < 10 min are more equally distributed, with tendency towards the slower kinetic phase. This might show that lid-closure events are equally distributed along the complete observation time (Figure 4-3, b). In contrast, the ß-strand swap kinetics show a third fast exponential phase, centred at t = 50 sec. This phase

presents the main component (> 50 %), a second phase is centred at t = 3 min (> 30 %) and the third phase of > 10 min won't be detectable. The additional, fast kinetic phase might explain the shape of the ß-strand swap histogram (Figure 4-3, c). Thus, one-colour smPET microscopy data actually mirror the data obtained from ensemble measurements. However, the overall kinetics are not comparable, because the slow kinetics are missing in single molecule experiments.

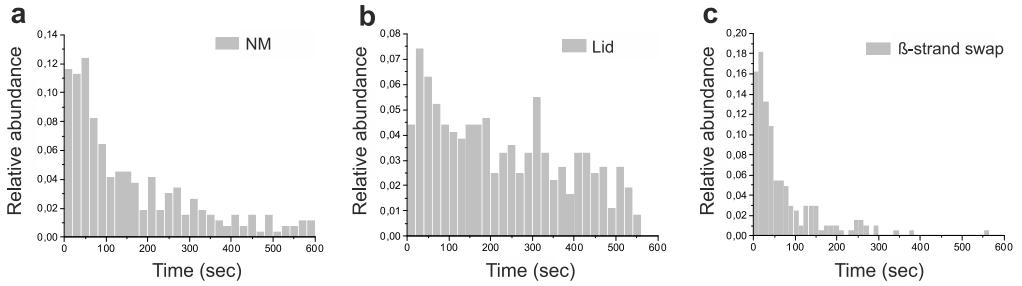

Figure 4-3: One-colour single molecule data of NM-association (a), Lid-Closure (b) and ß-strand swap (c) reporter systems. Histograms are calculated with a bin size of 20 sec. The relative abundance of conformational switching events at different timescales is shown. NM-association: N = 267 events; Lid-Closure: N = 365 events; ß-strand swap: N = 204 events. Modified from (Schubert, 2017)

One-colour single molecule PET microscopy measurements revealed that it is possible to detect local conformational motions, monitored by PET-reporter systems, at the single-molecule level. The newly developed technique provided the platform to achieve the actual goal: simultaneous observation of local motions at remote positions using two-colour single-molecule PET. Oxygen destruction of PET-reactive complexes was used for identification of possible fluorophore candidates for application in two-colour smPET microscopy (Figure 3-17). At a first glance, the fluorescence recovery effect of Atto542 PET-quenched complexes seemed to be only minor, compared to the effect of buffer exchange, measured for AttoOxa11 (Figure 3-13). It should be noted, that the change in localizations over time does not only represent the fluorescence recovery of PET-reactive complexes. Also photobleaching events are included, such that the actual number of oxygen destructed PET-complexes is underestimated.

Performing two-colour measurements with AMP-PNP emerged as non-applicable due to the sparse yield of co-localizing molecules, in which both fluorophores are stable over the observation time of the experiment and additionally show fluorescence recovery through PET-complex destruction by oxygen. Performing

measurements in presence of ATP is actually favourable, as this is the physiological nucleotide, triggering the chaperone cycle. Additionally, repeated cycles of ATP-hydrolysis better mimic the *in vivo* ATPase cycle, in which the cycle has reached an equilibrium between the different states of the ATPase cycle which are apo-states, ATP-bound-states and ADP-bound-states (disregarding the complex regulation mechanisms at cellular conditions). Some co-localizing heterodimers showed simultaneous fluorescence fluctuations in presence of ATP. Such a phenomenon was not identifiable in absence of ATP. Furthermore, the green fluorophore showed very stable photon emission, fluorescence intermittency was rarely detectable. Off-on switches of Atto 542 fluorophore were almost solely accompanied by the same kind of event of AttoOxa 11 fluorophore. However, AttoOxa 11 showed high frequent fluorescence intermittency, being of photo-physical nature. This behaviour complicated data evaluation, as no reliable statement could be given about whether or not local motions occur simultaneously or in a specific sequence or random. Nonetheless, off-states, which were only detected for one fluorophore, rather represented a stochastic, thermal fluctuation, than an ATPase active state. Occupation of the closed clamp configuration is only possible if the ATP-lids are closed and the N- and M-domains are associated. Furthermore, the ß-strand can't swap subunits as long as NTD's are not dimerized. Thus, off-states of the reporter systems have to overlap at least transiently.

Identification of a dimmed state in PET-quenched complexes enabled a more reliable data evaluation. Fluorescence fluctuations that reached background signal were clearly assignable to photo-physical events. However, dimmed states were not detected for all reporter systems. The NM-reporter system showed no dimmed state, neither when conjugated to AttoOxa11 nor to Atto542. This reporter showed the highest PET-quenching efficiency in ensemble measurements (~ 80 % fluorescence reduction, compare Figure 3-4). Lid reporter showed the lowest fluorescence reduction (~ 60 %) and dimmed states were detected for both fluorophores. This indicates that a clearly distinguishable dimmed state is dependent on the PET quenching efficiency of the chosen reporter system. The higher the quenching efficiency, the lower the difference between dimmed state and off-state. However, that a dimmed state could only be detected for ß-strand swap reporter (~ 70 % fluorescence reduction in ensemble) when conjugated to Atto542, is puzzling.

The applied data evaluation script only counted photo-switching events, if they occurred simultaneously within a time window of ± 15 frames (1 frame = 0.3 sec). This filter was incorporated, because in some cases the red dye switched off far earlier or switched on far later than the green dye, resulting in longer off-states as compared to the green fluorophore. If those earlier off-switches and later on-switches of the red fluorophore would be of biological nature, a swap of fluorophores should result in an inverse time-offset histogram shape (compare Figure 3-23, e – g). However, prolonged off-states were almost solely assignable to the red fluorophore. When the lid-reporter system was used, the photophysical nature of earlier off-switches or delayed on-switches of AttoOxa11 was detectable by distinguishing between dimmed and off-states. An example is shown in Figure 4-4, a-b. Furthermore, the simultaneous on-off switch filter also served to eliminate prolonged off-times which are caused by short fluorescence fluctuations, stretching only over 1 or 2 frames that occur immediately before the actual PET-quenched state is occupied. The data evaluation software smoothens the data by a Gaussian function. Thus, fast fluctuating blinking events are filtered out. However, fluorescence switches like displayed in Figure 4-4, c are mistaken as earlier off switch and later on switch of the red dye. The displayed example would be filtered out by the software tool, because green and red off-switch occur in a time-window > 15 frames. However, if the difference between the red and green off-switch is shorter, such an event is counted by the software. By manual data evaluation, some of these false positives are further filtered out. However, some might remain. This explains why the tail of the closure histograms in Figure 3-23 is directed towards positive values (earlier off-switch of the red-fluorophore), while the tail of opening offsets is minimally directed towards negative values (earlier on-switch of green fluorophore). This demonstrates that the shift is rather of photophysical than of biological nature.

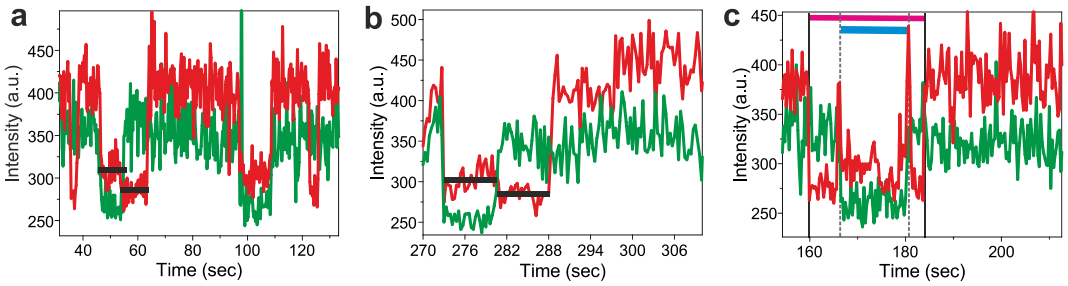

Figure 4-4: Examplary traces of lid-AttoOxa11 and NM-Atto542 reporter heterodimers, showing prolonged off-states of the red fluorophore, which are not due to longer residence times in the PET-complexed state, but due to photophysical events. PET-events and photophysical quenched events are distinguishable, because the PET-complexed state is not completely dark (dimmed state). The difference between dimmed and dark state is indicated by black bars (a, b). In c, the prolonged off state is caused by photoblinking immediately before and after the actual PET-event. Bars indicate the detected off-state residence time of the red fluorophore (magenta, black solid lines mark the borders) and the actual residence time (cyan, dashed gray lines). This event would be filtered out, because the red and green off-switch is not occurring simultaneously in a time window of ± 15 frames.

Results suggest that conformational switches into the closed clamp configuration but also opening of the investigated elements occur simultaneously within the time resolution of the experiment. However, the photophysical behaviour of the red dye complicates a reliable statement. A faster depopulation of non-radiative states, like triplet states and long-lived radical ion states, can be achieved through a combination of a reducing and oxidizing system (ROXS). Triplet states are depopulated via electron transfer, causing formation of a radical ion, which is further depopulated via reaction with the complementary redox reagent. The vitamin E derivative Trolox is often applied as anti-blinking reagent in single molecule applications. In buffer two forms are present: the reducing form Trolox and the oxidizing quinoid form, which is formed through reaction with molecular oxygen. Photoblinking is reduced according to the ROXS scheme (Cordes et al., 2009). It was shown that Trolox and ROXS systems consisting of reductant ascorbic acid and oxidant methylviologen efficiently reduce photoblinking of some rhodamine and cyanine dyes like Atto647N and Cy5. However, no effect was visible for oxazine dyes MR121 and Atto655 (Vogelsang et al., 2008; Cordes et al., 2009). Nonetheless, it was investigated within this work if Trolox might reduce AttoOxa11 photoblinking behaviour. But as expected, no differences were detected.

The stronger photoblinking behaviour of AttoOxa11 in two-colour experiments compared to one-colour experiments is very likely caused by the increased laser

excitation power. Stronger laser-power was necessary to receive a sufficiently high signal at shorter acquisition times, thus receiving a better time-resolution. A high time-resolution was not necessary in one-colour experiments, because motions were not measured simultaneously. In two-colour measurements, it was favourable to set the time-resolution as high as possible, because if motions occur in a specific sequence, this might happen within a very tiny time-window. However, measurements should be repeated with the same settings as used in one-colour microscopy experiments. If that way a reduced photoblinking behaviour is achieved, a more reliable statement can be given about local motions occurring simultaneous within a time window of 1 sec.

Open and closed state dwell times, listed in Table 3-4, indicate that the process of clamp-closure seems to be more heterogenic than the opening process, expressed by the bi-exponential and mono-exponential behaviour, respectively. This is not surprising, as the process of clamp closure is probably far more complex than the process of clamp opening. The process of clamp-closure might begin from different open-state conformers and/or might progress through intermediate states or might pass different free-energy barriers to switch from open to closed conformation. Opening of the clamp is quite likely resulting from one or only a few closed-clamp conformations which are likely of similar free energy. Gained results indicate that ground-state heterogeneity or different energy pathways are more likely the origin of multi-exponential kinetics of open-state dwell-times (closure kinetics) than intermediate states, which are represented by local motions which occur in a specific sequence (compare section 4.4). The distribution of time offsets in Figure 3-23 suggests that motions at remote positions are occurring cooperatively within a time window of ± 1.5 sec, but more likely in a random-order or simultaneously than in a specific order. Latter assumption is made, because the shapes of the different time-offset histograms are similar, even when the same local motions were investigated but with swapped fluorophore-attachment sites. Whether conformational switches occur simultaneously within the chosen time-window of 0.3 sec can't be concluded with certainty.

Open-state dwell-time distributions are populated on a much shorter timescale than those measured in one-colour smPET (compare Figure 3-23 with Figure 3-15 and Figure 4-3). Furthermore, the mean kinetics of clamp-closure are much faster

than those measured in bulk experiments (compare with Table 3-4). But of note, one-colour single-molecule and bulk measurements were performed in presence of AMP-PNP, such that once shifted to the closed clamp configuration, the clamp is trapped in this conformation. In presence of ATP the ATPase can progress repeatedly through the different steps of the ATPase cycle. For example, transition into an ATP-bound closed clamp conformation might result in ATP-hydrolysis, but also a back-reaction to the previous open-state conformer is possible. From this conformation, the closed clamp might be occupied again and much faster as from an ATP-unbound open-state. As transition steps within the cycle are reversible, not each ATP-binding and clamp-closure event results in ATP-hydrolysis, which further explains the discrepancy between ATP-hydrolysis rate and clamp-closure rate in two-colour experiments. In contrast, in presence of AMP-PNP closed-clamp transitions represent progression through the complete ATPase-cycle, as no-back transition from a closed-clamp conformer to an open conformer is possible. Thus, the open-state dwell-times observed in presence of AMP-PNP all begin with nucleotide-unbound open-state conformers and are likely to represent the sum of all forward rate constants of the ATPase cycle. The open-state dwell times in presence of ATP might result from different steps within the ATPase cycle, so that not only forward but also backward reactions within the ATPase cycle are included.

5 Conclusion and Outlook

This work demonstrates that quenching of extrinsic fluorophores by the natural amino acid Trp, which has been developed into a 1-nm sensitive tool for evaluation of rapid nanosecond to millisecond protein folding dynamics, also provides a platform for detection of local conformational transitions on prolonged timescales of milliseconds up to minutes at the single-molecule level. So far, such a wide timespan (nanoseconds to minutes) for observation of structural changes was only accessible for long range conformational transitions (2 to 10 nm) within biomolecules, monitored by FRET-based reporter systems. The developed two-colour single molecule PET microscopy method presents a complement to FRET-based and PET-FCS techniques, providing access to slow short-range (< 1 nm) conformational changes.

The idea for the presented project arose as the primary supervisor of this thesis, Dr. Hannes Neuweiler, listened to a talk given by Prof. Dr. Laurence Pearl (University of Sussex, UK), who presented the crystal structure of the closed clamp of Hsp90, obtained by his group. When compared to structures of isolated Hsp90-domains, representative for the apo-state structure, this structure revealed that specific structural elements undergo intramolecular conformational transitions that are essential for formation of the N-terminal dimerization interface. As the spatial scale of structural reconfigurations was too small for investigation by commonly applied spectroscopic tools, no further information could be gained about the individual role of each element as well as cooperativity of motions during formation of the closed clamp. The reason for the slow transition kinetics into the closed-clamp conformation remained elusive.

As the pioneer of the PET-FCS technique, which was successfully implemented into protein science for investigation of rapid protein dynamics, Dr. Hannes Neuweiler had the idea of designing PET-reporter systems to get access to the mechanistically crucial steps within the Hsp90 ATPase cycle, which are represented by

local conformational rearrangements. Additionally, Hsp90 provided the perfect system to investigate the applicability of PET-reporter systems for detection of not only fast motions within a biomolecule at equilibrium conditions, but also slow conformational transitions that are triggered by external stimuli. In bulk-experiments, this transition between states only becomes visible upon a clear shift in the equilibrium between states. As the non-hydrolysable ATP-derivate AMP-PNP traps Hsp90 in the closed clamp-configuration, which was proven in FRET-experiments, this prerequisite was granted (Hessling et al., 2009).

Observing biomolecular processes in bulk experiments was a good starting point with regard to the design of PET-reporter systems. Bulk measurements are easier to perform and especially the data evaluation is more easy than in single-molecule measurements. Changes in the overall kinetics of a local motion, due to a mutation or through interaction with an external factor like a cochaperone, are faster and more reliable to analyse, as the kinetics represent the average over a very high number of molecules. Measuring such a high number of molecules separately in single-molecule experiments would need an inconceivably high number of recorded image series.

Bulk measurements revealed that kinetics of local motions occur on similar time-scales. Additionally, functional mutations that affect a specific structural element, showed that local motions at remote positions are impacted similarly, demonstrating cooperative behaviour and interdependence of local motions. ß-strand swap seemed to be more loosely coupled to lid-Closure and NM-domain association, as indicated by introduction of a TrpZip-motif. However, as this motif causes a slowed detachment of the ß-strand, it would have been interesting to investigate how the detachment kinetics are coupled with lid-closure and NM-association.

This can be investigated in future experiments by application of the reporter A2C/E162W (both mutations on the same subunit), which was not applicable in one-colour bulk measurements, as PET-complex formation stabilized the structure folded on its own domain. But this reporter can be applied in two-colour single-molecule experiments, to determine if ß-strand detachment and lid-Closure or NM-association occur simultaneously. Furthermore, the influence of TrpZip and

A107N mutant on local motions should be measured simultaneously on the single-molecule level to show more reliable that there is a time-delay between ß-strand swap and lid closure as well as NM-association. Additionally, PET-FCS experiments of Δ8-constructs, lacking the N-terminal ß-strand, might reveal the impact of this structure on lid-mobility. Vice versa, lidless Hsp90 mutants might reveal the impact of this structure on ß-strand mobility. Furthermore, new mutants have already been designed, which are expected to rigidify the ß-strand structure similar to the TrpZip-motif, but hopefully won't cause aggregation when applied on the PET-FCS reporter that monitors lid-dynamics.

Oxidation of PET-reactive complexes by molecular oxygen, which was applied in one-colour-experiments to discriminate between PET-complex and photobleaching, did not provide more information as obtained in bulk-experiments. At the time one-colour measurements were performed, only AMP-PNP conditions were applicable, as there was no way to distinguish between PET and photobleaching at ATP-conditions, in which the ATPase cycles repeatedly between different open and closed conformers. But as identified in two-colour experiments, some reporter systems showed a clearly distinguishable dimmed state of the fluorescence quenched PET-complex, compared to the bleached state. Reporters that fulfil the criteria of a dimmed state, might be applicable to one-colour experiments to measure open and closed state transitions in presence of ATP.

Two-colour smPET microscopy allowed for the first time the observation of distinct local motions simultaneously and in real-time. Data suggests that motions occur simultaneously upon closure as well as opening of the clamp. Nonetheless, the photophysical behaviour of the AttoOxa11 fluorophore has to be improved for a reliable statement. But as many photostabilizing systems like ROXS systems and oxygen scavenger systems, in general don't show an effect on oxazine dyes, further red dyes should be investigated for their applicability in two-colour smPET microscopy. Maybe a fluorophore will be found, which allows for an even higher time-resolution, as a specific sequence of molecular events might happen within a time-span of only milliseconds.

Hsp90's chaperone cycle is highly regulated by interaction with a plethora of cochaperones. The influence of Aha1 on local motions was investigated in PET-

FCS and bulk experiments, showing that it acts early in the chaperone cycle by mobilization of the ATP-lid and promoting NM-domain association. Aha1 accelerates the clamp closure process, such that the stimulatory effect on kinetics of local motions was accessible in bulk-experiments. But most cochaperones do not have a stimulatory effect and are acting transiently at specific steps of the chaperone cycle. It would be interesting to monitor the process of binding of a cochaperone on Hsp90, using a FRET-reporter system, determine its residence time on the chaperone and simultaneously measure its influence on local conformational changes by a PET-reporter system in single molecule experiments. Additionally, the effect of a downstream interactor, acting at a later step within the ATPase cycle, on the cochaperones residence time could be investigated. This would provide information about if both molecules interact cooperatively with Hsp90, or if the former bound cochaperone is displaced. Furthermore, it would be interesting to observe the effect of Hsp90 interaction on the structure of a client. It is proposed that some client proteins are recognized by an unfolding mechanism, such that structurally labile proteins can be selected (Verba et al., 2016). Reporter systems should be designed, which report on changes within the client's structure.

The presented novel method provides a platform, for the in-depths investigation of open questions in the field of protein folding and the mechanism of biomolecular machines. For the biomolecular machine Hsp90 it brought new mechanistically insights with regard to the function and regulatory role of structural elements, which represent the mechanistic core of the ATP-hydrolysis cycle. It should also be noted, that this method enables the observation two-motions simultaneously using only two-extrinsic fluorophores. In comparison, in FRET-reporter systems two fluorophores report on only one motion.

But of course, new methods are never perfect right from the beginning. There is room for optimization of the photochemical aspects mentioned within this work, but also a faster data evaluation technique is desirable, making this technique easier applicable. I hope that this work is just the starting point and that this technique will become more easily and generally applicable for investigation of local transitions in biomolecules, yielding new mechanistic insights into the many enigmatic biochemical processes.

Bibliography

Aitken, C.E., Marshall, R.A., and Puglisi, J.D. (2008). An oxygen scavenging system for improvement of dye stability in single-molecule fluorescence experiments. Biophysical Journal *94*, 1826-1835.

Ali, M.M.U., Roe, S.M., Vaughan, C.K., Meyer, P., Panaretou, B., Piper, P.W., Prodromou, C., and Pearl, L.H. (2006). Crystal structure of an Hsp90–nucleotide–p23/Sba1 closed chaperone complex. Nature *440*, 1013-1017.

Anfinsen, C.B. (1973). Principles that Govern the Folding of Protein Chains. Science *181*, 223-230.

Antonik, M., Felekyan, S., Gaiduk, A., and Seidel, C.A.M. (2006). Separating structural heterogeneities from stochastic variations in fluorescence resonance energy transfer distributions via photon distribution analysis. The journal of physical chemistry. *110*, 6970-6978.

Arganda-Carreras, I., Sorzano, C.O.S., Marabini, R., Carazo, J.M., Ortiz-de-Solorzano, C., and Kybic, J. (2006). Consistent and Elastic Registration of Histological Sections Using Vector-Spline Regularization. Springer, Berlin, Heidelberg *4241*, 85-95.

Arndt, K.M., Pelletier, J.N., Müller, K.M., Plückthun, A., and Alber, T. (2002). Comparison of In Vivo Selection and Rational Design of Heterodimeric Coiled Coils. Structure *10*, 1235-1248.

Avellaneda, M.J., Koers, E.J., Naqvi, M.M., and Tans, S.J. (2017). The chaperone toolbox at the single-molecule level: From clamping to confining. Protein Science *26*, 1291-1302.

Balchin, D., Hayer-Hartl, M., and Hartl, F.U. (2016). In vivo aspects of protein folding and quality control. Science *353*, aac4354.

Beliu, G. (2013). Bachelorarbeit. Untersuchungen zur Dynamik der N-terminalen Domäne des molekularen Chaperons Hsp90 (Universität Würzburg).

Beliu, G. (2015). Masterarbeit. Untersuchungen zur Dynamik der ATP-Bindungsdomäne des Chaperons Hsp90 mittels Fluoreszenzkorrelationsspektroskopie (Universität Würzburg).

Benesch, R.E., and Benesch, R. (1953). Enzymatic Removal of Oxygen for Polarography and Related Methods. Science *118*, 447-448.

Bio-Logic. SFM-300-400 User's Manual *Version 2.7*.

Borgia, A., Williams, P.M., and Clarke, J. (2008). Single-Molecule Studies of Protein Folding. Annu. Rev. Biochem. *77*, 101-125.

Brujic, J., Hermans, R.I.Z., Garcia-Manyes, S., Walther, K.A., and Fernandez, J.M. (2007). Dwell-time distribution analysis of polyprotein unfolding using force-clamp spectroscopy. Biophysical Journal *92*, 2896-2903.

Butler, L.M., Ferraldeschi, R., Armstrong, H.K., Centenera, M.M., and Workman, P. (2015). Maximizing the Therapeutic Potential of HSP90 Inhibitors. Molecular cancer research *13*, 1445-1451.

Chan, H.S., and Dill, K.A. (1991). Polymer Principles In Protein Structure And Stability. Annual Review of Biophysics and Biomolecular Structure *20*, 447-490.

Chatterjee, S., and Burns, T.F. (2017). Targeting Heat Shock Proteins in Cancer: A Promising Therapeutic Approach. International journal of molecular sciences *18*.

Chen, Y., Ding, F., Nie, H., Serohijos, A.W., Sharma, S., Wilcox, K.C., Yin, S., and Dokholyan, N.V. (2008). Protein folding: Then and now. Archives of Biochemistry and Biophysics *469*, 4-19.

Cochran, A.G., Skelton, N.J., and Starovasnik, M.A. (2001). Tryptophan zippers: stable, monomeric beta -hairpins. Proceedings of the National Academy of Sciences *98*, 5578-5583.

Cordes, T., Vogelsang, J., and Tinnefeld, P. (2009). On the Mechanism of Trolox as Antiblinking and Antibleaching Reagent. J. Am. Chem. Soc. *131*, 5018-5019.

Cunningham, C.N., Krukenberg, K.A., and Agard, D.A. (2008). Intra- and Inter-monomer Interactions Are Required to Synergistically Facilitate ATP Hydrolysis in Hsp90. Journal of Biological Chemistry *283*, 21170-21178.

Cunningham, C.N., Southworth, D.R., Krukenberg, K.A., and Agard, D.A. (2012). The conserved arginine 380 of Hsp90 is not a catalytic residue, but stabilizes the closed conformation required for ATP hydrolysis. Protein Science *21*, 1162-1171.

Doose, S., Neuweiler, H., and Sauer, M. (2005). A Close Look at Fluorescence Quenching of Organic Dyes by Tryptophan. ChemPhysChem *6*, 2277-2285.

Doose, S., Neuweiler, H., and Sauer, M. (2009). Fluorescence Quenching by Photoinduced Electron Transfer: A Reporter for Conformational Dynamics of Macromolecules. ChemPhysChem *10*, 1389-1398.

Dutta, R., and Inouye, M. (2000). GHKL, an emergent ATPase/kinase superfamily. Trends Biochem. Sci. *25*, 24-28.

Finka, A., and Goloubinoff, P. (2013). Proteomic data from human cell cultures refine mechanisms of chaperone-mediated protein homeostasis. Cell stress and chaperones *18*, 591-605.

Gebhardt, J.C.M., Clemen, A.E.-M., Jaud, J., and Rief, M. (2006). Myosin-V is a mechanical ratchet. Proceedings of the National Academy of Sciences *103*, 8680-8685.

Gorenberg, E.L., and Chandra, S.S. (2017). The Role of Co-chaperones in Synaptic Proteostasis and Neurodegenerative Disease. Frontiers in neuroscience *11*, 248.

Gracanin, M., Hawkins, C.L., Pattison, D.I., and Davies, M.J. (2009). Singlet-oxygen-mediated amino acid and protein oxidation: formation of tryptophan peroxides and decomposition products. Free radical biology & medicine *47*, 92-102.

Graf, C., Lee, C.-T., Eva Meier-Andrejszki, L., Nguyen, M.T.N., and Mayer, M.P. (2014). Differences in conformational dynamics within the Hsp90 chaperone family reveal mechanistic insights. Frontiers in molecular biosciences *1*, 4.

Grecco, H.E., and Verveer, P.J. (2011). FRET in Cell Biology: Still Shining in the Age of Super-Resolution? ChemPhysChem *12*, 484-490.

Haenni, D., Zosel, F., Reymond, L., Nettels, D., and Schuler, B. (2013). Intramolecular Distances and Dynamics from the Combined Photon Statistics of Single-Molecule FRET and Photoinduced Electron Transfer. J. Phys. Chem. B *117*, 13015-13028.

Hanahan, D., and Weinberg, R.A. (2011). Hallmarks of cancer: the next generation. Cell *144*, 646-674.

Hartl, F.U., Bracher, A., and Hayer-Hartl, M. (2011). Molecular chaperones in protein folding and proteostasis. Nature *475*, 324-332.

Hayer-Hartl, M., Bracher, A., and Hartl, F.U. (2016). The GroEL-GroES Chaperonin Machine: A Nano-Cage for Protein Folding. Trends in Biochemical Sciences *41*, 62-76.

Heilemann, M., van de Linde, S., Schüttpelz, M., Kasper, R., Seefeldt, B., Mukherjee, A., Tinnefeld, P., and Sauer, M. (2008). Subdiffraction-Resolution Fluorescence Imaging with Conventional Fluorescent Probes. Angew. Chem. Int. Ed. *47*, 6172-6176.

Helmerich, D.A. (2015). Bachelorarbeit. Untersuchungen zur Konformationsdynamik der ATP Bindungsdomäne im C-terminal verkürzten Chaperon Hsp90 (Universität Würzburg).

Hessling, M., Richter, K., and Buchner, J. (2009). Dissection of the ATP-induced conformational cycle of the molecular chaperone Hsp90. Nat Struct Mol Biol *16*, 287-293.

Hua, B., Han, K.Y., Zhou, R., Kim, H., Shi, X., Abeysirigunawardena, S.C., Jain, A., Singh, D., Aggarwal, V., and Woodson, S.A., et al. (2014). An improved surface passivation method for single-molecule studies. Nature methods *11*, 1233-1236.

Hübner, C.G., Renn, A., Renge, I., and Wild, U.P. (2001). Direct observation of the triplet lifetime quenching of single dye molecules by molecular oxygen. J. Chem. Phys. *115*, 9619.

Inoue, H., Nojima, H., and Okayama, H. (1990). High efficiency transformation of Escherichia coli with plasmids. Gene *96*, 23-28.

Jahn, M., Buchner, J., Hugel, T., and Rief, M. (2015). Folding and assembly of the large molecular machine Hsp90 studied in single-molecule experiments. Proceedings of the National Academy of Sciences *113*, 1232-1237.

Jeyachandran, Y., Mielczarski, J., Mielczarski, E., and Rai, B. (2010). Efficiency of blocking of non-specific interaction of different proteins by BSA adsorbed on hydrophobic and hydrophilic surfaces. Journal of Colloid and Interface Science *341*, 136-142.

Jhaveri, K., Ochiana, S.O., Dunphy, M.P.S., Gerecitano, J.F., Corben, A.D., Peter, R.I., Janjigian, Y.Y., Gomes-DaGama, E.M., Koren, J., and Modi, S., et al. (2014). Heat shock protein 90 inhibitors in the treatment of cancer. Current status and future directions. Expert Opinion on Investigational Drugs *23*, 611-628.

Kampinga, H.H., and Craig, E.A. (2010). The HSP70 chaperone machinery: J proteins as drivers of functional specificity. Nature reviews. Molecular cell biology *11*, 579-592.

Karagöz, G.E., Duarte, A.M.S., Ippel, H., Uetrecht, C., Sinnige, T., van Rosmalen, M., Hausmann, J., Heck, A.J.R., Boelens, R., and Rüdiger, S.G.D. (2011). N-terminal domain of human Hsp90 triggers binding to the cochaperone p23. Proceedings of the National Academy of Sciences *108*, 580-585.

Kim, Y.E., Hipp, M.S., Bracher, A., Hayer-Hartl, M., and Ulrich Hartl, F. (2013). Molecular Chaperone Functions in Protein Folding and Proteostasis. Annu. Rev. Biochem. *82*, 323-355.

Kityk, R., Vogel, M., Schlecht, R., Bukau, B., and Mayer, M.P. (2015). Pathways of allosteric regulation in Hsp70 chaperones. Nature communications *6*, 8308.

Kleckner, I.R., and Foster, M.P. (2011). An introduction to NMR-based approaches for measuring protein dynamics. Biochimica et biophysica acta *1814*, 942-968.

Krukenberg, K.A., Street, T.O., Lavery, L.A., and Agard, D.A. (2011). Conformational dynamics of the molecular chaperone Hsp90. Quart. Rev. Biophys. *44*, 229-255.

Lai, B.T., Chin, N.W., Stanek, A.E., Keh, W., and Lanks, K.W. (1984). Quantitation and intracellular localization of the 85K heat shock protein by using monoclonal and polyclonal antibodies. Molecular and Cellular Biology *4*, 2802-2810.

Lakowicz, J.R. (op. 2006). Principles of fluorescence spectroscopy (New York: Springer).

Lavery, L.A., Partridge, J.R., Ramelot, T.A., Elnatan, D., Kennedy, M.A., and Agard, D.A. (2014). Structural Asymmetry in the Closed State of Mitochondrial Hsp90 (TRAP1) Supports a Two-Step ATP Hydrolysis Mechanism. Molecular Cell *53*, 330-343.

Levinthal, C. (1968). Are There Pathways for Protein Folding. Journal de Chimie Physique *1*, 44-45.

Li, J., Soroka, J., and Buchner, J. (2012). The Hsp90 chaperone machinery: Conformational dynamics and regulation by co-chaperones. Biochimica et Biophysica Acta - Molecular Cell Research *1823*, 624-635.

Liu, H., and Naismith, J.H. (2008). An efficient one-step site-directed deletion, insertion, single and multiple-site plasmid mutagenesis protocol. BMC biotechnology *8*, 91.

Lotz, G.P., Lin, H., Harst, A., and Obermann, W.M.J. (2003). Aha1 Binds to the Middle Domain of Hsp90, Contributes to Client Protein Activation, and Stimulates the ATPase Activity of the Molecular Chaperone. Journal of Biological Chemistry *278*, 17228-17235.

Lum, J.K., Neuweiler, H., and Fersht, A.R. (2012). Long-Range Modulation of Chain Motions within the Intrinsically Disordered Transactivation Domain of Tumor Suppressor p53. J. Am. Chem. Soc. *134*, 1617-1622.

Mashaghi, A., Kramer, G., Lamb, D.C., Mayer, M.P., and Tans, S.J. (2013). Chaperone Action at the Single-Molecule Level. Chem. Rev. *114*, 660-676.

Mayer, M.P. (2013). Hsp70 chaperone dynamics and molecular mechanism. Trends in Biochemical Sciences *38*, 507-514.

Mayer, M.P., and Le Breton, L. (2015). Hsp90: Breaking the Symmetry. Molecular Cell *58*, 8-20.

McLaughlin, S.H., Ventouras, L.-A., Lobbezoo, B., and Jackson, S.E. (2004). Independent ATPase Activity of Hsp90 Subunits Creates a Flexible Assembly Platform. Journal of Molecular Biology *344*, 813-826.

Meyer, P., Prodromou, C., Hu, B., Vaughan, C., Roe, S.M., Panaretou, B., Piper, P.W., and Pearl, L.H. (2003). Structural and Functional Analysis of the Middle Segment of Hsp90: Implications for ATP Hydrolysis and Client Protein and Cochaperone Interactions. Molecular Cell *11*, 647-658.

Meyer, P., Prodromoue, C., Liao, C., Hu, B., Roe, S.M., Vaughan, C.K., Vlasic, I., Panaretou, B., Piper, P.W., and Pearl, L.H. (2004). Structural basis for recruitment of the ATPase activator Aha1 to the Hsp90 chaperone machinery. EMBO J *23*, 1402-1410.

Mickler, M., Hessling, M., Ratzke, C., Buchner, J., and Hugel, T. (2009). The large conformational changes of Hsp90 are only weakly coupled to ATP hydrolysis. Nat Struct Mol Biol *16*, 281-286.

Mishra, P., Flynn, J.M., Starr, T.N., and Bolon, D.N.A. (2016). Systematic Mutant Analyses Elucidate General and Client-Specific Aspects of Hsp90 Function. Cell reports *15*, 588-598.

Motojima, F. (2015). How do chaperonins fold protein? Biophysics (Nagoya-shi, Japan) *11*, 93-102.

Nathan, D.F., and Lindquist, S. (1995). Mutational analysis of Hsp90 function: interactions with a steroid receptor and a protein kinase. Molecular and Cellular Biology *15*, 3917-3925.

Neckers, L., and Trepel, J.B. (2014). Stressing the development of small molecules targeting HSP90. Clinical cancer research *20*, 275-277.

Neef, D.W., Jaeger, A.M., and Thiele, D.J. (2011). Heat shock transcription factor 1 as a therapeutic target in neurodegenerative diseases. Nature reviews. Drug discovery *10*, 930-944.

Neuweiler, H., Banachewicz, W., and Fersht, A.R. (2010). Kinetics of chain motions within a protein-folding intermediate. Proceedings of the National Academy of Sciences *107*, 22106-22110.

Onuchic, J.N., Luthey-Schulten, Z., and Wolynes, P.G. (1997). Theory of protein folding: the energy landscape perspective. Annual review of physical chemistry *48*, 545-600.

Panaretou, B., Prodromou, C., Roe, S.M., Ladbury, J.E., Piper, P.W., and Pearl, L.H. (1998). ATP binding and hydrolysis are essential to the function of the Hsp90 molecular chaperone invivo. The EMBO Journal *17*, 4829-4836.

Pelletier, J.N., Arndt, K.M., Plückthun, A., and Michnick, S.W. (1999). An in vivo library-versus-library selection of optimized protein-protein interaction. Nature Biotechnology *17*, 683-690.

Prodromou, C. (2012). The 'active life' of Hsp90 complexes. Biochimica et Biophysica Acta - Molecular Cell Research *1823*, 614-623.

Prodromou, C. (2016). Mechanisms of Hsp90 regulation. The Biochemical journal *473*, 2439-2452.

Prodromou, C., Panaretou, B., Chohan, S., Siligardi, G., O'Brien, R., Ladbury, J.E., Roe, S.M., Piper, P.W., and Pearl, L.H. (2000). The ATPase cycle of Hsp90 drives a molecular 'clamp' via transient dimerization of the N-terminal domains. EMBO J *19*, 4383-4392.

Prodromou, C., Roe, S.M., O'Brien, R., Ladbury, J.E., Piper, P.W., and Pearl, L.H. (1997). Identification and structural characterization of the ATP/ADP-binding site in the Hsp90 molecular chaperone. Cell *90*, 65-75.

Ratzke, C., Hellenkamp, B., and Hugel, T. (2014). Four-colour FRET reveals directionality in the Hsp90 multicomponent machinery. Nature communications *5*, 4192.

Ratzke, C., Mickler, M., Hellenkamp, B., Buchner, J., and Hugel, T. (2010). Dynamics of heat shock protein 90 C-terminal dimerization is an important part of its conformational cycle. Proceedings of the National Academy of Sciences *107*, 16101-16106.

Retzlaff, M., Hagn, F., Mitschke, L., Hessling, M., Gugel, F., Kessler, H., Richter, K., and Buchner, J. (2010). Asymmetric Activation of the Hsp90 Dimer by Its Cochaperone Aha1. Molecular Cell *37*, 344-354.

Richter, K., Moser, S., Hagn, F., Friedrich, R., Hainzl, O., Heller, M., Schlee, S., Kessler, H., Reinstein, J., and Buchner, J. (2006). Intrinsic Inhibition of the Hsp90 ATPase Activity. Journal of Biological Chemistry *281*, 11301-11311.

Richter, K., Muschler, P., Hainzl, O., and Buchner, J. (2001). Coordinated ATP Hydrolysis by the Hsp90 Dimer. Journal of Biological Chemistry *276*, 33689-33696.

Richter, K., Reinstein, J., and Buchner, J. (2002). N-terminal residues regulate the catalytic efficiency of the Hsp90 ATPase cycle. Journal of Biological Chemistry *277*, 44905-44910.

Richter, K., Soroka, J., Skalniak, L., Leskovar, A., Hessling, M., Reinstein, J., and Buchner, J. (2008). Conserved Conformational Changes in the ATPase Cycle of Human Hsp90. Journal of Biological Chemistry *283*, 17757-17765.

Röhl, A., Rohrberg, J., and Buchner, J. (2013). The chaperone Hsp90: changing partners for demanding clients. Trends in Biochemical Sciences *38*, 253-262.

Roy, R., Hohng, S., and Ha, T. (2008). A practical guide to single-molecule FRET. Nature methods *5*, 507-516.

Rupp, B. (2013). Biomolecular crystallography. Principles, practice, and application to structural biology (Moorpark, California: Taylor & Francis Ltd).

Sadler, B.M., and Swami, A. (1998). Analysis of Wavelet Transform Multiscale Products for Step Detection and Estimation. IEEE Trans Information Theory *45*, 1043-1051.

Sauer, M., Hofkens, J., and Enderlein, J. (op. 2011). Handbook of fluorescence spectroscopy and imaging. From single molecules to ensembles (Weinheim, Germany: Wiley-VCH).

Sauer, M., and Neuweiler, H. (2014). PET-FCS: Probing Rapid Structural Fluctuations of Proteins and Nucleic Acids by Single-Molecule Fluorescence Quenching. In Engelborghs Y., Visser A. (eds) Fluorescence Spectroscopy and Microscopy. Methods in Molecular Biology (Methods and Protocols), pp. 597–615.

Schubert, J. (2017). Masterarbeit. Einzelmoleküldetektion lokaler Konformationsdynamik im molekularen Chaperon Hsp90 (Universität Würzburg).

Schuler, B., and Hofmann, H. (2013). Single-molecule spectroscopy of protein folding dynamics—expanding scope and timescales. Current Opinion in Structural Biology *23*, 36-47.

Schulze, A. (2013). Masterarbeit. Untersuchungen zur Konformationsdynamik des molekularen Chaperons Hsp90 mittels Fluoreszenzlöschung (Universität Würzburg).

Schulze, A., Beliu, G., Helmerich, D.A., Schubert, J., Pearl, L.H., Prodromou, C., and Neuweiler, H. (2016). Cooperation of local motions in the Hsp90 molecular chaperone ATPase mechanism. Nature chemical biology *12*, 628-635.

Shi, Y. (2014). A glimpse of structural biology through X-ray crystallography. Cell *159*, 995-1014.

Shiau, A.K., Harris, S.F., Southworth, D.R., and Agard, D.A. (2006). Structural Analysis of E. coli hsp90 Reveals Dramatic Nucleotide-Dependent Conformational Rearrangements. Cell *127*, 329-340.

Siligardi, G., Hu, B., Panaretou, B., Piper, P.W., Pearl, L.H., and Prodromou, C. (2004). Co-chaperone Regulation of Conformational Switching in the Hsp90 ATPase Cycle. Journal of Biological Chemistry *279*, 51989-51998.

Southworth, D.R., and Agard, D.A. (2008). Species-Dependent Ensembles of Conserved Conformational States Define the Hsp90 Chaperone ATPase Cycle. Molecular Cell *32*, 631-640.

Taipale, M., Jarosz, D.F., and Lindquist, S. (2010). HSP90 at the hub of protein homeostasis: emerging mechanistic insights. Nat Rev Mol Cell Biol *11*, 515-528.

Teufel, D.P., Johnson, C.M., Lum, J.K., and Neuweiler, H. (2011). Backbone-Driven Collapse in Unfolded Protein Chains. Journal of Molecular Biology *409*, 250-262.

Tsutsumi, S., Mollapour, M., Prodromou, C., Lee, C.-T., Panaretou, B., Yoshida, S., Mayer, M.P., and Neckers, L.M. (2012). Charged linker sequence modulates eukaryotic heat shock protein 90 (Hsp90) chaperone activity. Proceedings of the National Academy of Sciences *109*, 2937-2942.

van de Linde, S., Krstic, I., Prisner, T., Doose, S., Heilemann, M., and Sauer, M. (2011). Photoinduced formation of reversible dye radicals and their impact on super-resolution imaging. Photochemical & photobiological sciences *10*, 499-506.

Vaughan, C.K., Piper, P.W., Pearl, L.H., and Prodromou, C. (2009). A common conformationally coupled ATPase mechanism for yeast and human cytoplasmic HSP90s. FEBS Journal *276*, 199-209.

Verba, K.A., Wang, R.Y.-R., Arakawa, A., Liu, Y., Shirouzu, M., Yokoyama, S., and Agard, D.A. (2016). Atomic structure of Hsp90-Cdc37-Cdk4 reveals that Hsp90 traps and stabilizes an unfolded kinase. Science (New York, N.Y.) *352*, 1542-1547.

Vogelsang, J., Kasper, R., Steinhauer, C., Person, B., Heilemann, M., Sauer, M., and Tinnefeld, P. (2008). A Reducing and Oxidizing System Minimizes Photobleaching and Blinking of Fluorescent Dyes. Angew. Chem. Int. Ed. *47*, 5465-5469.

Wang, W. (1999). Instability, stabilization, and formulation of liquid protein pharmaceuticals. International journal of pharmaceutics *185*, 129-188.

Wegele, H. (2003). Dissection of the Contribution of Individual Domains to the ATPase Mechanism of Hsp90. Journal of Biological Chemistry *278*, 39303-39310.

Whitesell, L., and Lin, N.U. (2012). HSP90 as a platform for the assembly of more effective cancer chemotherapy. Biochimica et Biophysica Acta - Molecular Cell Research *1823*, 756-766.

Whitesell, L., and Lindquist, S. (2009). Inhibiting the transcription factor HSF1 as an anticancer strategy. Expert opinion on therapeutic targets *13*, 469-478.

Whitesell, L., and Lindquist, S.L. (2005). HSP90 and the chaperoning of cancer. Nature reviews. Cancer *5*, 761-772.

Wolmarans, A., Lee, B., Spyracopoulos, L., and LaPointe, P. (2016). The Mechanism of Hsp90 ATPase Stimulation by Aha1. Scientific reports *6*, 33179.

Wolter, S., Proppert, S., Aufmkolk, S., Lampe, A., and Klein, T. (2014). rapidSTORM manual. *Version 3.3*.

Wolter, S., Schüttpelz, M., Tscherepanow, M., van de Linde, S., Heilemann, M., and Sauer, M. (2010). Real-time computation of subdiffraction-resolution fluorescence images. Journal of microscopy *237*, 12-22.

Zierer, B.K., Rübbelke, M., Tippel, F., Madl, T., Schopf, F.H., Rutz, D.A., Richter, K., Sattler, M., and Buchner, J. (2016). Importance of cycle timing for the function of the molecular chaperone Hsp90. Nature structural & molecular biology *23*, 1020-1028.

Zoldák, G., and Rief, M. (2013). Force as a single molecule probe of multidimensional protein energy landscapes. Current Opinion in Structural Biology *23*, 48-57.

Zuehlke, A.D., and Neckers, L. (2016). Clients Place Unique Functional Constraints on Hsp90. Trends in Biochemical Sciences *41*, 562-564.

Publications

Schulze, A., Beliu, G., Helmerich, D.A., Schubert, J., Pearl, L.H., Prodromou, C., and Neuweiler, H. (2016). Cooperation of local motions in the Hsp90 molecular chaperone ATPase mechanism. Nature chemical biology 12 (8), 628-635.

Acknowledgements

At this point, I would like to express my thanks to everyone who supported me during the last years.

A special thanks goes to Hannes Neuweiler for letting me work on this exciting project. Thank you, Hannes, for extensive discussions and for the enthusiasm you have placed into this work. That was highly motivating and I really enjoyed the time in your group.

Thank you, Markus Sauer, for co-supervision of this work and especially for the nice atmosphere within your department. Even if I had a tough start at learning skiing, in the end it was much fun!

I would also like to thank Thomas Müller for co-supervision and for constructive criticism and good suggestions for improvement of my experiments.

For a fruitful collaboration, I would like to thank Laurence Pearl and Chrisostomos Prodromou (University of Sussex, UK).

Thanks to the graduate school of life sciences for the financial support which enabled me to work on this project.

Gerti Beliu, Jonathan Schubert, Suhaila Rajab, Dominic Helmerich – thanks to all of you for working together with me on this and related projects. It is nice to see that you all are going to be part of the "next generation" of PhD students. Julia, I think the remaining time in the lab will be great with them.

To all my colleagues and friends at the department – it was much fun with you. Sina, Felix, Franzi, Sarah and Juli – thank you that you introduced me into the world of outdoor sports. Nora and Jan, your laughter always made my day! Tracy, thank you for always having an open ear.

Fabi, Anne, Lena and Sebastian – thanks for sharing the office with me and for all the funny moments.

Thanks to my friends Katharina, Robert, Manu and Markus and to Carsten, Anna and Daniel. You are the best.

Great thanks to my family. My parents for always supporting me and my three older brothers for preparing me for life.

Last but not least, thank you Sebastian for your patience and for always supporting me, morally and scientifically. Your optimism and your trust always encourages me and makes me belief that everything is going to work out anyhow.